AD-A174 952 FINITE-DIFFERENCE SOLUTIONS FOR COMPRESSIBLE LAMINAR BOUNDARY-LAYER FLOWS (U) TORONTO UNIV DOWNSVIEW (ONTARIO) INST FOR AEROSPACE STUDIES B Y WANG ET AL 1/2

UNCLASSIFIED AUG 86 UTIAS-311 AFOSR-TR-86-2151 F/G 20/4 NL

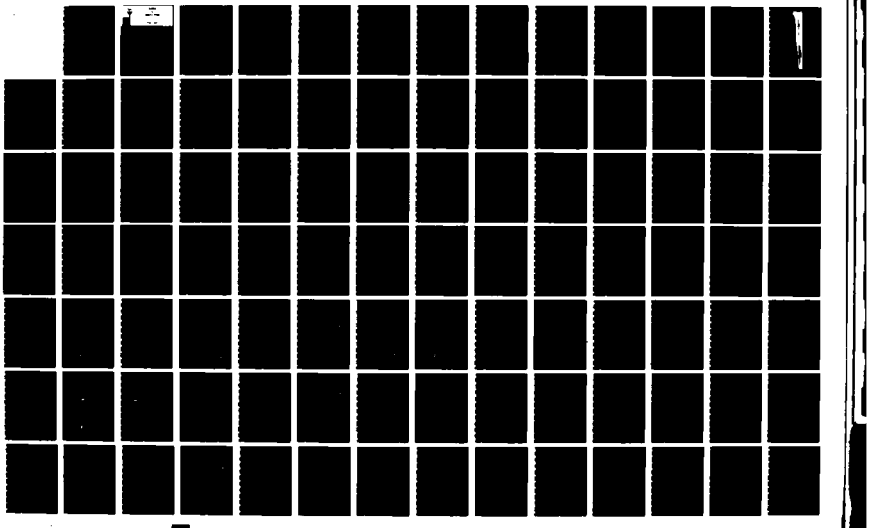

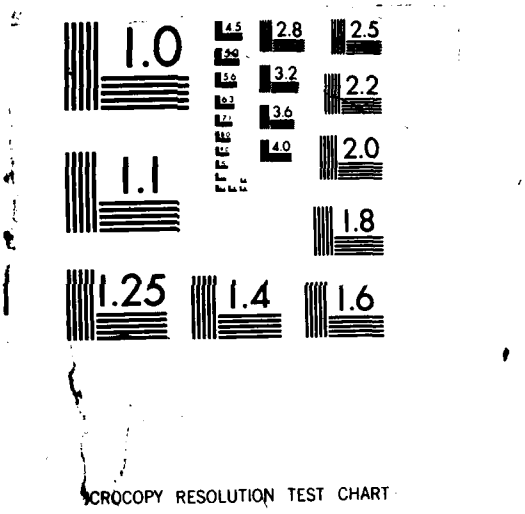

CROCOPY RESOLUTION TEST CHART

INSTITUTE

FOR

AEROSPACE STUDIES

UNIVERSITY OF TORONTO

REPORT DOCUMENTATION PAGE

READ INSTRUCTIONS BEFORE COMPLETING FORM

1. REPORT NUMBER: AFOSR-TR- 86-2151	2. GOVT ACCESSION NO.
3. RECIPIENT'S CATALOG NUMBER	
4. TITLE (and Subtitle): FINITE-DIFFERENCE SOLUTIONS FOR COMPRESSIBLE LAMINAR BOUNDARY-LAYER FLOWS OF A DUSTY GAS OVER A SEMI-INFINITE FLAT PLATE	5. TYPE OF REPORT & PERIOD COVERED: Interim
	6. PERFORMING ORG. REPORT NUMBER: UTIAS Report No. 311
7. AUTHOR(s): Wang, B. Y., Glass, I. I.	8. CONTRACT OR GRANT NUMBER(s): AFOSR-82-0096
9. PERFORMING ORGANIZATION NAME AND ADDRESS: University of Toronto, Inst. for Aerospace Studies, 4925 Dufferin Street, Downsview, Ontario, Canada, M3H 5T6	10. PROGRAM ELEMENT, PROJECT, TASK AREA & WORK UNIT NUMBERS: 61102F 2307/A1
11. CONTROLLING OFFICE NAME AND ADDRESS: Air Force Office of Scientific Research/NA, Bldg. 410, Bolling Air Force Base, DC 20332, U.S.A. NA	12. REPORT DATE
	13. NUMBER OF PAGES
14. MONITORING AGENCY NAME & ADDRESS (if different from Controlling Office): same as 11	15. SECURITY CLASS. (of this report): Unclassified
	15a. DECLASSIFICATION/DOWNGRADING SCHEDULE

16. DISTRIBUTION STATEMENT (of this Report)

Approved for public release; distribution unlimited.

17. DISTRIBUTION STATEMENT (of the abstract entered in Block 20, if different from Report)

Approved for public release;
distribution unlimited.

18. SUPPLEMENTARY NOTES

19. KEY WORDS (Continue on reverse side if necessary and identify by block number)

1. Dusty-gas flows, 2. Two-phase flows, 3. Boundary-layer flows,
4. Partial-differential equations, 5. Numerical analysis.

20. ABSTRACT (Continue on reverse side if necessary and identify by block number)

A finite-difference method is used to investigate compressible, laminar boundary-layer flows of a dilute dusty gas over a semi-infinite flat plate. Details are given of the implicit finite-difference schemes as well as the boundary conditions, initial conditions and compatibility conditions for →

Continued

solving the gas-particle boundary-layer equations. The flow profiles for both the gas and particle phases were obtained numerically along the whole length of the plate from the leading edge to far downstream of it. The finite-difference solutions in the large-slip region and the small-slip region are compared with the asymptotic solutions and good agreement is achieved. The boundary-layer characteristics of interest, including the wall shear stress, the wall heat-transfer rate and the displacement thickness, are calculated. The alteration of the flow properties owing to the presence of particles is discussed in detail. It was found that the boundary-layer flow of a dusty gas can be divided into three distinct flow regimes which are characterized by quasi-frozen, nonequilibrium and quasi-equilibrium flows and that at a critical distance from the leading edge the particle velocity at the wall decelerates to zero and near-equilibrium is achieved between the gas and particle flows. For the laminar boundary layer of a dusty gas, the shear stress and the heat-transfer at the wall are increased and the displacement thickness is decreased compared with the pure-gas case alone. (Canada)

FINITE-DIFFERENCE SOLUTIONS FOR COMPRESSIBLE LAMINAR BOUNDARY-LAYER FLOWS OF A DUSTY GAS OVER A SEMI-INFINITE FLAT PLATE

by

B. Y. Wang and I. I. Glass

Submitted February, 1986

UTIAS Report No. 311
CN ISSN 0082-5255

Acknowledgements

We wish to thank Dr. W. S. Liu and Prof. J. P. Sislian for their valuable discussions.

One of us (B. Y. Wang) is grateful to the Institute of Mechanics, Academia Sinica, Beijing, China, and to UTIAS for the opportunity to study and to do research during the past two years.

The financial assistance received from the Natural Science and Engineering Research Council of Canada under grant No. A1647, the U.S. Air Force under grant AF-AFOSR-82-0096, from the U.S. Defence Nuclear Agency under DNA Contract 001-85-0368, and the Defence Research Establishment Suffield (DRES), is acknowledged with thanks.

Summary

A finite-difference method is used to investigate compressible, laminar boundary-layer flows of a dilute dusty gas over a semi-infinite flat plate. Details are given of the implicit finite-difference schemes as well as the boundary conditions, initial conditions and compatibility conditions for solving the gas-particle boundary-layer equations. The flow profiles for both the gas and particle phases were obtained numerically along the whole length of the plate from the leading edge to far downstream of it. The finite-difference solutions in the large-slip region and the small-slip region are compared with the asymptotic solutions and good agreement is achieved. The boundary-layer characteristics of interest, including the wall shear stress, the wall heat-transfer rate and the displacement thickness, are calculated. The alteration of the flow properties owing to the presence of particles is discussed in detail. It was found that the boundary-layer flow of a dusty gas can be divided into three distinct flow regimes which are characterized by quasi-frozen, nonequilibrium and quasi-equilibrium flows and that at a critical distance from the leading edge the particle velocity at the wall decelerates to zero and near-equilibrium is achieved between the gas and particle flows. For the laminar boundary layer of a dusty gas, the shear stress and the heat-transfer at the wall are increased and the displacement thickness is decreased compared with the pure-gas case alone.

Contents

Notation

A_n^i	coefficients of the finite-difference equations, Eqs. (3.12)-(3.20) and (3.26)-(3.27)
a_n	grid parameters for the six-point difference scheme, Eq. (3.14)
a_T	coefficient for fitting a polynomial to the gas temperature near the wall, Eq. (5.11)
a_u	coefficient for fitting a polynomial to the gas velocity near the wall, Eq. (5.10)
B_n^i	coefficients of the finite-difference equations, Eqs. (3.12)-(3.20) and (3.26)-(3.27)
b_n	grid parameters for the six-point difference scheme, Eq. (3.14)
b_T	coefficient for fitting a polynomial to the gas temperature near the wall, Eq. (5.11)
b_u	coefficient for fitting a polynomial to the gas velocity near the wall, Eq. (5.10)
C_D	general drag coefficient for a sphere in a viscous fluid
C_{D_o}	Stokesian drag coefficient for a sphere in a viscous fluid
C_n^i	coefficients of the finite-difference equations, Eqs. (3.12)-(3.20) and (3.26)-(3.27)
c_n	grid parameters for the six-point difference scheme, Eq. (3.14)
c_p	specific heat at constant pressure for the gas phase
c_s	specific heat for the particle phase
c_T	coefficient for fitting a polynomial to the gas temperature near the wall, Eq. (5.11)
c_u	coefficient for fitting a polynomial to the gas velocity near the wall, Eq. (5.10)
D	normalized drag coefficient for a sphere in a viscous fluid

D_n^i	coefficients of the finite-difference equations, Eqs. (3.12)-(3.20) and (3.26)-(3.27)
d	diameter of the particles
d_n	grid parameters for the six-point difference scheme, Eq. (3.14)
d_T	coefficient for fitting a polynomial to the gas temperature near the wall, Eq. (5.11)
d_u	coefficient for fitting a polynomial to the gas velocity near the wall, Eq. (5.10)
Ec	gas Eckert number based on the freestream temperature, $Ec = u_\infty^{*2}/c_p^* T_\infty^*$
E_n^i	recurrence coefficients in the Thomas algorithm, Eq. (4.1)
F	integrated function of the nondimensional displacement thickness, Eq. (5.14)
F_n^i	recurrence coefficients in the Thomas algorithm, Eq. (4.1)
f	transformation function for the asymptotic solution
G_n^i	recurrence coefficients in the Thomas algorithm, Eq. (4.1)
K	ratio of consecutive step sizes in the y-direction, $K = \Delta y_n / \Delta y_{n-1}$
k	heat conductivity for the gas phase
m	grid line in the y-direction
N	grid point at the outer edge of the boundary layer
Nu	Nusselt number based on the particle diameter
n	grid line in the x-diretion
Pr	gas Prandtl number, $Pr = c_p^* \mu^* / k^*$
p	gas pressure
$\dot{q}$	heat-transfer rate
R	gas constant

Re_∞	flow Reynolds number based on the particle equilibrium length, $Re_\infty = \rho^*_\infty u^*_\infty \lambda^*_\infty / \mu^*_\infty$
T	temperature
u	tangential velocity in the x-direction
v	normal velocity in the y-direction
W	function representing any flow property, u, v, ρ or T
x	coordinate along the wall
y	coordinate normal to the wall

Greek Symbols

α	ratio of the specific heats for the two phases, $\alpha = c^*_p / c^*_s$
β	mass loading ratio of the particles in the freestream, $\beta = \rho^*_{p_\infty} / \rho^*_\infty$
δ	displacement thickness of the boundary layer
ε	small quantity used in testing for the outer edge of the boundary layer, Eq. (4.6)
η	similarity variable for the asymptotic solution
θ	weighting factor for the finite-difference schemes
λ^*_∞	particle velocity-equilibrium length, $\lambda^*_\infty = \rho^*_s d^{*2} u^*_\infty / 18 \mu^*_\infty$
μ	dynamic viscosity for the gas phase
μ'	derivative of the gas viscosity with respect to the gas temperature, $\mu' = d\mu/dT$
ρ	density
ρ_s	density of the particle material
τ	shear stress
ω	power index for the gas viscosity

Subscripts

asy	asymptotic solution

cri	critical point
m	grid line in the y-direction
n	grid line in the x-direction
p	particle
s	slip quantity
w	wall conditions
∞	freestream conditions
o	initial conditions

Superscripts

*	dimensional
i	index for dependent variables: i = 1, 2, 3, 4, 5, 6 represent u, T, u_p, v_p, T_p and ρ_p, respectively

PLATE 1: ILLUSTRATION OF A DUSTY-GAS BOUNDARY LAYER. THE PHOTOS SHOW THE AIR-SAND BOUNDARY-LAYER DEVELOPMENT STARTING FROM THE SHORE OF THE GULF OF AQUABA, JORDAN, AS VIEWED FROM EILAT, ISRAEL (PHOTOS BY I. I. GLASS).

1. INTRODUCTION

Boundary-layer flows of a dusty gas have been investigated using several analytical methods: a series method [1-7], an integral method [8-11], and a finite-difference method [12-15]. All the work mentioned above, however, dealt with incompressible-flow cases for the gas phase. Very few authors [16-18] considered the problems of compressible boundary-layer flows where the density of the gas phase can be changed due to compressibility. As pointed out by Singleton [17], Chiu [16] employed incorrect boundary-layer equations and assumed that the particle density is constant. Singleton extended Marble's analysis [1] to compressible boundary-layer flows. He applied the coordinate perturbation method and obtained asymptotic solutions for two limiting regions (see Fig. 1): for the large-slip (or quasi-frozen) region near the leading edge (I) and for the small-slip (or quasi-equilibrium) region far downstream of the leading edge (III). Zhao [18] used a similar series-expansion method and improved Singleton's analysis. However, these series solutions in the form of asymptotic expansions could provide only one term in addition to the frozen or equilibrium-flow values, owing to the complexity of the problem. Moreover, this solution does not provide any information on the boundary-layer development in the nonequilibrium transition region where the slip is moderate. A thorough understanding of the compressible dusty-gas boundary-layer over the entire-flow region is important, since these flows have practical applications in many scientific and technical fields such as solid rocket exhaust nozzles, nuclear reactors with gas-solid feeds, ablation cooling, blast waves moving over the Earth's surface, conveying of powdered materials, fluidized bed and environmental pollution, as mentioned in Refs. [12, 19].

In the present paper, the behaviour of compressible, laminar boundary-layer flows of a dusty gas over a semi-infinite flat plate along the whole length of the plate is studied using a finite-difference method. The problem of two-phase suspension flows is solved in the framework of a model of two interpenetrating and interacting continuous media, which is called a two-way coupling model or a two-fluid approach [20,21]. The following assumptions are made in this analysis: (1) The gas-particle mixture is a dilute system where the volume fraction of the particle phase is neglected. (2) The gas phase is a perfect gas. (3) The particles are spheres of uniform size without random kinetic motion. There are no mutual collisions or other interactions among the particles. (4) Only the drag and heat-transfer processes couple the particles to the gas. The momentum and energy exchange between the two phases can be calculated from available analytical solutions for the viscous flow field around a single sphere.

Finite-difference methods of solution of single-phase boundary-layer equations have been studied for many years. A review of this work is given in Ref. [22]. Flügge-Lotz and Blottner [23] developed an implicit difference technique. They used a six-point scheme for the momentum and energy equations and a four-point scheme for the continuity equation. This finite-difference procedure was applied successfully to various studies of

pure-gas boundary-layer flows. However, in the dusty-gas case, the nature of the governing equations requires some changes which result in considerable complexity. First, in addition to some new interaction terms in the conservation equations for the gas phase, there is an extra set of conservation equations for the particle phase. The partial differential equations for the gas phase are of second order, while those for the particle phase are of first order. Secondly, there is no correponding state equation for the particle phase, since the particle phase has no analog of flow pressure. In order to close the system of basic equations, the y-momentum equation for the particle phase cannot be omitted as for the gas phase. Finally, the flow properties of the particles present quite different features in different flow regions. In the near leading-edge region, very large velocity slip and temperature defect between the two phases appear, whereas a quasi-equilibrium state can be reached in the far-downstream region where the flow profiles for the two phases are almost the same. Between these two regions, there is a transition region which is characterized by a nonequilibrium flow. In general, the two phases in this region have moderate differences in velocity and temperature across the boundary layer. It is interesting to note that in the transition region, there exists a special position along the flat plate, which is defined as the critical point in this analysis. At the critical point, the tangential velocity of the particles at the wall vanishes, that is, there is no slip between the particles and the gas. This is due to the fact that in the two-phase boundary layer, the gas decelerates from its freestream velocity at the outer edge to zero at the wall and then the particles are retarded by the gas. The velocity of the particles at the wall may be reduced to zero provided the distance is long enough for the particles to adjust to the gas. Of course, equalization of the gas and particle velocities at the wall does not mean that the disparity of the two phases has died out because across the boundary layer, equilibrium between the particles and the gas is still not attained. Nevertheless, it can be said that at the critical point, the two-phase system completes essentially the transition from a nonequilibrium flow to an equilibrium flow, since the equilibrium state is reached first on the surface of the plate and this process is continued until the two phases are in equilibrium across the whole boundary layer far downstream. As the particles are slowed down, the density of the particle phase near the wall increases. When the particle velocity becomes zero, the particles tend to accumulate at the wall. In other words, deposition of the particles at the wall may occur if there is no diffusion. Therefore, as discussed by Soo [24,25], there are two possible situations when the particle velocity decelerates to near zero:

(1) For large particles, their Brownian motion is neglected, the particles slowed down at the wall will deposit and form a sliding layer (or bed of particles). This compacted layer may build up or erode away, and even a steady equilibrium condition may be achieved when the shear stresses in this dense layer of the particulate matter and in the suspension mixture are equalized. The velocity at which such a layer moves depends on the materials and surfaces of the particles and the wall. Because of deposition of the particle phase, the density of the particles at the

wall becomes very large. However, if the particle density is too high, the present analysis will fail since the assumptions concerning the interactions between the two phases or among the particles in this paper can be considered correct just for a dilute gas-particle system.

(2) For small particles, the Brownian diffusion is significant in the region near the wall, although the intensity of Brownian motion of the particulate cloud is usually small across the boundary layer. The density of the particle phase at the wall is then controlled by the Brownian diffusion process. The layer of deposited particles may not exist at all because the diffusion due to the Brownian motion prevents the formation of a dense bed of particles. It is shown in Soo's analyses that, if the Schmidt number of the particle Brownian diffusion is of order unity or less, the whole two-phase system behaves like a gaseous mixture and the density profiles for the particle phase reduces to its original one as in the freestream. Soo studied only the incompressible boundary-layer case. Marble [1,26] treated the case of compressible flows and obtained a similar result. Some other studies [17,18] on the compressible boundary-layer flow of a gas-particle mixture came to the same conclusion. From the asymptotic solution for the small-slip limit, it is found that the zeroth-order approximation of the dimensionless density for the particle phase is the same as that for the gas phase. This means that the loading ratio of the particles is constant across the boundary layer and equal to its original value in the freestream. Physically, in this quasi-equilibrium flow region, the particles always remain attached or fixed to their original gas mass and move together with the gas. Then the gas-particle mixture behaves like a perfect gas with the modified properties. This implies that the flow process in the small-slip region is mainly diffusion-controlled for both the gas and particles. Therefore, in this paper, it is assumed that, after the critical point, the particle density is determined from the gas density and the loading ratio. Using these considerations, the finite-difference schemes for the dusty-gas boundary-layer flows can be constructed. In this analysis, the finite-difference scheme developed by Flügge-Lotz and Blottner [22,23] were employed for the gas phase. For the particle phase, a four-point scheme was used. For comparison, the six-point scheme was used to solve the x-momentum and energy equations of the particles, employing additional boundary conditions obtained from the compatibility conditions. After the critical point, very simple compatibility conditions for the tangential velocity and temperature of the particles can be derived: at the wall, the particles have the same velocity and temperature as the gas.

With this finite-difference scheme, the flow properties of the dusty-gas boundary layer over the entire length of a semi-infinite flat-plate were calculated numerically. The flow profiles of u, v and T for the two phases are presented at different distances from the leading edge. From these results, it is shown that the boundary-layer flows of a dusty gas have different characteristics in the three distinct regions. In the large-slip

region, the particles have a little deviation from their freestream uniform motion and then the differences in the flow quantities of the two phases are quite large. While slipping through the gas downstream, interaction between the two phases increases the gas velocity and temperature but decreases the particle velocity and temperature as well. Thus, in the transition region, the differences in the flow properties of the two phases are significantly reduced. Of course, the particles and the gas are still in nonequilibrium. In this region, the velocity slip and temperature defect are moderate compared with those in the other two limiting regions. In the small-slip region far downstream, the flow profiles for the particle phase become almost identical with those for the gas phase, that is, the two phases approach nearly equilibrium and the slip quantities are very small. In fact, the only reason the particles do not actually attain the local gas velocity and temperature is that slip is induced along the gas streamlines by the gas retardation associated with thickening of the gas boundary layer. In addition to the flow profiles of u, v and T, some boundary-layer characteristic quantities of interest, i.e., the shear stress and heat-transfer rate at the wall and the displacement thickness, are calculated in this analysis. It is noted that owing to the presence of the particles, the shear stress and heat transfer increase while the displacement thickness decreases in the case of laminar boundary-layer flows, since the interaction between the gas and particles causes an increase in the gas velocity and temperature.

In this paper, the quasi-frozen flow properties in the near leading-edge region and the quasi-equilibrium flow properties in the far-downstream region were compared with the corresponding asymptotic values [27]. The agreement was very good. For the finite-difference solution in the nonequilibrium transition region, it is found that the results are physically reasonable. Although it is not possible at present to make any direct comparison between our finite-difference solution and other relevant results, since there are no experimental or other analytical data available for the nonequilibrium-flow region. Nevertheless, the fact that the finite-difference solution in the far-downstream region agrees quite well with the asymptotic small-slip solution provides confidence in the difference solution for this transition region, since the boundary-layer equations are parabolic, which is classified as a marching problem [30]. Thus, the solution procedure of finite difference begins with certain initial profiles at or near the leading edge, then through the large-slip region, the transition region, and finally ends in the small-slip region downstream. It is clear that the finite-difference solution for the small-slip region would not be correct if there were some mistakes in the difference solution for the transition region.

The numerical study of boundary-layer flows in dusty gases provides a good introduction to the dynamics of a two-phase system. The quasi-frozen flow, nonequilibrium flow and quasi-equilibrium flow are all encountered and analysed using the finite-difference method. The difference solution gives the complete and exact information about modifications of the boundary-layer

flows due to gas-particle interaction. Moreover, it provides a basis for the experimental investigation of dusty-gas boundary-layer flows.

2. MATHEMATICAL DESCRIPTION OF COMPRESSIBLE, LAMINAR, DUSTY-GAS BOUNDARY-LAYER FLOWS

The basic boundary-layer equations for steady, two-dimensional, compressible, laminar, dusty-gas flows over a flat plate are given by [27]

Continuity:

$$\frac{\partial}{\partial x^*}\,\rho^* u^* + \frac{\partial}{\partial y^*}\,\rho^* v^* = 0 \tag{2.1}$$

Momentum:

$$\rho^*\left(u^*\,\frac{\partial u^*}{\partial x^*} + v^*\,\frac{\partial u^*}{\partial y^*}\right) = \frac{\partial}{\partial y^*}\left(\mu^*\,\frac{\partial u^*}{\partial y^*}\right) + \rho_p^*(u_p^* - u^*)\,\frac{u_\infty^*}{\lambda_\infty^*}\,\frac{\mu^*}{\mu_\infty^*}\,D \tag{2.2}$$

Energy:

$$\rho^* c_p^*\left(u^*\,\frac{\partial T^*}{\partial x^*} + v^*\,\frac{\partial T^*}{\partial y^*}\right) = \frac{\partial}{\partial y^*}\left(k^*\,\frac{\partial T^*}{\partial y^*}\right) + \mu^*\left(\frac{\partial u^*}{\partial y^*}\right)^2 + \rho_p^*\left[(u_p^* - u^*)^2\right.$$

$$\left. + (v_p^* - v^*)^2\right]\,\frac{u_\infty^*}{\lambda_\infty^*}\,\frac{\mu^*}{\mu_\infty^*}\,D + \frac{1}{3Pr}\,\rho_p^* c_p^*(T_p^* - T^*)\,\frac{u_\infty^*}{\lambda_\infty^*}\,\frac{\mu^*}{\mu_\infty^*}\,Nu \tag{2.3}$$

State:

$$p^* = \rho^* R^* T^* \tag{2.4}$$

for the gas phase, and

Continuity:

$$\frac{\partial}{\partial x^*}\,\rho_p^*\,u_p^* + \frac{\partial}{\partial y^*}\,\rho_p^*\,v_p^* = C \tag{2.5}$$

x-momentum:

$$\rho_p^*\left(u_p^*\,\frac{\partial u_p^*}{\partial x^*} + v_p^*\,\frac{\partial u_p^*}{\partial y^*}\right) = -\rho_p^*(u_p^* - u^*)\,\frac{u_\infty^*}{\lambda_\infty^*}\,\frac{\mu^*}{\mu_\infty^*}\,D \tag{2.6}$$

y-momentum:

$$\rho_p^*\left(u_p^*\,\frac{\partial v_p^*}{\partial x^*} + v_p^*\,\frac{\partial v_p^*}{\partial y^*}\right) = -\rho_p^*(v_p^* - v^*)\,\frac{u_\infty^*}{\lambda_\infty^*}\,\frac{\mu^*}{\mu_\infty^*}\,D \tag{2.7}$$

Energy:

$$\rho_p^* c_s^* \left(u_p^* \frac{\partial T_p^*}{\partial x^*} + v_p^* \frac{\partial T_p^*}{\partial y^*}\right) = -\frac{1}{3Pr} \rho_p^* c_p^* (T_p^* - T^*) \frac{u_\infty^*}{\lambda_\infty^*} \frac{\mu^*}{\mu_\infty^*} Nu \qquad (2.8)$$

for the particle phase. In the equations above, the particle velocity-equilibrium length λ_∞^* is

$$\lambda_\infty^* = \frac{\rho_s^* d^{*2}}{18\mu_\infty^*} u_\infty^*$$

The starred quantities in Eqs. (2.1)-(2.8) have dimensions. The independent variables are the space coordinates x* and y* which are parallel and perpendicular to the wall, respectively. The dependent variables are the density ρ^*, the velocity components u* and v* and the temperature T* for the gas phase as well as the corresponding quantities ρ_p^*, u_p^*, v_p^* and T_p^* for the particle phase. For the flat-plate boundary layer, the gas pressure p* is constant and equal to its freestream value. Hence, in the dusty-gas boundary-layer problem, there are eight simultaneous equations with eight unknowns so that this system is closed. Of course, it is required that the other physical quantities appearing in Eqs. (2.1)-(2.8) are known functions of the flow variables. The normalized drag coefficient D and the Nusselt number Nu can be expressed in terms of the slip Reynolds number and the Prandtl number. Here, the normalized drag coefficient D is defined as

$$D = \frac{C_D}{C_{D_0}} \qquad (2.9)$$

where C_D and C_{D_0} are the real drag coefficient for the flow situation under consideration and the drag coefficient from the Stokes relation. In this analysis, only Stokes' relation is used and consequently D = 1.0 and Nu = 2.0. Regarding the thermodynamic properties, the following assumptions are made: (1) The specific heats for the gas and particle phases (c_p^* and c_s^*) are constant; (2) the Prandtl number of the gas (Pr) is constant; (3) the viscosity coefficient of the gas (μ^*) has a power-law form with temperature. Consequently, the expression for the gas viscosity is given by

$$\mu^* = \mu_\infty^* \left(\frac{T^*}{T_\infty^*}\right)^\omega \qquad (2.10)$$

where ω is the power index for the viscosity coefficient.

It is advantageous to write the basic equations and relative expressions in nondimensional form before the numerical computations are performed. For the investigation of two-phase boundary-layer flows, it is convenient to choose the velocity-equilibrium length λ_∞^* as the characteristic length, and the following nondimensional quantities are defined,

$$x = \frac{x^*}{\lambda_\infty^*}, \qquad y = \frac{y^*}{\lambda_\infty^*}\sqrt{Re_\infty},$$

$$u = \frac{u^*}{u_\infty^*}, \qquad v = \frac{v^*}{u_\infty^*}\sqrt{Re_\infty}, \qquad \rho = \frac{\rho^*}{\rho_\infty^*}, \qquad T = \frac{T^*}{T_\infty^*} \tag{2.11}$$

$$u_p = \frac{u_p^*}{u_\infty^*}, \qquad v_p = \frac{v_p^*}{u_\infty^*}\sqrt{Re_\infty}, \qquad \rho_p = \frac{\rho_p^*}{\rho_\infty^*}, \qquad T_p = \frac{T_p^*}{T_\infty^*},$$

$$\mu = \frac{\mu^*}{\mu_\infty^*}$$

where the flow Reynolds number based on the particle velocity-equilibrium length Re_∞ is

$$Re_\infty = \frac{\rho_\infty^* u_\infty^* \lambda_\infty^*}{\mu_\infty^*}$$

Now, a nondimensional form of the boundary-layer equations results in

$$\frac{\partial}{\partial x}\rho u + \frac{\partial}{\partial y}\rho v = 0 \tag{2.12}$$

$$\rho\left(u\frac{\partial u}{\partial x} + v\frac{\partial u}{\partial y}\right) = \mu\frac{\partial^2 u}{\partial y^2} + \left(\frac{d\mu}{dT}\cdot\frac{\partial T}{\partial y}\right)\frac{\partial u}{\partial y} + \rho_p(u_p - u)\mu D \tag{2.13}$$

$$\rho\left(u\frac{\partial T}{\partial x} + v\frac{\partial T}{\partial y}\right) = \frac{\mu}{Pr}\frac{\partial^2 T}{\partial y^2} + \frac{1}{Pr}\frac{d\mu}{dT}\left(\frac{\partial T}{\partial y}\right)^2 + Ec\,\mu\left(\frac{\partial u}{\partial y}\right)^2 + Ec\,\rho_p\left[(u_p - u)^2\right.$$

$$\left. + \frac{1}{Re_\infty}(v_p - v)^2\right]\mu D + \frac{1}{3Pr}\rho_p(T_p - T)\mu Nu \tag{2.14}$$

$$\rho = \frac{1}{T} \tag{2.15}$$

$$\frac{\partial}{\partial x}\rho_p u_p + \frac{\partial}{\partial y}\rho_p v_p = 0 \tag{2.16}$$

$$u_p \frac{\partial u_p}{\partial x} + v_p \frac{\partial u_p}{\partial y} = -(u_p - u)\mu D \tag{2.17}$$

$$u_p \frac{\partial v_p}{\partial x} + v_p \frac{\partial v_p}{\partial y} = -(v_p - v)\mu D \tag{2.18}$$

$$u_p \frac{\partial T_p}{\partial x} + v_p \frac{\partial T_p}{\partial y} = -\frac{\alpha}{3Pr}(T_p - T)\mu Nu \tag{2.19}$$

where the gas Eckert number Ec, the gas Prandtl number Pr and the ratio of specific heats for the two phases α are respectively defined as

$$Ec = \frac{u_\infty^{*2}}{c_p^* T_\infty^*}, \qquad Pr = \frac{c_p^* \mu^*}{k^*}, \qquad \alpha = \frac{c_p^*}{c_s^*}$$

The viscosity relation in nondimensional form can be written as

$$\mu = T^\omega \tag{2.20}$$

In order to obtain a unique solution to the problem, it is necessary to satisfy the boundary conditions. Inspecting the basic equations (2.12)-(2.19), there are seven partial differential equations and two of them are of second order. Therefore, nine boundary conditions should be specified. If the partcle phase is in equilibrium with the gas phase in the external flow, the nondimensional boundary conditions are given by:

(1) At the wall of the flat plate

$$u(x, 0) = 0, \qquad v(x, 0) = 0, \qquad T(x, 0) = T_w, \qquad v_p(x,0) = 0 \tag{2.21}$$

(2) At the outer edge of the boundary layer

$$u(x, \infty) = 1, \qquad T(x, \infty) = 1,$$
$$u_p(x, \infty) = 1, \qquad T_p(x, \infty) = 1, \qquad \rho_p(x, \infty) = \beta \tag{2.22}$$

where the mass loading ratio of the particles β is

$$\beta = \frac{\rho_{p_\infty}^*}{\rho_\infty^*}$$

Besides, owing to the parabolic character of boundary-layer equations, the initial profiles of the dependent variables are required across the boundary layer at some point x_0:

$$\begin{aligned} u(x_0, y) &= u_0(y), & v(x_0, y) &= v_0(y) \\ T(x_0, y) &= T_0(y), & \rho(x_0, y) &= \rho_0(y) \\ u_p(x_0, y) &= u_{p_0}(y), & v_p(x_0, y) &= v_{p_0}(y) \\ T_p(x_0, y) &= T_{p_0}(y), & \rho_p(x_0, y) &= \rho_{p_0}(y) \end{aligned} \tag{2.23}$$

At the initial position x_0, the finite-difference solution procedure starts and then proceeds downstream.

3. FINITE-DIFFERENCE SCHEMES AND RESULTING FINITE-DIFFERENCE EQUATIONS

The basic boundary-layer equations (2.12)-(2.19) with the boundary conditions (2.21)-(2.22) and the initial conditions (2.23) can be solved numerically using a finite-difference method. In this way, the partial differential equations are approximated by finite-difference equations and the flow field is divided into a rectangular grid or mesh. Generally, either equal or unequal intervals can be used. In this report, equal intervals in the x-direction and unequal intervals in the y-direction were used in order to reduce the computation time (see Fig. 2). The step size in the y-direction was increased in a geometric progression as

$$\frac{\Delta y_n}{\Delta y_{n-1}} = K$$

where K is a constant and it is set with a value slightly greater than unity. When K = 1.0, the unequal-interval mesh reduces to an equal-interval mesh. In the difference procedure, it is assumed that the flow quantities are known at the grid points in the column (m) and unknown at the grid points in the column (m+1). The computation starts stepwise downstream with the initial profiles.

When the finite-difference scheme is employed, the derivatives are replaced by difference quotients. There are numerous ways of constructing difference quotients. For the sake of stability, implicit schemes, which can be six-point or four-point, are used in this analysis [28].

For the momentum and energy equations of the gas phase, a six-point difference scheme was used. With this scheme, six grid points (m, n-1), (m, n), (m, n+1), (m+1, n-1), (m+1, n) and (m+1, n+1) are involved. Any function w(x, y) and its derivatives are evaluated at a mid-point (m+θ, n):

$$W = \theta W_{m+1,n} + (1-\theta) W_{m,n} \tag{3.1}$$

$$\frac{\partial W}{\partial x} = \frac{1}{\Delta x} (W_{m+1,n} - W_{m,n}) \tag{3.2}$$

$$\frac{\partial W}{\partial y} = \frac{\theta}{(K+1)\Delta y_n} [W_{m+1,n+1} + (K^2-1)W_{m+1,n} - K^2 W_{m+1,n-1}]$$

$$+ \frac{1-\theta}{(K+1)\Delta y_n} [W_{m,n+1} + (K^2-1)W_{m,n} - K^2 W_{m,n-1}] \tag{3.3}$$

$$\frac{\partial^2 W}{\partial y^2} = \frac{2\theta K}{(K+1)\Delta y_n^2} [W_{m+1,n+1} - (K+1)W_{m+1,n} + KW_{m+1,n-1}]$$

$$+ \frac{2(1-\theta)K}{(K+1)\Delta y_n^2} [W_{m,n+1} - (K+1)W_{m,n} + KW_{m,n-1}] \tag{3.4}$$

where the weighting factor θ can be chosen as any value between zero and unity. When $\theta = 0.5$, it reduces to the six-point Crank-Nicolson scheme where the truncation error is of order (Δx^2) [29]. When θ takes the value of zero or unity, it gives the full explicit or implicit scheme, respectively. The last two schemes involve only four grid points and have a truncation error of order (Δx). But with respect to the variable y, all three schemes above are of second order (Δy^2), since the central difference formula is used for derivatives in the y-direction.

A four-point difference scheme is applied to the gas continuity equation. In this scheme, four grid points (m, n-1), (m, n), (m+1, n-1) and (m+1, n) are included and all the values of the function w(x, y) and its derivatives are calculated at a mid-point (m+θ, n - 1/2):

$$W = \frac{1}{2} [\theta(W_{m+1,n} + W_{m+1,n-1}) + (1-\theta)(W_{m,n} + W_{m,n-1})] \tag{3.5}$$

$$\frac{\partial W}{\partial x} = \frac{1}{2\Delta x} [(W_{m+1,n} - W_{m,n}) + (W_{m+1,n-1} - W_{m,n-1})] \tag{3.6}$$

$$\frac{\partial W}{\partial y} = \frac{\theta}{\Delta y_{n-1}} (W_{m+1,n} - W_{m+1,n-1}) + \frac{1-\theta}{\Delta y_{n-1}} (W_{m,n} - W_{m,n-1}) \tag{3.7}$$

When $\theta = 0$ or $\theta = 1$ in the above formulae, the truncation error in the x-direction is of order (Δx). When $\theta = 0.5$, the scheme is known as the four-point Wendroff scheme and the truncation error in the x-direction is of second order (Δx^2) [29]. However, from experience in the present analysis, the Wendroff scheme may produce an oscillation in the normal velocity of the

gas phase. It was found that this oscillation problem can be avoided by using $\theta = 0.75$, which produces a discretization error of order $(\Delta x^{1.5})$. In the y-direction, this four-point scheme has a truncation error of order (Δy^2) as in the six-point scheme.

For the particle phase, due to the stability requirement, the y-derivatives are approximated by backward difference quotients instead of the central difference quotients which are used in the above schemes for the gas. Then, another four-point difference scheme for the particles is constructed as follows. The function $w(x, y)$ and its derivatives are estimated at the point $(m+\theta, n)$. The derivatives, both in the x- and y-directions, are replaced by backward quotients.

For the x-momentum, energy and continuity equations of the particles, the grid points (m, n), (m, n+1), (m+1, n) and (m+1, n+1) are involved and the difference scheme is

$$W = \theta W_{m+1,n} + (1-\theta) W_{m,n} \tag{3.8}$$

$$\frac{\partial W}{\partial x} = \frac{1}{\Delta x} (W_{m+1,n} - W_{m,n}) \tag{3.9}$$

$$\frac{\partial W}{\partial y} = \frac{\theta}{\Delta y_n} (W_{m+1,n+1} - W_{m+1,n}) + \frac{1-\theta}{\Delta y_n} (W_{m,n+1} - W_{m,n}) \tag{3.10}$$

For the y-momentum equation, the grid points (m, n), (m, n-1), (m+1, n) and (m+1, n-1) are involved and the difference scheme takes another form for the y-derivative instead of Eq. (3.10)

$$\frac{\partial W}{\partial y} = \frac{\theta}{\Delta y_{n-1}} (W_{m+1,n} - W_{m+1,n-1}) + \frac{1-\theta}{\Delta y_{n-1}} (W_{m,n} - W_{m,n-1}) \tag{3.11}$$

The function w and the x-derivative $\partial W/\partial x$ have the same forms as Eqs. (3.8) and (3.9).

Similarly, when θ is equal to zero or unity, which represents, respectively, the explicit or implicit scheme, the above four-point schemes (3.8)-(3.11) reduce to three-point schemes. These schemes have a truncation error of first order (Δy). For stability consideration, as mentioned before, the value of θ is chosen to be 0.75.

With the above formulae, the finite-difference equations for compressible, laminar boundary-layer flows of a dusty gas over a semi-infinite flat plate are given by:

(1) The momentum equation of gas phase,

$$A_n^1 u_{m+1,n+1} + B_n^1 u_{m+1,n} + C_n^1 u_{m+1,n-1} = D_n^1 \qquad (n = 2, 3, \ldots N-1) \tag{3.12}$$

where

$$A_n^1 = a_n(\rho v - \mu' T_y)_{m+\theta,n} - c_n \mu_{m+\theta,n}$$

$$B_n^1 = (\rho u)_{m+\theta,n} + a_n(K^2-1)(\rho v - \mu' T_y)_{m+\theta,n} + c_n(K+1)\mu_{m+\theta,n}$$

$$+ \theta\Delta x(\rho_p \mu D)_{m+1,n}$$

$$C_n^1 = -a_n K^2(\rho v - \mu' T_y)_{m+\theta,n} - c_n K \mu_{m+\theta,n}$$

$$D_n^1 = [(\rho u)_{m+\theta,n} - (1-\theta)\Delta x(\rho_p \mu D)_{m,n}]u_{m,n} - b_n(\rho v - \mu' T_y)_{m+\theta,n}\Delta u_{m,n}$$

$$+ d_n \mu_{m+\theta,n}\Delta^2 u_{m,n} + \Delta x(\rho_p u_p \mu D)_{m+\theta,n}$$

(2) The energy equation of gas phase,

$$A_n^2 T_{m+1,n+1} + B_n^2 T_{m+1,n} + C_n^2 T_{m+1,n-1} = D_n^2 \qquad (n = 2, 3, \ldots N-1) \quad (3.13)$$

where

$$A_n^2 = a_n\left(\rho v - \frac{\mu'}{Pr} T_y\right)_{m+\theta,n} - c_n\left(\frac{\mu}{Pr}\right)_{m+\theta,n}$$

$$B_n^2 = (\rho u)_{m+\theta,n} + a_n(K^2-1)\left(\rho v - \frac{\mu'}{Pr} T_y\right)_{m+\theta,n} + c_n(K+1)\left(\frac{\mu}{Pr}\right)_{m+\theta,n}$$

$$+ \theta\Delta x\left(\frac{1}{3Pr}\rho_p \mu Nu\right)_{m+1,n}$$

$$C_n^2 = -a_n K^2\left(\rho v - \frac{\mu'}{Pr} T_y\right)_{m+\theta,n} - c_n K\left(\frac{\mu}{Pr}\right)_{m+\theta,n}$$

$$D_n^2 = \left[(\rho u)_{m+\theta,n} - (1-\theta)\Delta x\left(\frac{1}{3Pr}\rho_p \mu Nu\right)_{m,n}\right]T_{m,n}$$

$$- b_n\left(\rho v - \frac{\mu'}{Pr} T_y\right)_{m+\theta,n} \Delta T_{m,n} + d_n\left(\frac{\mu}{Pr}\right)_{m+\theta,n}\Delta^2 T_{m,n}$$

$$+ \Delta x\left\{Ec\,\mu(u_y)^2 + Ec\,\rho_p\left[(u_p - u)^2 + \frac{1}{Re_\infty}(v_p - v)^2\right]\mu D + \frac{1}{3Pr}\rho_p T_p \mu Nu\right\}_{m+\theta,n}$$

For the coefficient D_n^2, the term $(v_p - v)^2/Re_\infty$ is a small quantity and can be neglected. In all the above coefficient expressions, some parameters are given by

$$a_n = \frac{\theta \Delta x}{(K+1)\Delta y_n}, \qquad b_n = \frac{(1-\theta)\Delta x}{(K+1)\Delta y_n}$$

$$c_n = \frac{2\theta K \Delta x}{(K+1)\Delta y_n^2}, \qquad d_n = \frac{2(1-\theta)K\Delta x}{(K+1)\Delta y_n^2}$$

$$\Delta W_{m,n} = W_{m,n+1} + (K^2-1)W_{m,n} - K^2 W_{m,n-1} \tag{3.14}$$

$$\Delta^2 W_{m,n} = W_{m,n+1} - (K+1)W_{m,n} + KW_{m,n-1}$$

$$(W_y)_{m,n} = \frac{W_{m,n+1} + (K^2-1)W_{m,n} - K^2 W_{m,n-1}}{(K+1)\Delta y_n}$$

where the function W represents the flow properties such as velocity, temperature, density, etc.

(3) The state equation of the gas phase:

$$\rho_{m+1,n} = \frac{1}{T_{m+1,n}} \qquad (n = 1, 2, \ldots, N) \tag{3.15}$$

(4) The continuity equation of the gas phase:

$$(\rho v)_{m+1,n} = (\rho v)_{m+1,n-1} - \frac{1-\theta}{\theta}\left[(\rho v)_{m,n} - (\rho v)_{m,n-1}\right]$$

$$- \frac{\Delta y_{n-1}}{2\theta \Delta x}\left[(\rho u)_{m+1,n} - (\rho u)_{m,n} + (\rho u)_{m+1,n-1} - (\rho u)_{m,n-1}\right] \qquad (n = 2, 3, \ldots N) \tag{3.16}$$

(5) The x-momentum equation of the particle phase:

$$A_n^3 u_{p_{m+1,n+1}} + B_n^3 u_{p_{m+1,n}} = C_n^3 \qquad (n = 1, 2, \ldots N-1) \tag{3.17}$$

where

$$A_n^3 = \frac{\theta\Delta x}{\Delta y_n} v_{\rho_{m+\theta,n}}$$

$$B_n^3 = u_{\rho_{m+\theta,n}} - \frac{\theta\Delta x}{\Delta y_n} v_{\rho_{m+\theta,n}} + \theta\Delta x(\mu D)_{m+1,n}$$

$$C_n^3 = -\left[\frac{(1-\theta)\Delta x}{\Delta y_n} v_{\rho_{m+\theta,n}}\right] u_{\rho_{m,n+1}} + \left[u_{\rho_{m+\theta,n}} + \frac{(1-\theta)\Delta x}{\Delta y_n} v_{\rho_{m+\theta,n}}\right.$$

$$\left. - (1-\theta)\Delta x(\mu D)_{m,n}\right] u_{\rho_{m,n}} + \Delta x(u\mu D)_{m+\theta,n}$$

(6) The y-momentum equation of the particle phase,

$$A_n^4 v_{\rho_{m+1,n}} + B_n^4 v_{\rho_{m+1,n-1}} = C_n^4 \qquad (n = 2, 3, \ldots, N) \qquad (3.18)$$

where

$$A_n^4 = u_{\rho_{m+\theta,n}} + \frac{\theta\Delta x}{\Delta y_{n-1}} v_{\rho_{m+\theta,n}} + \theta\Delta x(\mu D)_{m+1,n}$$

$$B_n^4 = -\frac{\theta\Delta x}{\Delta y_{n-1}} v_{\rho_{m+\theta,n}}$$

$$C_n^4 = \left[u_{\rho_{m+\theta,n}} - \frac{(1-\theta)\Delta x}{\Delta y_{n-1}} v_{\rho_{m+\theta,n}} - (1-\theta)\Delta x(\mu D)_{m,n}\right] v_{\rho_{m,n}}$$

$$+ \left[\frac{(1-\theta)\Delta x}{\Delta y_{n-1}} v_{\rho_{m+\theta,n}}\right] v_{\rho_{m,n-1}} + \Delta x(v\mu D)_{m+\theta,n}$$

(7) The energy equation of the particle phase,

$$A_n^5 T_{\rho_{m+1,n+1}} + B_n^5 T_{\rho_{m+1,n}} = C_n^5 \qquad (n = 1, 2, \ldots, N-1) \qquad (3.19)$$

where

$$A_n^5 = \frac{\theta\Delta x}{\Delta y_n} v_{p_{m+\theta,n}}$$

$$B_n^5 = u_{p_{m+\theta,n}} - \frac{\theta\Delta x}{\Delta y_n} v_{p_{m+\theta,n}} + \theta\Delta x \left(\frac{\alpha}{3Pr} \mu Nu\right)_{m+1,n}$$

$$C_n^5 = -\left[\frac{(1-\theta)\Delta x}{\Delta y_n} v_{p_{m+\theta,n}}\right] T_{p_{m,n+1}} + \left[u_{p_{m+\theta,n}} + \frac{(1-\theta)\Delta x}{\Delta y_n} v_{p_{m+\theta,n}}\right.$$

$$\left. - (1-\theta)\Delta x \left(\frac{\alpha}{3Pr} \mu Nu\right)_{m,n}\right] T_{p_{m,n}} + \Delta x \left(\frac{\alpha}{3Pr} T\mu Nu\right)_{m+\theta,n}$$

(8) The continuity equation of the particle phase,

$$A_n^6 \rho_{p_{m+1,n+1}} + B_n^6 \rho_{p_{m+1,n}} = C_n^6 \qquad (n = 1, 2, \ldots, N-1) \qquad (3.20)$$

where

$$A_n^6 = \frac{\theta\Delta x}{\Delta y_n} v_{p_{m+\theta,n}}$$

$$B_n^6 = 2\theta u_{p_{m+1,n}} + (1-2\theta) u_{p_{m,n}} + \frac{\theta^2\Delta x}{\Delta y_n} \left(v_{p_{m+1,n+1}} - 2v_{p_{m+1,n}}\right)$$

$$+ \frac{\theta(1-\theta)\Delta x}{\Delta y_n} \left(v_{p_{m,n+1}} - 2v_{p_{m,n}}\right)$$

$$C_n^6 = -\left[\frac{(1-\theta)\Delta x}{\Delta y_n} v_{p_{m+\theta,n}}\right] \rho_{p_{m,n+1}} + \left[(2\theta-1) u_{p_{m+1,n}} + 2(1-\theta) u_{p_{m,n}}\right.$$

$$\left. - \frac{\theta(1-\theta)\Delta x}{\Delta y_n} \left(v_{p_{m+1,n+1}} - 2v_{p_{m+1,n}}\right) - \frac{(1-\theta)^2\Delta x}{\Delta y_n} \left(v_{p_{m,n+1}} - 2v_{p_{m,n}}\right)\right] \rho_{p_{m,n}}$$

Using the finite-difference equations in the form (3.12)-(3.20), a stable and convergent numerical solution to the dusty-gas boundary-layer equations was obtained when x is smaller than x_{cri}. After the critical point ($x > x_{cri}$), quite simple compatibility conditions were derived for the particle velocity and temperature. These conditions provided supplemental boundary conditions at the wall so that the six-point scheme could be used for the x-momentum and energy equations of the particles when $x > x_{cri}$. At

the wall ($y = 0$), with the boundary conditions $u = 0$ and $v_p = 0$, Eqs. (2.17) and (2.19) become

$$\frac{u_{p_w}}{\partial x} = -(\mu D)_w \tag{3.21}$$

$$u_{p_w} \frac{\partial T_{p_w}}{\partial y} = -\frac{\alpha}{3Pr}(T_{p_w} - T_w)(\mu Nu)_w \tag{3.22}$$

These two equations, Eqs. (3.21) and (3.22), are termed as compatibility equations from which compatibility conditions can be derived. From Eq. (3.21), it is known that, as x increases, the particle velocity at the wall decreases until it becomes zero. The position of the critical point is determined by

$$u_{p_w}(x_{cri}) = 0 \tag{3.23}$$

After the critical point ($x > x_{cri}$), the two phases have zero velocity at the wall and then the drag vanishes ($D_w = 0$). Thus, for $x > x_{cri}$, Eq. (3.21) leads to

$$u_{p_w} = 0 \tag{3.24}$$

Substituting Eq. (3.24) into Eq. (3.22) yields

$$T_{p_w} = T_w \tag{3.25}$$

Equation (3.25) is valid for $x > x_{cri}$, too. Equations (3.24) and (3.25) mean that after the critical point the particles and gas are in equilibrium at the wall. Now, concerning the tangential velocity and temperature of the particles, there exist two boundary conditions: one is at the wall and the other is at the outer edge of the boundary layer, as in the case of the gas phase. For the normal velocity, however, no such simple compatibility conditions, such as Eqs. (3.24) and (3.25), can be derived.

With the six-point scheme, the x-momentum and energy equations of the particle phase are replaced by the following difference equations:

(1) Momentum:

$$A_n^7 u_{p_{m+1,n+1}} + B_n^7 u_{p_{m+1,n}} + C_n^7 u_{p_{m+1,n-1}} = D_n^7 \qquad (n = 2, 3, \ldots, N-1) \tag{3.26}$$

where

$$A_n^7 = a_n v_{\rho_{m+\theta,n}}$$

$$B_n^7 = u_{p_{m+\theta,n}} + a_n(K^2-1)v_{p_{m+\theta,n}} + \theta\Delta x(\mu D)_{m+1,n}$$

$$C_n^7 = -a_n K^2 v_{p_{m+\theta,n}}$$

$$D_n^7 = [u_{p_{m+\theta,n}} - (1-\theta)\Delta x(\mu D)_{m,n}]u_{p_{m,n}} - b_n v_{p_{m+\theta,n}} \Delta u_{p_{m,n}} + \Delta x(u\mu D)_{m+\theta,n}$$

(2) Energy:

$$A_n^8 T_{p_{m+1,n+1}} + B_n^8 T_{p_{m+1,n}} + C_n^8 T_{p_{m+1,n-1}} = D_n^8 \qquad (n = 2, 3, \ldots, N-1) \tag{3.27}$$

where

$$A_n^8 = a_n v_{p_{m+\theta,n}}$$

$$B_n^8 = u_{p_{m+\theta,n}} + a_n(K^2-1)v_{p_{m+\theta,n}} + \theta\Delta x\left(\frac{\alpha}{3Pr}\,\mu Nu\right)_{m+1,n}$$

$$C_n^8 = -a_n K^2 v_{p_{m+\theta,n}}$$

$$D_n^8 = [u_{p_{m+\theta,n}} - (1-\theta)\Delta x\left(\frac{\alpha}{3Pr}\,\mu Nu\right)_{m,n}]T_{p_{m,n}} - b_n v_{p_{m+\theta,n}} \Delta T_{p_m} + \Delta x\left(\frac{\alpha}{3Pr}\,T\mu Nu\right)_{m+\theta,n}$$

Therefore, when $x > x_{cri}$, the difference equations are composed of Eqs. (3.12), (3.13), (3.15), (3.16), (3.18), (3.26) and (3.27) with the assumption that the particle density is determined by $\rho_p = \beta\rho$. The detailed derivations of all the finite-difference equations above are given in Appendices A and B.

It is noted that the boundary-layer equations (2.12)-(2.19) are a coupled nonlinear partial-differential system. To avoid the coupling and nonlinearity, in the process of discretizing every conservation equation, only one corresponding variable appears as an unknown in the resulting difference equation and the difference expressions for the products of the unknown variables, functions or derivatives are chosen such that the unknown variables appear linearly in the products. This procedure leads to a linear system of algebraic equations which are not coupled. As pointed out by Blottner [22] the coupling between the equations results in a tridiagonal matrix which is somewhat more complicated to solve than in the uncoupled case. In addition, for linear algebraic equations, there are several effective methods of solution available. For example, the Thomas algorithm is a very powerful and convenient technique to solve the linear equations with the tridiagonal matrix of the coefficients.

4. METHODS OF SOLUTION OF THE FINITE-DIFFERENCE EQUATIONS

The methods of solution depend upon the characters of the finite-difference equations. For the six-point scheme, the resulting difference equations constitute the system of simultaneous algebraic equations with a tridiagonal matrix of the coefficients. Advantage can be taken of this tridiagonal form of the coefficient matrix to solve the algebraic equations by use of the Thomas algorithm [30]. With the Thomas algorithm, the solution is obtained by

$$W^i_{m+1,n} = \frac{G^i_n - E^i_n W^i_{m+1,n+1}}{F^i_n} \tag{4.1}$$

where

$$E^i_n = A^i_n, \qquad F^i_n = B^i_n - C^i_n \frac{E^i_{n-1}}{F^i_{n-1}}, \qquad G^i_n = D^i_n - C^i_n \frac{G^i_{n-1}}{F^i_{n-1}}$$

The recurrence relation, Eq. (4.1), can be used to solve difference equations (3.12) and (3.13), or (3.26) and (3.27). Correspondingly, $W^1 = u$, $W^2 = T$, $W^7 = u_p$ and $W^8 = T_p$.

By using the following procedure, the flow profiles can be determined:

(1) With the boundary conditions at the wall, calculate quantities E^i_n, F^i_n, G^i_n from the wall towards the outer edge.

(2) With the boundary conditions at the outer edge, calculate the flow properties W^i_n from the outer edge towards the wall.

After the gas temperature $T_{m+1,n}$ is known, the gas density $\rho_{m+1,n}$ can be calculated directly from the state equation (3.15). Then, starting at the wall and using the gas continuity equation (3.16), the normal velocity $v_{m+1,n}$ can be obtained.

When $x < x_{cri}$, the differential equations for the particle phase are discretized using the four-point difference schemes. The methods for solving the difference equations (3.17) to (3.20) are not difficult. After starting either at the wall (only for the y-momentum equation) or at the outer edge of the boundary layer, the calculations proceed consecutively from one grid point to another in recursion, until the whole boundary layer has been traversed:

$$W^i_{m+1,n} = \frac{C^i_n - A^i_n W^i_{m+1,n+1}}{B^i_n} \qquad (i = 3, 5, 6) \tag{4.2}$$

$$W^{i}_{m+1,n} = \frac{C^{i}_{n} - B^{i}_{n} W^{i}_{m+1,n-1}}{A^{i}_{n}} \qquad (i = 4) \qquad (4.3)$$

where $W^3 = u_p$, $W^4 = v_p$, $W^5 = T_p$ and $W^6 = \rho_p$. After the critical point ($x > x_{cri}$), the x-momentum and energy equations of the particle phase can be discretized with the six-point scheme and then solved by the Thomas algorithm, as for the gas phase.

Before solving the difference equations numerically using the methods described above, some considerations are required:

(1) How to evaluate the coefficient matrix elements;

(2) How to give the boundary conditions in a form suitable for the numerical computation;

(3) How to obtain the initial profiles;

(4) How to determine the value of x_{cri}, the nondimensional coordinate for the critical point.

First, the finite-difference equations can be solved provided that the values of all the coefficients A^i_n, B^i_n, C^i_n and D^i_n are known. However, from the expressions of these coefficients, it is seen that they depend on unknown values of the variables at the grid line $(m + 1)$, since the difference scheme is an implicit one. This difficulty can be surmounted by using an iteration procedure. Of course, the iteration technique increases the computation time very much. The other way to overcome the difficulty is to use a linearization approximation: the quantities appearing in the coefficients are evaluated at the previous grid line (m) if these quantities are still unknown at the grid line (m + 1). Otherwise, they take on their updated values. In this analysis, this linearization approach was employed, since it is easier to program and requires less computer storage. Of course, it is less accurate compared with the iteration approach. However, satisfactory accuracy can be achieved by reducing the step size.

Second, in order to solve the system of simultaneous algebraic equations at every new grid line $(m + 1)$, it is necessary to have the boundary conditions in a suitable form. In this analysis this is straightforward, since there are no derivatives involved in the boundary conditions of the Dirichlet type. In the finite-difference scheme, the boundary conditions at the wall, Eq. (2.21), are written as

$$u_{m+1,1} = 0, \quad v_{m+1,1} = 0, \quad T_{m+1,n} = T_w, \quad v_{p_{m+1,1}} = 0 \qquad (4.4)$$

Similarly, the boundary conditions at the outer edge, Eq. (2.22), are given in the form,

$$u_{m+1,N} = 1, \qquad T_{m+1,N} = 1$$

$$u_{p_{m+1,N}} = 1, \qquad T_{p_{m+1,N}} = 1, \qquad \rho_{p_{m+1,N}} = \beta \tag{4.5}$$

Here, concerning the outer-edge boundary conditions, another difficulty arises: How to select the number N, the maximum value for the number of grid points at the column (m+1). In other words, in the computation process, it is required to know how far to calculate the flow variables across the boundary layer. In order to guarantee that the value of N used represents the freestream condition, one can specify a large number N_{max} for the grid points at the last grid line (m_{max}) far downstream, where the computation terminates. For all the previous grid lines ($0 < m < m_{max}$), the same number N_{max} is used to define the outer edge of the boundary layer. This method is direct but inefficient, since it needs more computation time. There is another approach in which a special value of N is chosen for a given grid line (m). In the latter method, N is determined as follows [31]:

(1) It is assumed that N_{m+1} at the new grid line (m + 1) is equal to N_m, the number of grid points at the previous line (m).

(2) The finite-difference equations are solved with the assumed N_{m+1} and the values of the flow quantities at the last two consecutive grid points, $W_{m+1,N-1}$ and $W_{m+1,N}$, can be found.

(3) The difference between $W_{m+1,N-1}$ and $W_{m+1,N}$ is compared with a certain small quantity ε. If the condition of smooth conjugation

$$|W_{m+1,N} - W_{m+1,N-1}| < \varepsilon \tag{4.6}$$

is satisfied, the selection of N_{m+1} is correct and the computation can proceed to the next step.

(4) If the condition (4.6) is not fulfilled, it is required to assume $N_{m+1} = N_m + 1$ and then to obtain the new values of $W_{m+1,N-1}$ and $W_{m+1,N}$. If the condition (4.6) is not fulfilled again, it is necessary to increase N_{m+1} with unity, and so forth, until the smooth-conjugation condition is satisfied. With this method, the number of grid points across the boundary layer varies as the thickness of the boundary layer increases.

Next, in order to initiate the computation, the initial flow profiles must be given. In most pure-gas boundary-layer studies, the initial profiles are obtained from similarity solutions. For dusty-gas boundary-layer flows, however, no analogous similarity solutions exist. In previous work on finite-difference solutions for incompressible dusty-gas boundary-layer equations, the initial profiles were specified in two ways:

(1) The Blasius similarity profiles were chosen for the gas phase and uniform profiles for the particle phase [14].

(2) The initial profiles were obtained by using an integral method [13, 15].

It is well known that all the integral methods for boundary-layer analysis do not attempt to satisfy the basic equations at every point; instead, they guess or assume a suitable expression for the velocity and temperature profiles and satisfy the boundary-layer equations only on an average extended over the thickness of the boundary layer. In general, the initial profiles obtained from integral methods are quite approximate. From the studies of the behaviour of dusty-gas boundary-layer flows near the leading edge [17, 18, 27], it is also known that the similarity profiles for the gas phase and the uniform profiles for the particle phase are the zeroth-order approximation in the large-slip region. The zeroth-order asymptotic profiles are physically reasonable and were tested in this analysis. More accurate initial profiles up to the first order can be obtained from the asymptotic large-slip solution to the compressible laminar boundary-layer equations for the gas-particle flow over a semi-infinite flat plate by using a series-expansion method [27]. Thus, it is suggested here to employ the first-order asymptotic solution as the initial profiles. However, in this approach, it is required to obtain the asymptotic solution first and then to solve the difference equations starting at a given initial position which may be very near the leading edge but cannot be exactly at the leading edge, since the asymptotic solution involves a singularity at the leading edge. Wu [32] once proposed the following type of initial profiles at the leading edge in pure-gas cases:

(1) The tangential velocity u^* and temperature T^* have their freestream values at all the grid points across the boundary layer except at the wall.

(2) At the wall, the tangential velocity u_w^* is zero and the temperature T_w^* corresponds to the wall temperature.

(3) The normal velocity v^* is assumed zero at all the grid points.

Clearly, this method is very advantageous for starting numerical computation without any preliminary calculations of initial profiles. Flügge-Lotz and Blottner [23] studied the possibility of using the Wu-type initial profiles in pure-gas boundary-layer cases and concluded that the Wu-type of initial profiles can give reasonable results if the proper mesh sizes are chosen. In the dusty-gas case, similar initial profiles can be set up by using Wu-type profiles for the gas phase and uniform profiles for the particle phase. Soo [24] applied such initial profiles to his analysis of incompressible, laminar boundary-layer flow of a dilute particulate suspension. The profiles are termed here as the extended Wu-type. In this report, the above three different types, i.e., the first-order

asymptotic-type, the zeroth-order asymptotic-type and the extended Wu-type, were used respectively as the initial profiles in order to compare them.

As mentioned before, the asymptotic types of initial profiles can be obtained from the large-slip solution [27]. However, because of the different notations, certain relations must be established with the asymptotic large-slip solution as follows:

$$x = (x)_{asy}, \qquad y = (\sqrt{2x}\ \eta)_{asy}$$

$$u = (u)_{asy}, \qquad v = \left(\frac{1}{\sqrt{2x}}\ (\eta u - f)\right)_{asy}, \qquad T = (T)_{asy}, \qquad \rho = (\rho)_{asy} \tag{4.7}$$

$$u_p = \left(\frac{1}{\rho_p}\ \frac{\partial f_p}{\partial \eta}\right)_{asy}, \qquad v_p = -\left(\frac{\sqrt{2x}}{\rho_p}\ \left(\frac{\partial f_p}{\partial x} + \frac{f_p}{2x} - \frac{\eta}{2x}\ \frac{\partial f_p}{\partial \eta}\right)\right)_{asy}$$

$$T_p = (T_p)_{asy}, \qquad \rho_p = \beta(\rho_p)_{asy}$$

Similarly, a set of relations can be written for connecting the finite-difference solution with the asymptotic small-slip solution. In this analysis, nondimensional slip quantities for the particle phase are defined as

$$u_s = u_p - u, \qquad v_s = v_p - v, \qquad T_s = T_p - T \tag{4.8}$$

The corresponding relations are

$$x = (x)_{asy}, \qquad y = \frac{1}{\sqrt{1+\beta}}\ (\sqrt{2x}\ \eta)_{asy} \tag{4.9}$$

$$u_s = (u_s)_{asy}, \qquad v_s = \frac{1}{\sqrt{1+\beta}}\ \left(\frac{v_s}{\sqrt{2x}}\right)_{asy}, \qquad T_s = (T_s)_{asy}$$

These expressions are useful when comparing the finite-difference solution with the asymptotic small-slip solution. In Eqs. (4.7) and (4.9), the subscript 'asy' denotes the asymptotic solution.

Finally, as pointed out earlier, after the critical point ($x > x_{cri}$), it is assumed that the particle density is equal to the gas density times the mass loading ratio of the particles. It is equivalent to assume that there is no accumulation of particles on the surface of the plate and the flow is then mainly diffusion-controlled for the particle phase as well as for the

gas phase. In addition, after the critical point, quite simple compatibility conditions (3.24) and (3.25) are valid. The value of x_{cri} can be determined from the compatibility equation (3.21) and the condition (3.23). Equation (3.21) is an ordinary differential equation and the solution $u_{p_w}(x)$ can be obtained numerically or analytically. For instance, in the case of the Stokes relation (D = 1.0), Eq. (3.21) can be integrated analytically as

$$u_{p_w}(x) = 1 - \mu_w x \tag{4.10}$$

where $u_{p_w}(0) = 1$ is taken as the initial condition at x = 0. From the condition $u_{p_w}(x_{cri}) = 0$, Eq. (3.23), the critical value x_{cri} can be determined, say, for the Stokes case

$$x_{cri} = \frac{1}{\mu_w} \tag{4.11}$$

when $T_w = 0.5$ and $\omega = 0.5$, $x_{cri} = \sqrt{2}$ or $x^*_{cri} = \sqrt{2}\,\lambda^*_\infty$. If $\rho^*_s = 2.5$ g/cm^3, $d^* = 10$ μm, $T^*_\infty = 300$ K (or $\mu^*_\infty = 1.80\times10^{-5}$ NS/m^2) and $u^*_\infty = 500$ m/S, the typical values of relaxation parameters are obtained as: $\lambda^*_\infty = 0.386$m and $x^*_{cri} = 0.546$ m.

5. RELATIONS FOR SHEAR STRESS, HEAT TRANSFER, AND DISPLACEMENT THICKNESS

Once the gas flow profiles across the boundary layer are determined, some boundary-layer characteristics of practical interest can be calculated. The important quantities describing the behaviour of boundary-layer flows are shear stress at the wall, heat-transfer rate at the wall and displacement thickness. They are given in dimensional form as

(1) Shear stress at the wall:

$$\tau^*_w = \mu^*_w \left(\frac{\partial u^*}{\partial y^*}\right)_w \tag{5.1}$$

(2) Heat-transfer rate at the wall:

$$\dot{q}^*_w = -k^*_w \left(\frac{\partial T^*}{\partial y^*}\right)_w \tag{5.2}$$

(3) Displacement thickness:

$$\delta^* = \int_0^\infty \left(1 - \frac{\rho^* u^*}{\rho^*_\infty u^*_\infty}\right) dy^* \tag{5.3}$$

The corresponding nondimensional characteristic quantities are defined as

$$\tau_w = \frac{\tau_w^*}{\rho_\infty^* u_\infty^{*2}} \sqrt{Re_\infty} \tag{5.4}$$

$$\dot{q}_w = \frac{\dot{q}_w^*}{\rho_\infty^* u_\infty^{*3}} \sqrt{Re_\infty} \tag{5.5}$$

$$\delta = \frac{\delta^*}{\lambda_\infty^*} \sqrt{Re_\infty} \tag{5.6}$$

Substituting the nondimensional transformations (2.11) into the expressions (5.1)-(5.3), the nondimensional boundary-layer characteristics, Eqs. (5.4)-(5.6), can be written as

$$\tau_w = \mu_w \left(\frac{\partial u}{\partial y}\right)_w \tag{5.7}$$

$$\dot{q}_w = - \frac{\mu_w}{Pr\ Ec} \left(\frac{\partial T}{\partial y}\right)_w \tag{5.8}$$

$$\delta = \int_0^\infty (1 - \rho u) dy \tag{5.9}$$

For numerical computations, it is necessary to express the above relations in finite-difference form. By means of polynomial fitting, the gas velocity u and temperature T near the wall may be expressed with sufficient accuracy as

$$u = a_u + b_u y + c_u y^2 + d_u y^3 \tag{5.10}$$

$$T = a_T + b_T y + c_T y^2 + d_T y^3 \tag{5.11}$$

Taking the derivatives of the above variables with respect to y and setting $y = 0$, the formulae for shear stress and heat-transfer rate at the wall are obtained as

$$\tau_w = \mu_w b_u, \qquad \dot{q}_w = - \frac{\mu_w}{Pr\ Ec} b_T$$

The values of b_u and b_T can be determined by evaluating Eqs. (5.10) and (5.11) at the four grid points nearest the wall and solving the resulting equations. Then the shear stress and heat-transfer rate can be given by the following expressions (see Appendix C):

$$\tau_w = \mu_w \frac{(K^2 + K + 1)}{K^2 \Delta y_1} \left[u_2 - \frac{u_3}{K(K+1)} + \frac{u_4}{K(K^2 + K + 1)^2}\right] \qquad (5.12)$$

$$\dot{q}_w = - \frac{\mu_w}{Pr\ Ec} \frac{(K^2 + K + 1)}{K^2 \Delta y_1} \left[(T_2 - T_1) - \frac{T_3 - T_1}{K(K+1)} + \frac{T_4 - T_1}{K(K^2 + K + 1)^2}\right] \qquad (5.13)$$

where the subscripts 1, 2, 3, 4 denote the four grid points nearest the wall and $u_1 = u_w = 0$, $T_1 = T_w$.

To calculate the nondimensional displacement thickness δ, a three-point difference formula of integration was used. The formula can be applied to a nonequidistant step size [33]

$$\delta = \sum_{2}^{N-1} \frac{\Delta y_{n-1}}{6} \left[\frac{3K + 2}{K + 1} F_{n-1} + \frac{3K + 1}{K} F_n - \frac{1}{K(K+1)} F_{n+1}\right] \qquad (5.14)$$

where $F = 1 - \rho u$, and the subscripts n-1, n and n+1 represent three consecutive grid points at a given section.

6. COMPUTER PROGRAM

The computer program FDBLEP for solving boundary-layer equations of a dusty gas over a semi-infinite flat plate was written in Fortran language on a Perkin-Elmer computer system at UTIAS (see Appendix D).

Only the main features of the calculation procedure will be reviewed here. A rectangular-grid system indicated in Fig. 2 was adopted, with the m-lines in the y-direction (i.e., normal to the plate) and the n-lines in the x-direction (i.e., parallel to the plate). The y-axis is designated as the initial line for the m-lines and the x-axis for the n-lines. In the finite-difference procedure, the flow profiles along some m-line (say, the initial line m = 0) are known and the flow parameters along the (m+1)-line have to be determined.

Given below are the main steps in the computation procedure:

(1) Compute $u_{m+1,n}$.

Using the known solution at the m-line (linearized conditions) and the boundary conditions on the (m+1)-line, the new tangential velocity of the gas at all the grid points of the (m+1) line, $u_{m+1,n}$, are calculated.

(2) Test for the outer edge of the boundary layer while computing u. After the boundary layer has been traversed, the two consecutive values of u, $u_{m+1,N-1}$ and $u_{m+1,N}$, are compared to see if the difference between them is less than some small positive number ε. The value of ε is determined by the desired accuracy of the computation.

(3) Compute $T_{m+1,n}$.

Using the new values of $u_{m+1,n}$ with the other linearized conditions, the new gas temperatures $T_{m+1,n}$ across the boundary layer are calculated.

(4) Compute $\rho_{m+1,n}$.

Using the new values of $T_{m+1,n}$, the new gas density profile is calculated directly.

(5) Compute $v_{m+1,n}$.

Using the new values of $u_{m+1,n}$ and $\rho_{m+1,n}$, the new normal velocity of the gas $v_{m+1,n}$ across the boundary layer are calculated.

(6) Compute $u_{p_{m+1,n}}$.

Using the new tangential velocity profile $u_{m+1,n}$ for the gas phase and the linearized velocity profiles $u_{p_{m,n}}$ and $v_{p_{m,n}}$ for the particle phase, the new tangential velocity profile of the particles is computed.

(7) Compute $v_{p_{m+1,n}}$.

Using the new values of $v_{m+1,n}$ and $u_{p_{m+1,n}}$ with the linearized values of $v_{p_{m,n}}$, the new normal velocity profile for the particle phase is computed.

(8) Compute $T_{p_{m+1,n}}$.

Using the new values of $u_{p_{m+1,n}}$, $v_{p_{m+1,n}}$ and $T_{m+1,n}$ with the values of T_p at the previous line (m), the new temperature profile for the particle phase is computed.

(9) Compute $\rho_{p_{m+1,n}}$.

Using the new values of $u_{p_{m+1,n}}$ and $v_{p_{m+1,n}}$ with the values of u_p, v_p, ρ_p at the previous line (m), the new particle density profile is computed. However, when $x > x_{cri}$, the new particle density profile can be obtained by setting $\rho_{p_{m+1,n}} = \beta\rho_{m+1,n}$.

(10) Compute τ_w.

Using the first four values of velocity for the gas phase nearest the wall, i.e., $u_{m+1,1}$, $u_{m+1,2}$, $u_{m+1,3}$ and $u_{m+1,4}$, the shear stress at the wall is calculated.

(11) Compute $\dot{q}_w$.

Using the values of gas temperature at the four grid points nearest the wall, i.e., $T_{m+1,1}$, $T_{m+1,2}$, $T_{m+1,3}$ and $T_{m+1,4}$, the heat-transfer rate at the wall is calculated.

(12) Compute δ.

Using the density and tangential velocity profiles for the gas phase, $\rho_{m+1,n}$ and $u_{m+1,n}$, the displacement thickness can be obtained by integration.

To advance the computation from the (m+1)-line to the (m+2)-line and so on, the same procedure (1)-(12) is repeated until the desired value of x is reached. The flow diagram for the basic computer program is shown in Fig. 3. It is noted that the order of solving the difference equations is important. The equations for the gas phase are solved first where the momentum and energy equations must be solved before the continuity equation. Then the equations for the particle phase are solved and the energy and continuity equations must be solved after the momentum equations.

7. NUMERICAL RESULTS AND DISCUSSIONS

The present finite-difference technique was used to solve the compressible, laminar boundary-layer flows of a dusty gas over a semi-infinite flat plate. The difference solutions for the three flow regions were obtained: the quasi-frozen flow region near the leading edge, the nonequilibrium flow region and the quasi-equilibrium flow region far downstream. The asymptotic solutions in the two limiting regions (the large-slip and small-slip regions, respectively) were also solved numerically in order to independently verify the validity of the present implicit finite-difference scheme when it is applied to a gas-particle mixture.

In this analysis, the following set of parameters was chosen so that the finite-difference results could be compared with the asymptotic solutions by Singleton [17]:

(1) The power index of the gas viscosity is equal to 0.5 ($\omega = 0.5$).

(2) The Prandtl number of the gas is equal to unity ($Pr = 1.0$).

(3) The Eckert number of the gas is equal to unity ($Ec = 1.0$).

(4) The ratio of specific heats for the two phases is equal to unity ($\alpha = 1.0$).

(5) The mass loading ratio of the particles is equal to unity ($\beta = 1.0$).

(6) Stokes' relation applies for the interaction between the two phases ($D = 1.0$ and $Nu = 2.0$).

(7) The nondimensional temperature at the wall is equal to 0.5 ($T_w = 0.5$).

The flow in the large-slip region was considered first. The initial profiles at $x_0 = 0.005$ were obtained from the first-order asymptotic solution. The computation proceeded from $x_0 = 0.005$ to $x = 0.505$ with mesh parameters $\Delta x = 0.001$, $\Delta y_1 = 0.01$ and $K = 1.05$. The flow profiles for the two phases at $x = 0.055$, 0.105 and 0.305 are plotted in Figs. 4 to 6. As these results show, there is a very large slip between the particles and the gas in this near-leading-edge region. Then the flow is quasi-frozen. This situation can be explained as follows. In the freestream, the gas and particles are in equilibrium, that is, they have the same tangential velocity and temperature while their normal velocity is equal to zero. At the leading edge, due to viscous effects, the tangential gas velocity decreases from its freestream value at the outer edge to zero at the wall and the gas temperature also changes from its freestream value at the outer edge to the wall temperature at the wall, whereas the normal gas velocity acquires quite a large value. The particles, however, cannot accommodate these rapid changes and tend to keep their original state of motion in the freestream. It takes some time for the particles to attain their equilibrium with the gas. The relaxation process of the particles occurs throughout the velocity-equilibrium length λ_∞^*. This two-phase slip phenomenon implies that the viscous relaxation length for the gas is much shorter than the relaxation length for the particles owing to the drag and heat-transfer interactions between the two phases. By comparing the finite-difference solution with the asymptotic solution in the large-slip limit, it is seen that excellent agreement is obtained when $x \leq 0.1$. Therefore, the asymptotic large-slip solution is valid when $x \leq 0.1$.

Next, the dusty-gas boundary-layer flow in the nonequilibrium region was studied. The first-order asymptotic profiles at $x_0 = 0.05$ were taken as the initial profiles. The grid parameters were $\Delta x = 0.001$, $\Delta y_1 = 0.03$ and $K = 1.05$. The flow profiles of the two phases at $x = 0.55$, 1.05, 2.05 and 5.05 are shown in Figs. 7 to 10, respectively. The numerical results indicate that the slip between the particles and the gas diminishes gradually as x increases. However, in this transition region, the particles still have moderate slip against the gas and then the two-phase flow is characterized by nonequilibrium. At the critical point ($x = x_{cri}$), the particles achieve equilibrium with the gas at the wall. After that point, the two phases are in a state of near-equilibrium. From the experience of this analysis, after the critical point, the four-point scheme for the particle continuity equation became unstable. It was necessary to seek an appropriate treatment of the particle density. As mentioned before, based on the fact that the gas-particle mixture acts like a perfect gas with the total density $(1+\beta)\rho^*$ in the small-slip limit, it is assumed that the particle phase has the local density $\rho_p^* = \beta\rho^*$, which means that the mass loading ratio of the particles

is constant across the boundary layer. Of course, this assumption concerning the particle density for $x > x_{cri}$ may cause some inaccuracy in the prediction of the flow properties in the nonequilibrium region since this density distribution represents the zeroth-order approximation in the small-slip limit. Fortunately, a near-equilibrium state between the two phases is essentially reached after the critical point, as the difference solutions show. The effect of the particle density on the flow properties takes place only through the interaction terms. Under the near-equilibrium condition, these interaction terms will become small of second order compared with the viscous terms. Therefore, this approximate treatment of the particle density is acceptable. It provides an approach to solve the dusty-gas boundary-layer flow in the region $x > x_{cri}$. More discussion about the particle density is given in Appendix E. In Figs. 7 to 10, it is also noted that the relaxation of the tangential velocities of the two phases is terminated effectively at about $x = 5.0$ as well as the temperatures. In contrast with tangential velocity, there is still an apparent difference between the normal velocities of the two phases up to $x \sim 20.0$. It seems to mean that the relaxation of v_p and v occurs over a greater length than that for u_p and u. In fact, the main reason is that only one mechanism, i.e., the interaction between the phases, acts in the relaxation process for u_p and u while two mechanisms, the interaction between the phases and the continuity requirement, both play an important role in the process for v_p and v.

For the finite-difference solution in the small-slip region, the computation was started at $x_o = 5.05$ and continued until $x = 20.05$. The initial profiles were obtained from the finite-difference solution in the nonequilibrium region. All the mesh parameters used in this calculation were the same as those in the transition region. The numerical results for $x = 10.05$, 15.05 and 20.05 are shown in Figs. 11 to 13. It is seen that the quasi-equilibrium state between the particles and the gas has already been reached. In Fig. 14, the particle slip quantities u_s, v_s and T_s obtained from the difference solution are compared with those from the asymptotic small-slip solution. There is very good agreement between these two solutions. The comparison between the finite-difference solution and the asymptotic series-expansion solution in the small-slip region indicates that the finite-difference scheme presented in this paper has proved to be a useful method for studying dusty-gas boundary-layer flows and that the asymptotic small-slip solution is valid when $x > 10$.

It is found from Figs. 4 to 13 that the tangential velocity of the particles in the boundary layer is always greater than that of the gas and it decreases monotonically from its freestream value to the value at equilibrium with the gas as one advances downstream from the leading edge. Regarding the normal velocity, however, the situation is a little different. Near the leading edge, the normal velocity of the particles is smaller than that of the gas, i.e., $v_p < v$. With increasing distance x, the normal velocity of the particles becomes greater than that of the gas, which happens first near the wall and then extends over the whole thickness of the boundary layer. However, with increasing x, say $x \simeq 20$, the normal

velocities of the particles and the gas reach an equilibrium value as for the tangential velocities. This difference can be explained as follows. The normal velocities for the two phases are equal to zero in the freestream and induced to some values in the boundary layer whereas the tangential velocities for the two phases are equal to the freestream value and decrease in the boundary layer. In the boundary layer, the gas tangential velocity at the wall vanishes and its distribution across the boundary layer is similar to the profile for the pure-gas case. At the leading edge, the particles tend to keep their motion in the freestream and consequently the particle tangential velocity is greater than the gas velocity. Then, owing to the slip between the two phases, a drag force arises and the particles decrease their tangential velocity while the gas increases its tangential velocity. Marching downstream, the difference between the tangential velocities for the two phases becomes smaller and smaller. With the particle slip velocity approaching zero, the drag exerted on the particles by the gas approaches zero as well. When the particle velocity becomes the same as that of the gas, the interaction between the particles and the gas disappears. Therefore, the particle tangential velocity may become nearly the same as the gas tangential velocity but it cannot be smaller than that. By contrast, after entering the boundary layer at the leading edge, the normal gas velocity is induced first to satisfy the continuity requirement and the normal velocity of the particles is then induced due to the drag force exerted by the gas. Of course, this induced velocity for the particles cannot be greater than that of the gas. However, in addition to the interaction between the two phases, the continuity requirement for the particle phase is another important factor which determines the changes in the normal velocity. Since the tangential particle velocity decreases in the x-direction, a normal velocity must be induced to ensure mass conservation. Thus, the normal particle velocity may exceed the normal gas velocity. Especially in the region near the wall, where the particle slip velocity is quite large, the retardation of the particles is considerable and it results in a rapid increase of the normal particle velocity. In the region far downstream, where the thickness of the boundary layer varies very slowly, the effect of the interaction between the two phases becomes predominant and the normal velocities of the two phases tend to approach each other like the tangential velocities.

The numerical results shown above were obtained with the six-point scheme for the x-momentum and energy equations for the particle phase after the critical point. Instead, if the four-point scheme is still employed for the particle x-momentum and energy equations after the critical point, regardless of the compatibility conditions, the corresponding results are shown in Figs. 15 to 17. It is found that some small oscillations appear in the particle temperature profiles in the near-equilibrium flow region, for example, at $x = 4.05$ and 6.05 (see Figs. 15 and 16). The reason is mainly that the four-point scheme has a first-order truncation error in the y-direction, $O(\Delta y)$, while the six-point scheme is of second order, $O(\Delta y^2)$. In other words, the latter is more accurate and it can lead to a better result. It is also interesting to note that these oscillations are bound and damp out as x increases. In Fig. 17 ($x = 10.05$), it is seen that these

oscillations disappear. It means that in the small-slip region ($x > 10$), both the six-point scheme and the four-point scheme can be used.

The finite-difference computations were made with the mass loading ratio $\beta = 0$, using the same difference scheme for the dusty-gas boundary layer. Obviously, the two-phase system of a gas-particle mixture reduces to a single-phase system of a pure gas when $\beta = 0$. The results for the case of $\beta = 0$ should be identical with the similarity solution for the pure-gas boundary-layer equations. With $\beta = 0$, the numerical results for the positions $x = 1.05$, 2.05, 5.05 and 8.05 are respectively shown in Figs. 18 to 21. They are compared with the similarity solution of a pure-gas boundary-layer flow under similar conditions. Excellent agreement between these two solutions is achieved along the whole plate. This comparison provides further strong evidence that the present finite-difference scheme is correct.

Once the flow profiles across the boundary layer are known, the boundary-layer characteristics can be calculated. The three nondimensional quantities τ_w, $\dot{q}_w$ and δ as functions of the distance x from the leading edge are shown in Fig. 22 to 24. It is found that the curves for the shear stress τ_w and the heat-transfer rate $\dot{q}_w$ are nearly identical except in the nonequilibrium region. This is attributed to the Reynolds analogy between the heat-transfer and the shear stress [34]. It is well known that for the boundary-layer flow of a pure gas on a flat plate, the profiles for the velocity and the temperature become completely analogous if the Prandtl number has the value of unity. For the dusty-gas boundary-layer flows over a flat plate, there is no similar relation available. As pointed out before, however, the gas-particle system behaves like a gaseous mixture in the two limiting regions: (1) In the large-slip limit near the leading edge, the two-phase system responds as if there were no particles. For this analysis, the Prandtl number of the gas is just assumed to be equal to unity so that the Reynolds analogy holds in the large-slip region, or more exactly, with zeroth-order accuracy. (2) In the small-slip limit far downstream, the two-phase system acts like a pure gas with modified thermodynamic properties. The modified Prandtl number $\overline{Pr}$ is given by [26]

$$\overline{Pr} = Pr \frac{1 + \beta/\alpha}{1 + \beta}$$

In the case under consideration in this paper, $\alpha = 1.0$ and $\beta = 1.0$. This yields $\overline{Pr} = Pr = 1.0$. Consequently, the Reynolds analogy also holds in the small-slip region with zeroth-order accuracy. In Figs. 22 to 24, it is interesting to note that along every curve for the characteristic quantities, there is an inflection point which corresponds to the critical point. This fact means that for the boundary-layer flows of a gas-particle mixture, some significant changes in the flow properties occur at the critical point. In fact, as mentioned before, at the critical point, the two-phase system accomplishes essentially the transition from the

nonequilibrium flow to equilibrium flow. In Figs. 22 to 24, the corresponding results for the pure gas without particles are shown for comparison. It is seen that the shear stress and heat-transfer rate at the wall increase and the displacement thickness decreases owing to the presence of particles. Owing to the interaction between the particles and the gas in the two-phase boundary layer, the tangential velocity and temperature of the gas phase increase except at the wall and at the outer edge, where the same boundary conditions hold as in the pure-gas case. Compared with the pure-gas boundary layer, the velocity and temperature profiles for the dusty-gas boundary layer have a steeper gradient at the wall and a more even gradient near the outer edge. It is clear that, as a result of these changes in the flow profiles, the shear stress and heat transfer increase while the displacement thickness decreases. The same conclusion was obtained from the asymptotic analysis [27].

Finite-difference calculations were also done with other types of initial profiles: the zeroth-order asymptotic profiles and the extended Wu-type profiles. In the previous computations of this analysis, only the first-order asymptotic profiles were applied. The numerical results for these three different types of initial profiles are compared in Figs. 25 to 30. The difference solution for the extended Wu-type initial profiles started at the leading edge ($x_0 = 0.0$) and the solutions for the two asymptotic profiles at $x_0 = 0.05$. Figures 25 to 27 give the flow profiles of the two phases at $x = 0.15$, 1.05 and 5.05, and Figs. 28 to 30 give the nondimensional boundary-layer characteristics. The results for the extended Wu-type profiles indicate that employing them as the initial conditions can result in physically reasonable solutions which agree very well with the solution for the first-order asymptotic profiles. The results for the zeroth-order asymptotic profiles show that using the zeroth-order asymptotic profiles as the initial conditions may cause some deviations in the flow properties in the quasi-frozen and nonequilibrium regions but not in the quasi-equilibrium region, especially for the normal velocity of the particles. The reason is that the zeroth-order asymptotic profiles assume a zero velocity for the normal particle velocity at some distance from the leading edge (say, $x_0 = 0.05$) and it leads to some errors. With increasing x along the flat-plate, these deviations are damped out and all the three initial profiles yield identical results. It should be pointed out that the possibility of using the extended Wu-type initial profiles leads to a significant simplification in the computation procedure, since it is not necessary to solve the asymptotic solution in the large-slip limit.

8. CONCLUDING REMARKS

The complete set of nonlinear partial-differential equations for compressible, laminar, boundary-layer flows of a dusty gas over a semi-infinite flat plate was solved using implicit finite-difference schemes. The numerical solutions for the three distinct flow regimes, the quasi-frozen, nonequilibrium and quasi-equilibrium regimes, were obtained for the case of the Stokes relation. The finite-difference results for the

two limiting cases of large slip and small slip are in good agreement with the corresponding asymptotic solutions. The numerical examples indicate that the present finite-difference method provides a useful technique for studying two-phase boundary-layer flows.

From this analysis, it is shown that in order to get a finite-difference solution along the entire flat-plate length with the present basic equations, it is important to deal realistically with the particle density after the critical point. The assumption that the gas-particle system is treated as a binary gas with the given mass ratio of the components (β) after the critical point represents a practical approach for the case where diffusion is the main controlling process in the region $x > x_{cri}$. It yields physically reasonable results.

For the x-momentum and energy equations of the particles, both four-point and six-point schemes can be used. The numerical computations indicate that the six-point scheme leads to better results especially in the nonequilibrium-flow region, since it has an accuracy of second order. When using the six-point scheme it is necessary to obtain the compatibility conditions as additional boundary conditions. Fortunately, the compatibility conditions for the tangential velocity and temperature of the particles are very simple after the critical point.

A comparative study of the three different initial profiles (the first-order asymptotic, zeroth-order asymptotic and extended Wu-type) indicates that all three types of initial profiles can be used for the finite-difference solution but the zeroth-order asymptotic profiles might cause some errors in the near leading-edge and transition regions. It is suggested that the extended Wu-type initial profiles can be used, since they lead to a significant simplification in the numerical procedure.

The numerical results presented in this report indicate that the effects of the particles on the boundary-layer flows are considerable and that the modification in the flow properties owing to the presence of particles includes an alteration of the flow profiles, an increase in the shear stress and heat transfer at the wall and a decrease in the displacement thickness. These are the major features found in compressible, laminar boundary-layer flows of a gas-particle mixture.

REFERENCES

[1] Marble, F. E., Dynamics of a Gas Containing Small Solid Particles. Combustion and Propulsion, 5th AGARD Colloquium, Pergamon Press, Oxford, 1963.

[2] Liu, J. T. C., Flow Induced by the Impulsive Motion of an Infinite Flat Plate in a Dusty Gas. Astronautica Acta, Vol. 13, No. 4, 1967, pp. 369-377.

[3] Stulov, V. P., Equations of Laminar Boundary Layer in a Two-Phase Medium. Fluid Dynamics, Vol. 14, No. 1, 1979, pp. 37-44.

[4] Zung, L. B., Flow Induced in Fluid Particle Suspension by an Infinite Rotating Disk. The Physics of Fluids, Vol. 12, No. 1, January 1969, pp. 18-23.

[5] Otterman, B. and Lee, S. L., Particulate Velocity and Concentration Profiles for Laminar Flow of a Suspension Over a Flat Plate. Heat Transfer and Fluid Mechanics Institute, Monterey, California, June 10-12, 1970, Proceedings, Stanford University Press, pp. 311-322.

[6] Lee, S. L. and Chan, W. K., Two-Phase Laminar Boundary Layer Along a Vertical Flat Wall. Hydrotransport, Vol. 2, 1972, A4.45-A4.58.

[7] DiGiovanni, P. R. and Lee, S. L., Impulsive Motion in a Particle-Fluid Suspension Including Particulate Volume, Density and Migration Effects. Journal of Applied Mechanics, Vol. 41, No. 1, 1974, pp. 35-41.

[8] Soo, S. L., Fluid Dynamics of Multiphase Systems. Blaisdell Publishing Company, Waltham, Massachusetts, 1967.

[9] Tabakoff, W. and Hamed, A., Analysis of Cascade Particle Gas Boundary Layer Flows with Pressure Gradient. AIAA Paper No. 72-87.

[10] Hamed, A. and Tabakoff, W., The Boundary Layer of Particulate Gas Flow. Zeitschrift fur Flugwissenchaften, Vol. 20, October 1972, p. 373.

[11] Jain, A. C. and Ghosh, A., Gas-Particulate Laminar Boundary Layer on a Flat Plate. Z. Flugwise Weltraumersch, Vol. 3, 1979, pp. 379-385.

[12] Hamed, A. and Tabakoff, W., Analysis of Nonequilibrium Particulate Flow. AIAA Paper No. 73-687.

[13] Prabha, S. and Jain, A. C., On the Use of Compatibility Conditions in the Solution of Gas Particulate Boundary Layer Equations. Applied Scientific Research, Vol. 36, No. 2, 1980, pp. 81-91.

[14] Osiptsov, A. N., Structure of the Laminar Boundary Layer of a Disperse Medium on a Flat Plate. Fluid Dynamics, Vol. 15, No. 4, 1980, pp. 512-517.

[15] Prabha, S. and Jain, A. C., On the Nature of Gas-Particulate Flow. 13th International Symposium on Space Technology and Science, Tokyo, Japan, June 28-July 3, 1982, pp. 517-522.

[16] Chiu, H. H., Boundary Layer Flow with Suspended Particles. Princeton University, Report 620, August 1962.

[17] Singleton, R. E., The Compressible Gas-Solid Particle Flow Over a Semi-Infinite Flat Plate. ZAMP, Vol. 16, No. 4, 1965, pp. 421-449.

[18] Zhao, G. Y., Compressible Gas-Solid Particle Boundary Layer Over a Semi-Infinite Flat Plate. Acta Mechanica Sinica, Vol. 16, No. 5, September 1984, pp. 434-442.

[19] Lee, S. L., Aspects of Suspension Shear Flows. Advances in Applied Mechanics, Vol. 22, 1982, pp. 1-65.

[20] Crowe, C. T., Review - Numerical Models for Dilute Gas-Particle Flows. ASME Journal of Fluids Engineering, Vol. 104, September 1982, pp. 297-303.

[21] Di Giacinto, M., Sabetta, F. and Piva, R., Two-Way Coupling Effects in Dilute Gas-Particle Flows. ASME Journal of Fluids Engineering, Vol. 104, September 1982, pp. 304-312.

[22] Blottner, F. G., Finite Difference Methods of Solution of the Boundary-Layer Equations. AIAA Journal, Vol. 8, No. 2, February 1970, pp. 193-205.

[23] Flügge-Lotz, I. and Blottner, F. G., Computation of the Compressible Laminar Boundary-Layer Flow Including Displacement-Thickness Interaction Using Finite-Difference Methods. TR131, January 1962, Division of Engineering Mechanics, Stanford University.

[24] Soo, S. L., Laminar and Separated Flow of a Particulate Suspension. Astronautica Acta, Vol. 11, No. 6, 1965, pp. 422-431.

[25] Soo, S. L., Non-Equilibrium Fluid Dynamics - Laminar Flow Over a Flat Plate. ZAMP, Vol. 19, 1968, pp. 545-563.

[26] Marble, F. E., Dynamics of Dusty Gases. Annual Review of Fluid Mechanics, Vol. 2, 1970, pp. 397-446.

[27] Wang, B. Y. and Glass, I. I., Asymptotic Solutions to Compressible Laminar Boundary-Layer Equations for the Dusty-Gas Flow Over a Semi-Infinite Flat Plate. UTIAS Report No. 310, 1986.

[28] Roache, P. J., Computational Fluid Dynamics. Hermosa Publishers, 1976.

[29] Mitchell, A. R., Computational Methods in Partial Differential Equations. John Wiley and Sons, Ltd., 1969.

[30] Anderson, D. A., Tannehill, J. C. and Pletcher, R. H., Computational Fluid Mechanics and Heat Transfer. Hemisphere Publishing Corporation, 1984.

[31] Brailovskaya, I. Y. and Chudov, L. A., The Solution of Boundary Layer Equations by the Difference Method. AD 409560, 1963.

[32] Wu, J. C., The Solution of Laminar Boundary-Layer Equations by the Finite Difference Method. Douglas Aircraft Company, Inc., Report No. SM-37484, June 1, 1960.

[33] Liu, W. S., Finite-Difference Solutions for Nonequilibrium Laminar Boundary Layers in Ionizing-Argon Flows. UTIAS Report No. 226, May 1979.

[34] Schlichting, H., Boundary-Layer Theory. McGraw-Hill Book Company, Seventh Edition, 1979.

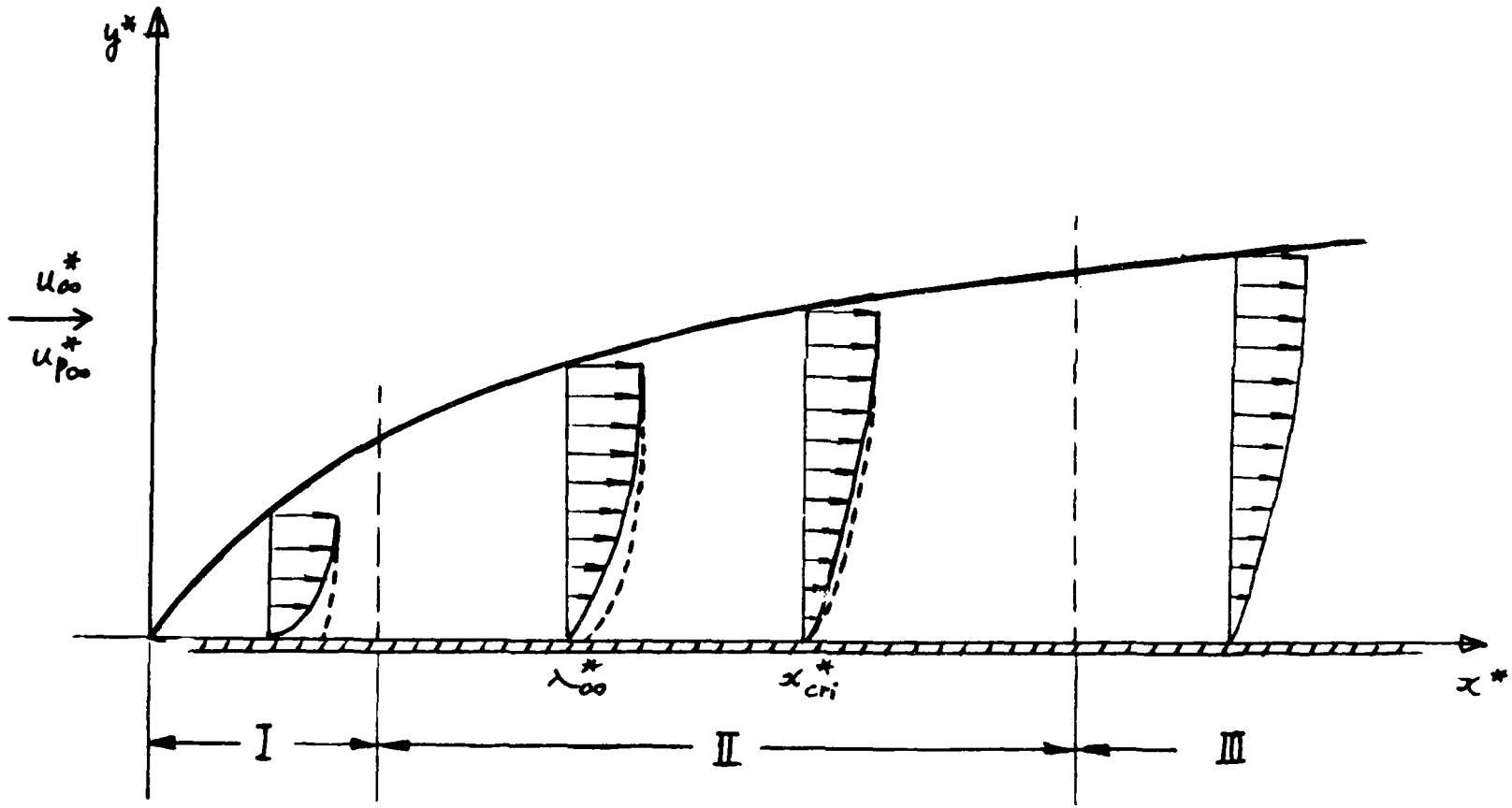

FIG. 1 SCHEMATIC DIAGRAM OF A DUSTY-GAS BOUNDARY-LAYER FLOW OVER A SEMI-INFINITE FLAT PLATE.

I: LARGE-SLIP REGION, II: MODERATE-SLIP REGION, III: SMALL-SLIP REGION.

——— GAS-VELOCITY PROFILE; ------ PARTICLE-VELOCITY PROFILE.

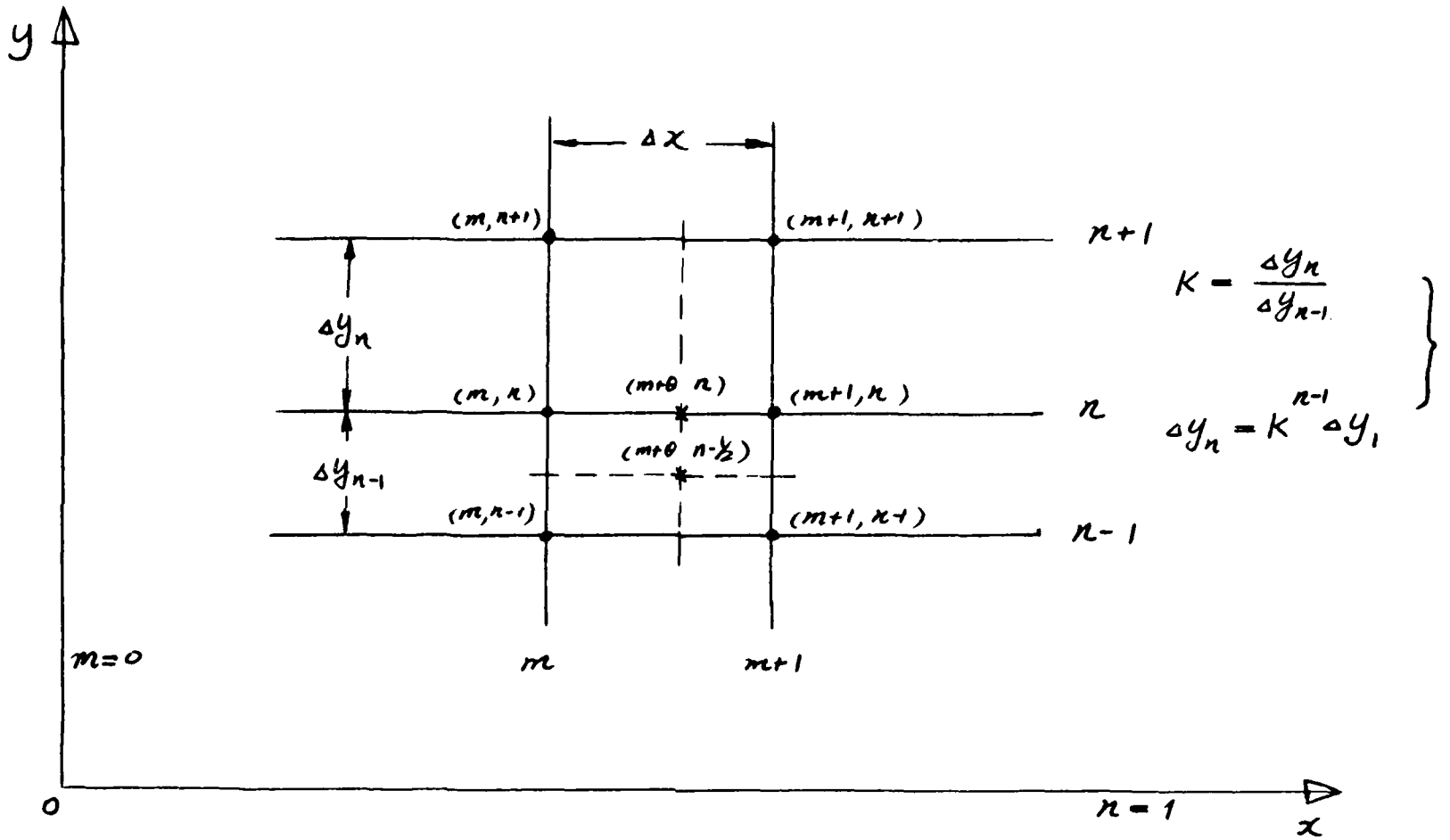

FIG. 2 GRID POINTS FOR FINITE-DIFFERENCE SCHEMES.

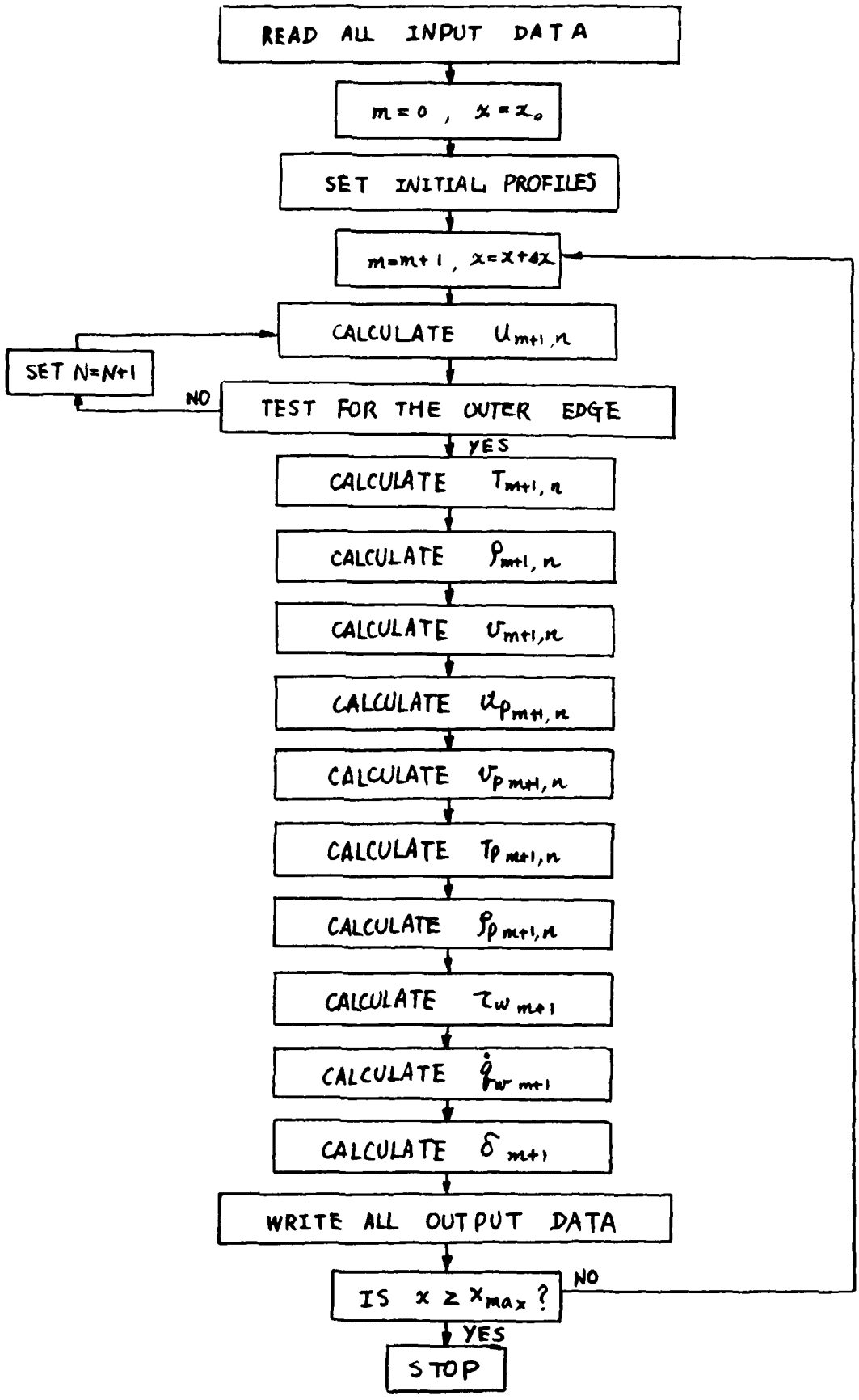

FIG. 3 FLOW CHART OF THE COMPUTER PROGRAM FDBLEP.

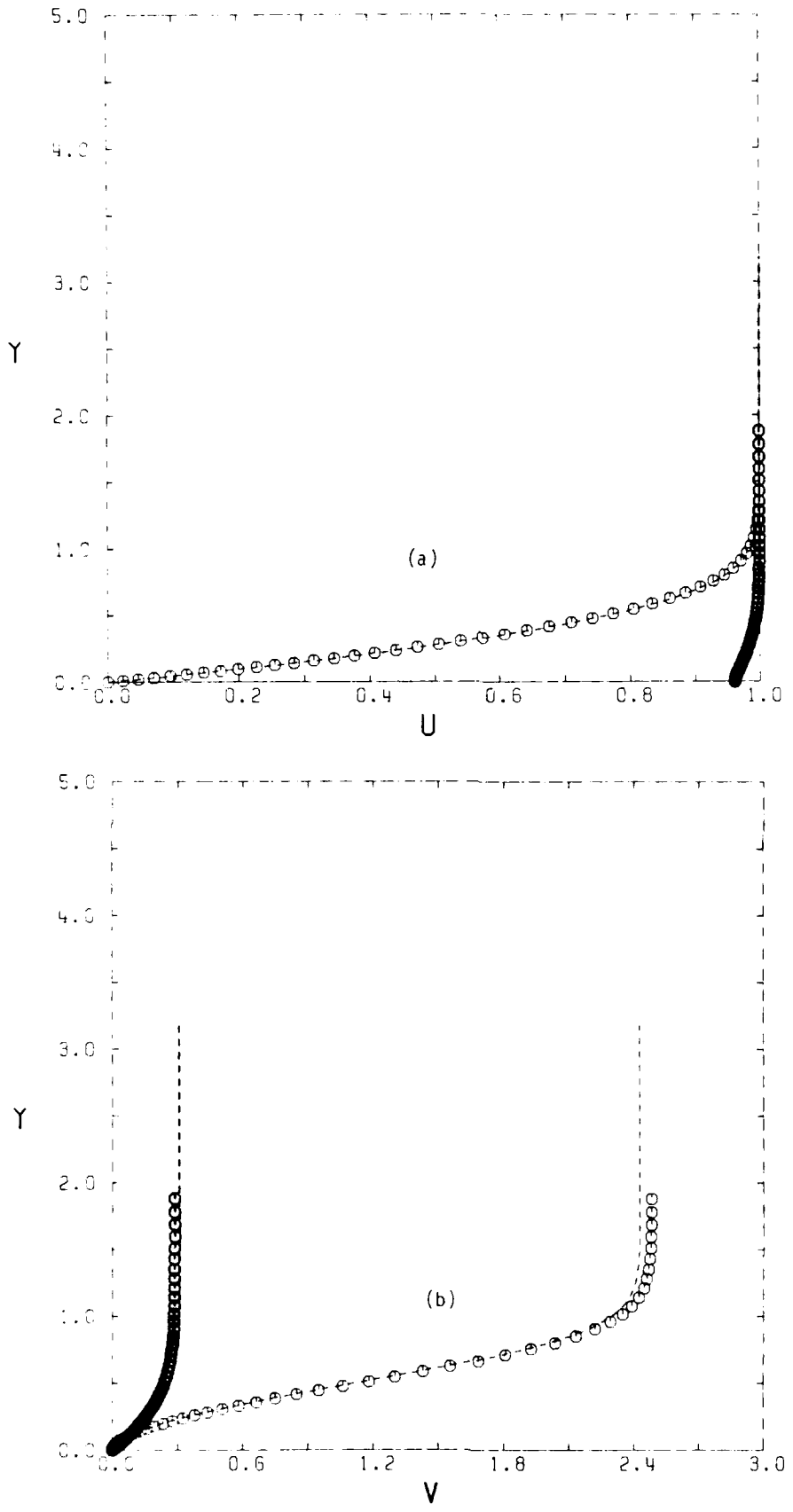

FIG. 4 FLOW PROFILES IN LARGE-SLIP REGION (x = 0.055).

(a) TANGENTIAL VELOCITY; (b) NORMAL VELOCITY; (c) TEMPERATURE.

○ DIFFERENCE SOLUTION FOR GAS; ● DIFFERENCE SOLUTION FOR PARTICLES;
--- ASYMPTOTIC SOLUTION FOR GAS; ▬▬ ASYMPTOTIC SOLUTION FOR PARTICLES.

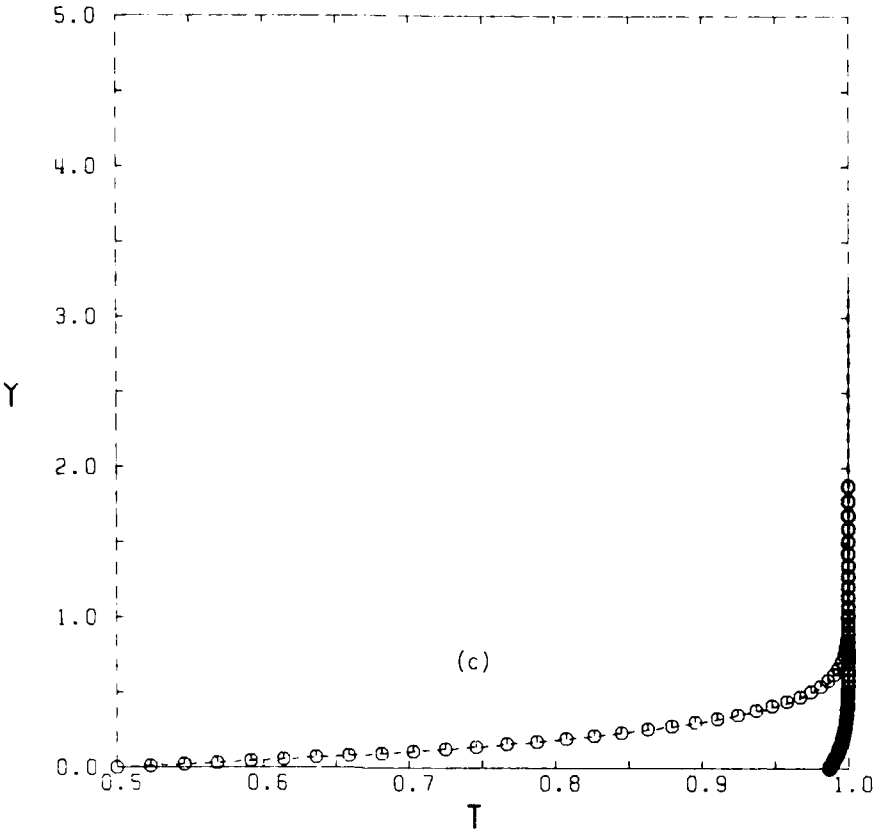

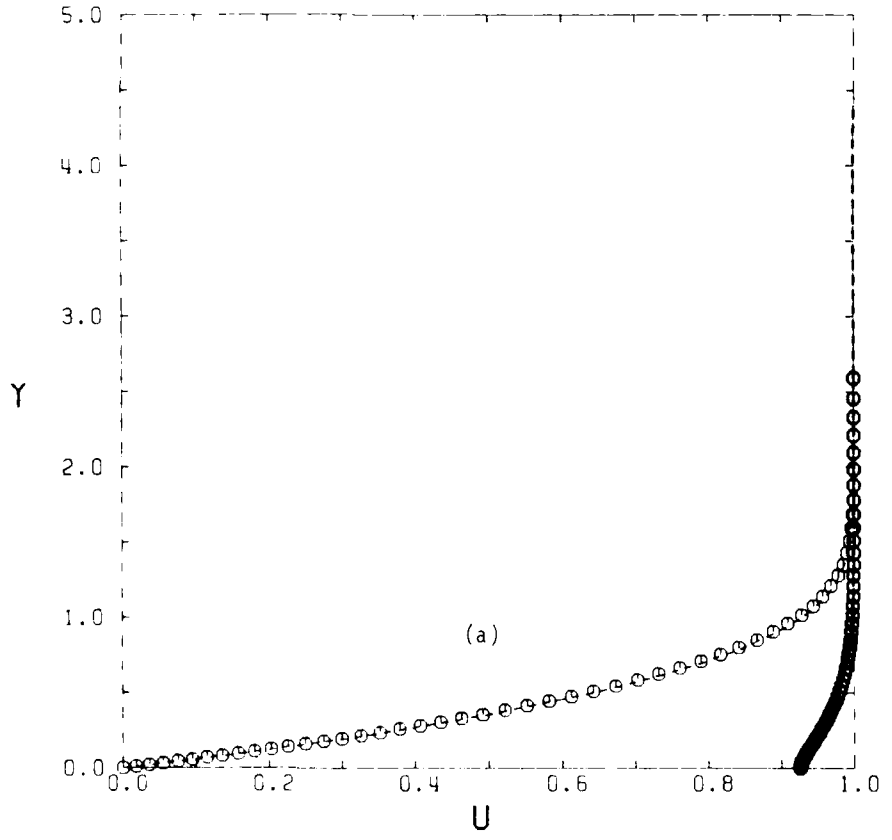

FIG. 5 FLOW PROFILES IN LARGE-SLIP REGION (x = 0.105).

(a) TANGENTIAL VELOCITY; (b) NORMAL VELOCITY; (c) TEMPERATURE.

○ DIFFERENCE SOLUTION FOR GAS; ● DIFFERENCE SOLUTION FOR PARTICLES;
--- ASYMPTOTIC SOLUTION FOR GAS; ▬▬ ASYMPTOTIC SOLUTION FOR PARTICLES.

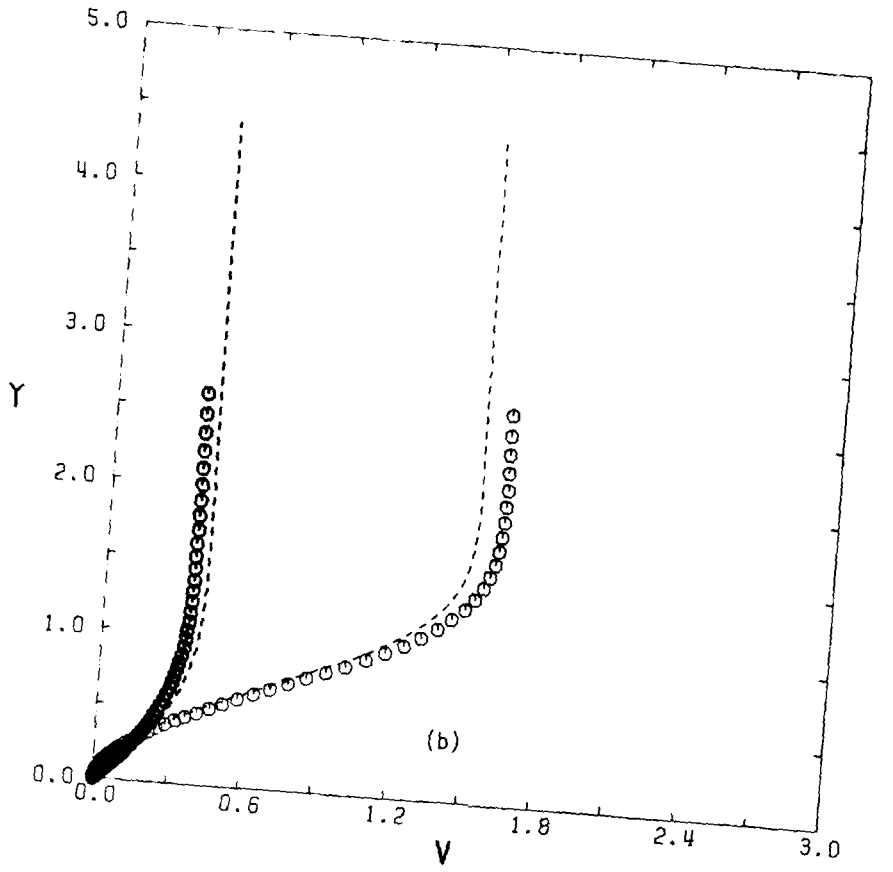
5.0
4.0
3.0
2.0
1.0
0.0
Y
0.0
0.6
1.2
1.8
2.4
3.0
V
(b)

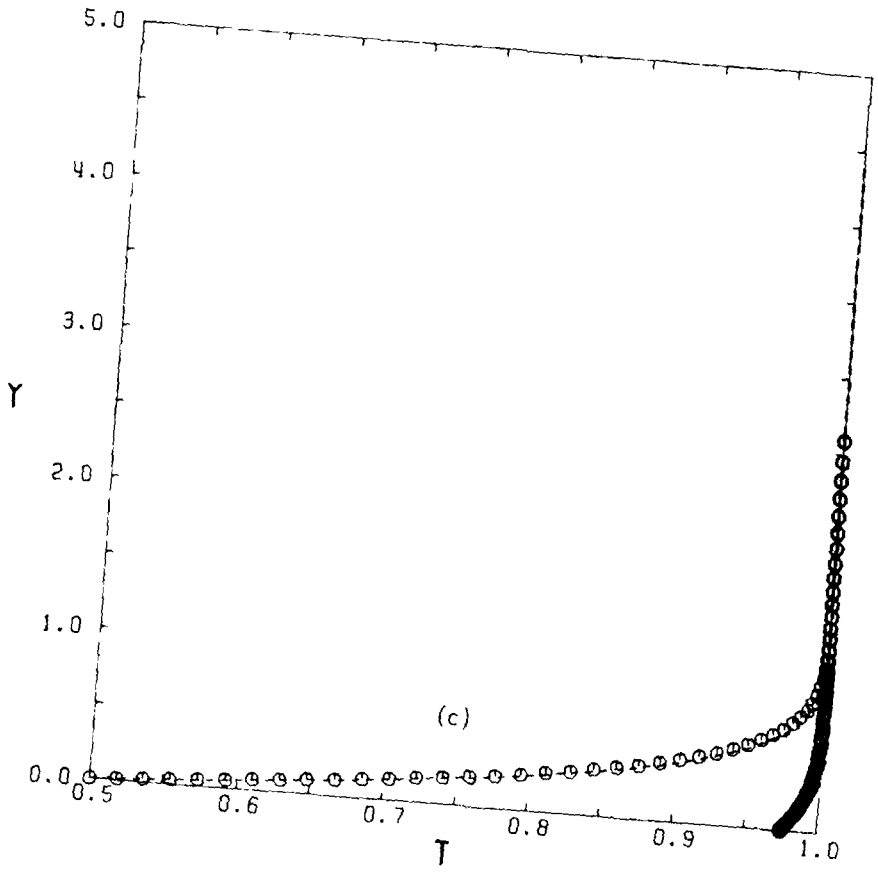
5.0
4.0
3.0
2.0
1.0
0.0
Y
0.5
0.6
0.7
0.8
0.9
1.0
T
(c)

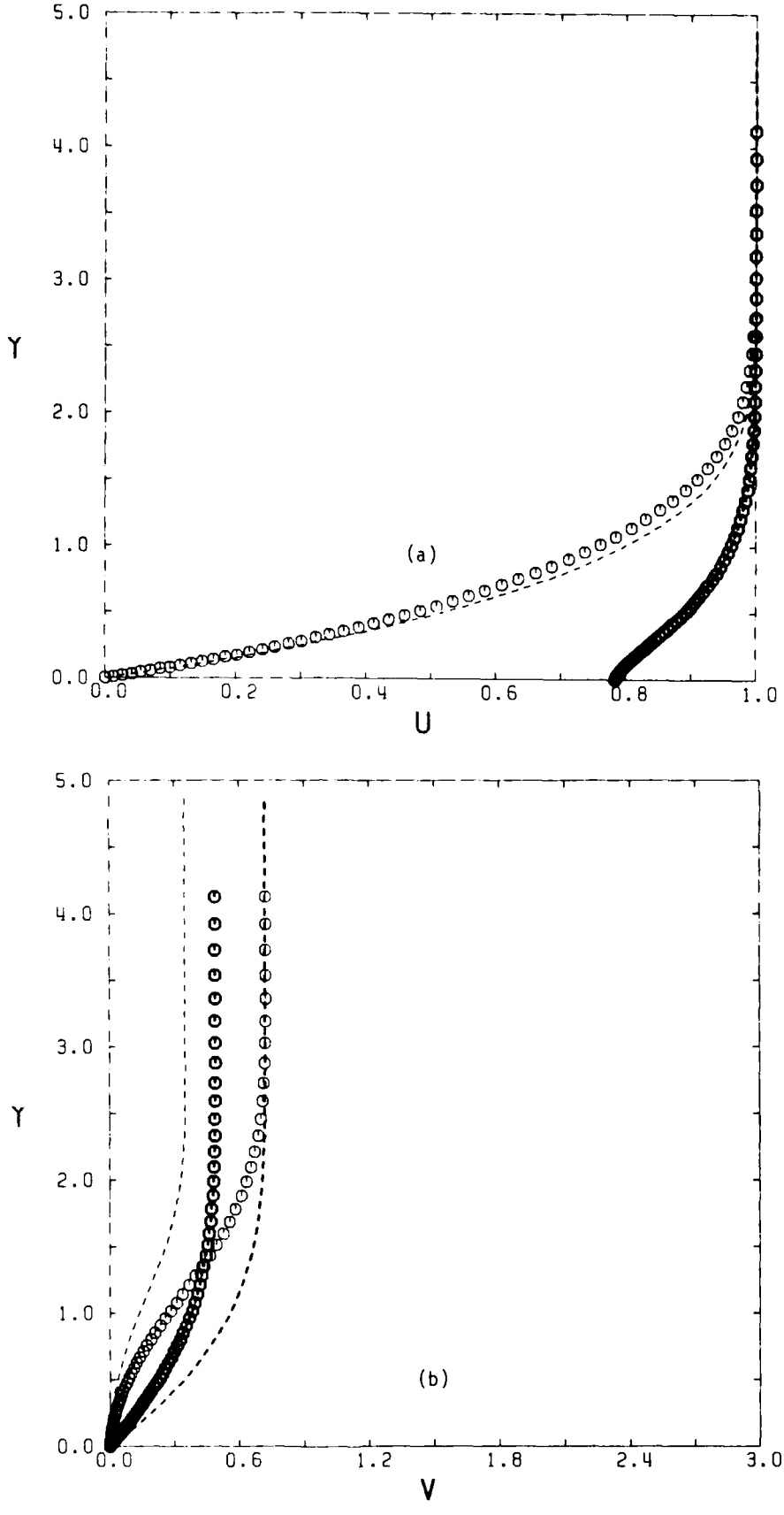

FIG. 6 FLOW PROFILES IN LARGE-SLIP REGION (x = 0.305).

(a) TANGENTIAL VELOCITY; (b) NORMAL VELOCITY; (c) TEMPERATURE.

○ DIFFERENCE SOLUTION FOR GAS; ● DIFFERENCE SOLUTION FOR PARTICLES;
--- ASYMPTOTIC SOLUTION FOR GAS; ▬▬ ASYMPTOTIC SOLUTION FOR PARTICLES.

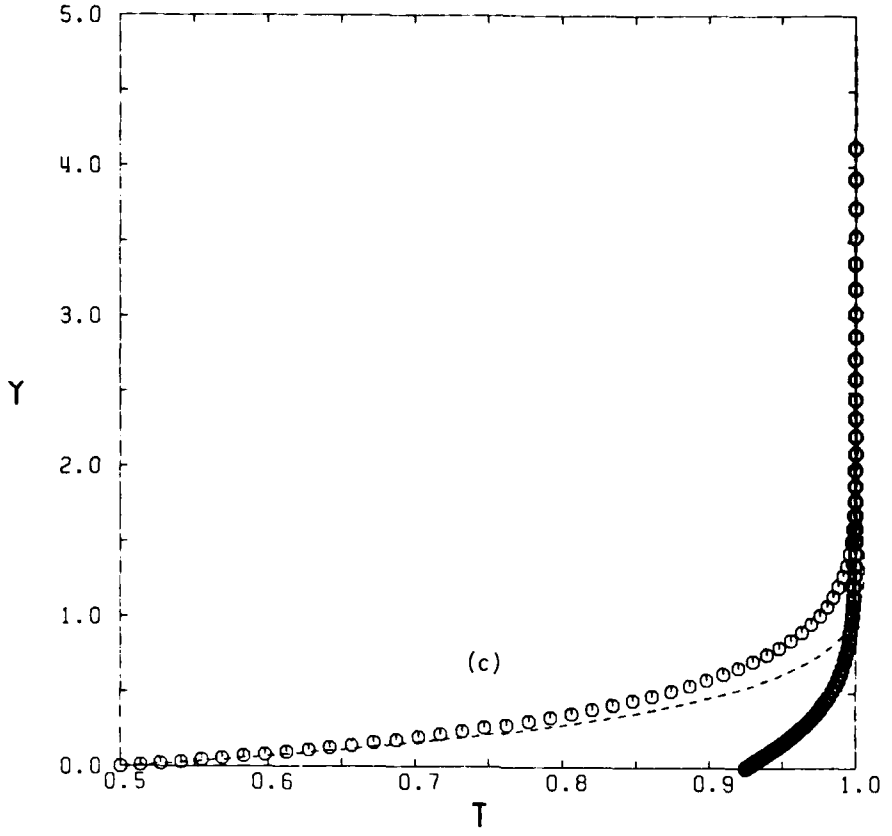

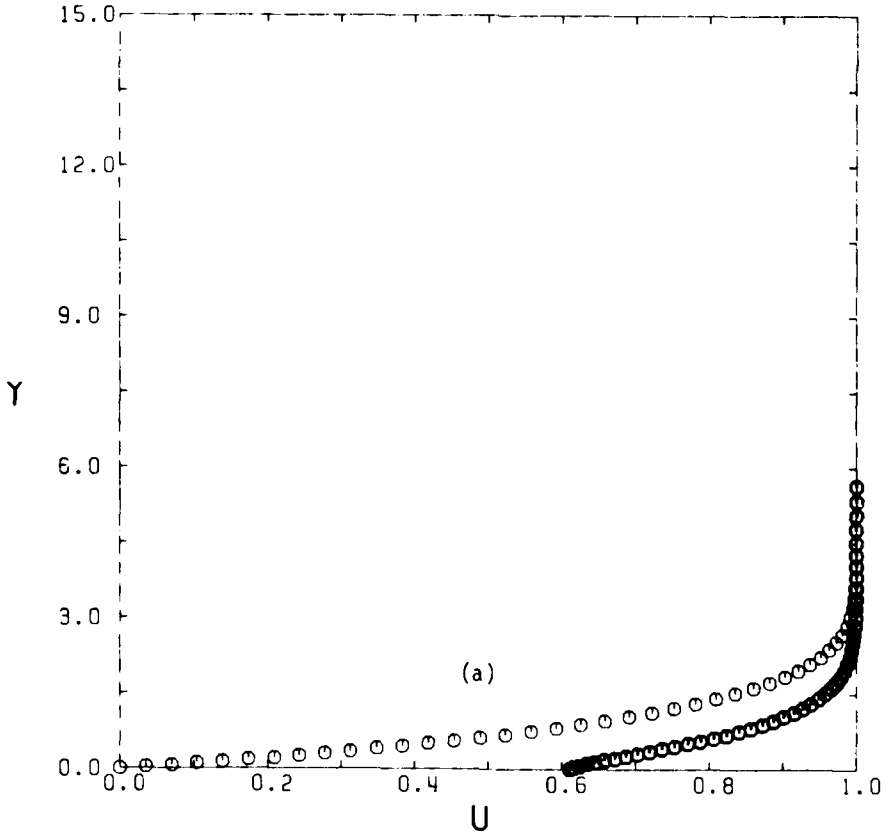

FIG. 7 FLOW PROFILES IN MODERATE-SLIP REGION (x = 0.55).

(a) TANGENTIAL VELOCITY; (b) NORMAL VELOCITY; (c) TEMPERATURE.

○ GAS; ● PARTICLES.

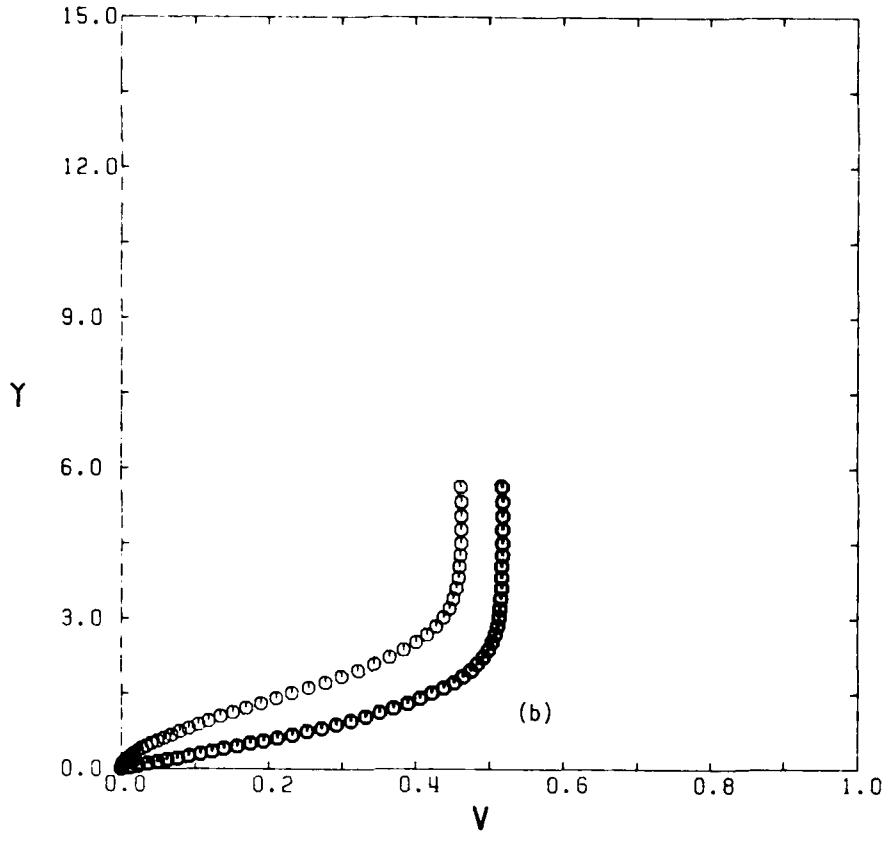
15.0
12.0
9.0
6.0
3.0
0.0
Y
0.0
0.2
0.4
0.6
0.8
1.0
V
(b)

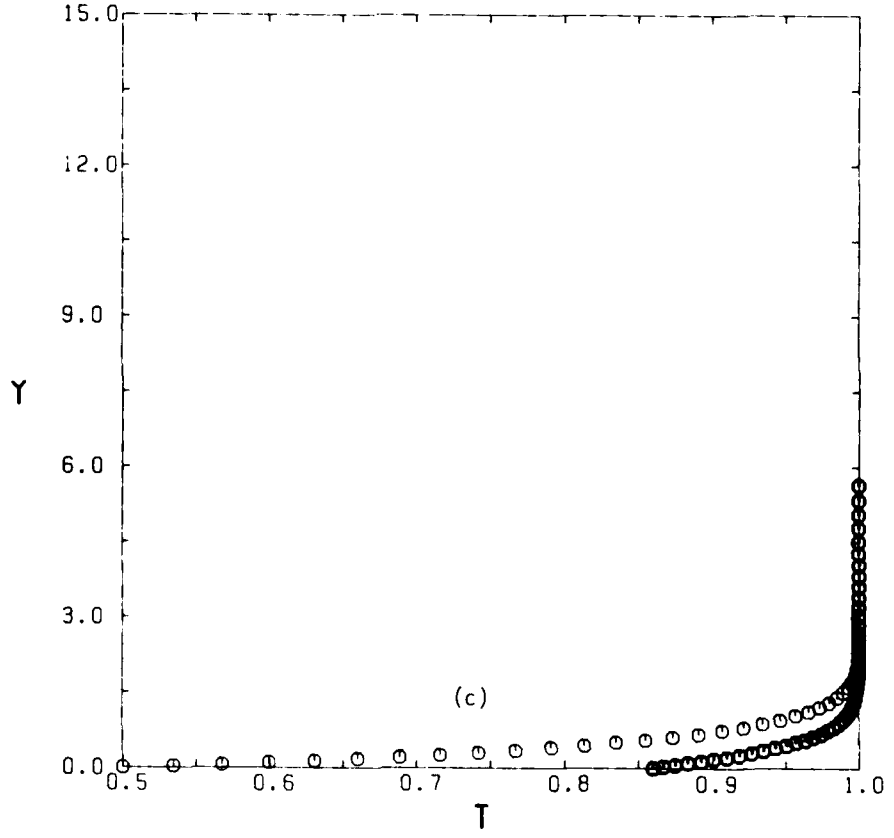
15.0
12.0
9.0
6.0
3.0
0.0
Y
0.5
0.6
0.7
0.8
0.9
1.0
T
(c)

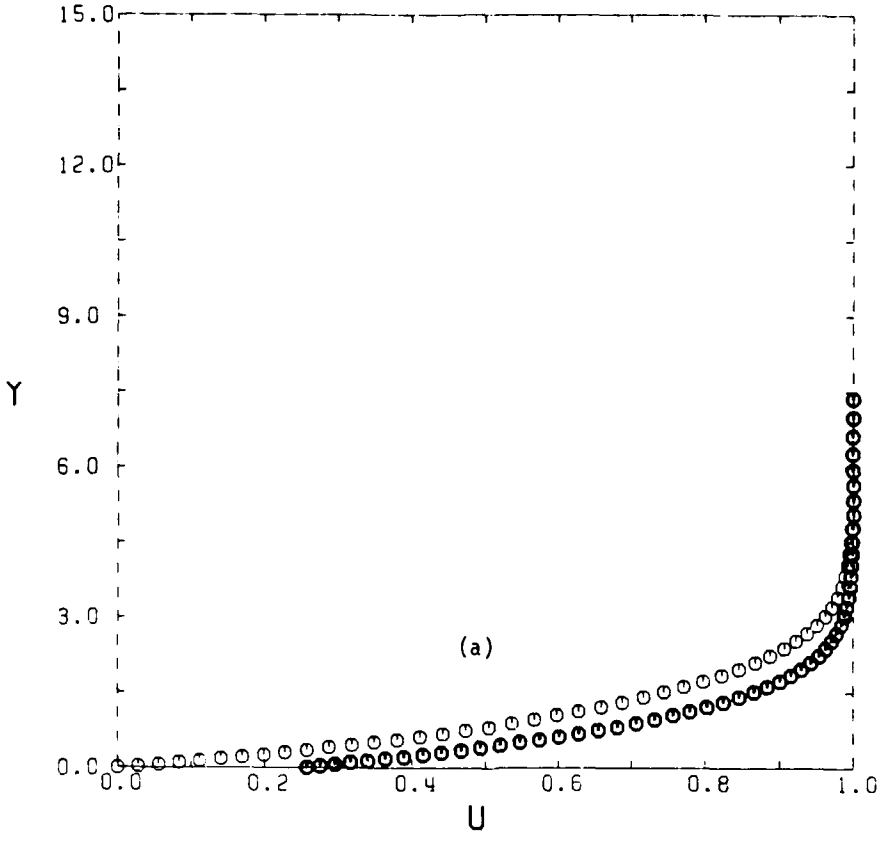

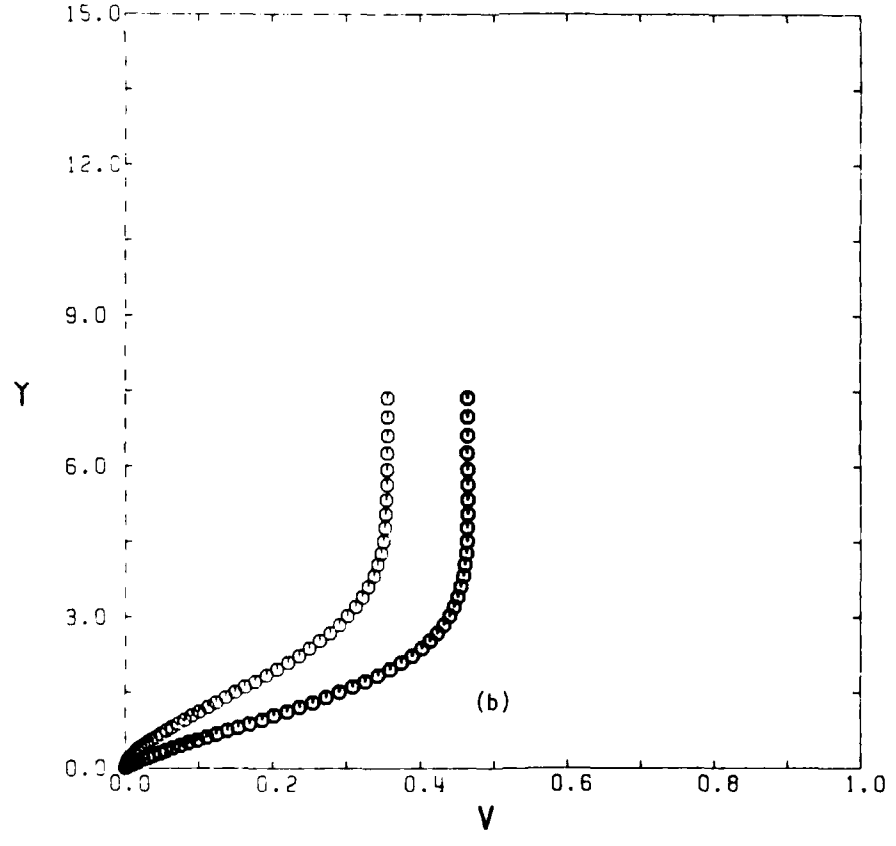

FIG. 8 FLOW PROFILES IN MODERATE-SLIP REGION (x = 1.05).

(a) TANGENTIAL VELOCITY; (b) NORMAL VELOCITY; (c) TEMPERATURE.

○ GAS; ● PARTICLES.

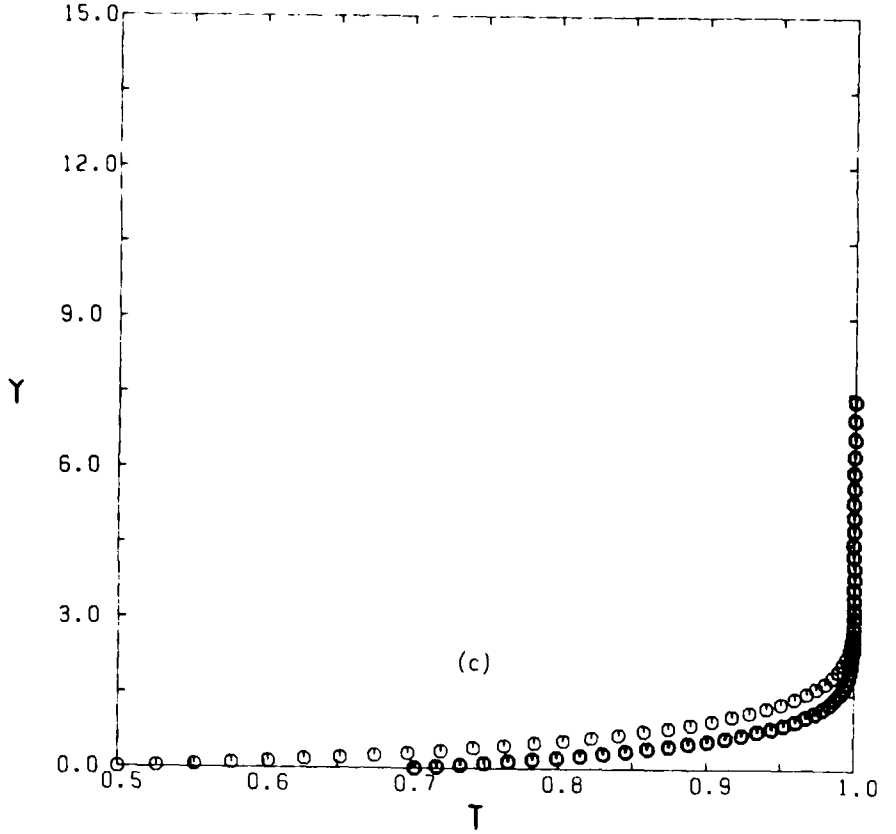

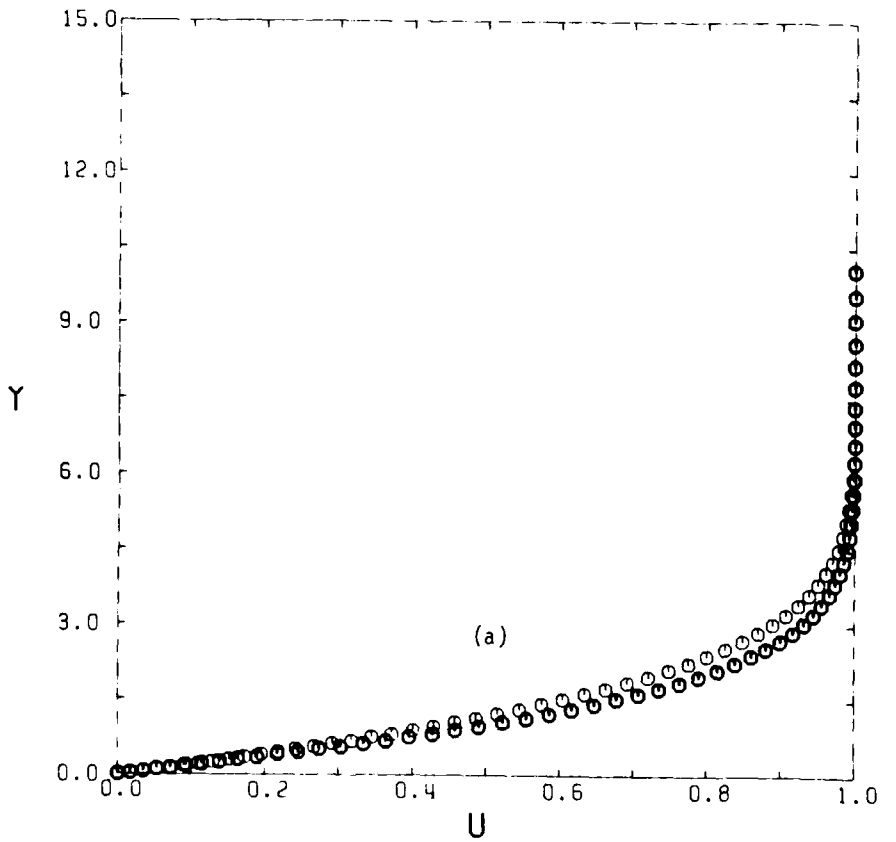

FIG. 9 FLOW PROFILES IN MODERATE-SLIP REGION (x = 2.05).

(a) TANGENTIAL VELOCITY; (b) NORMAL VELOCITY; (c) TEMPERATURE.

○ GAS; ● PARTICLES.

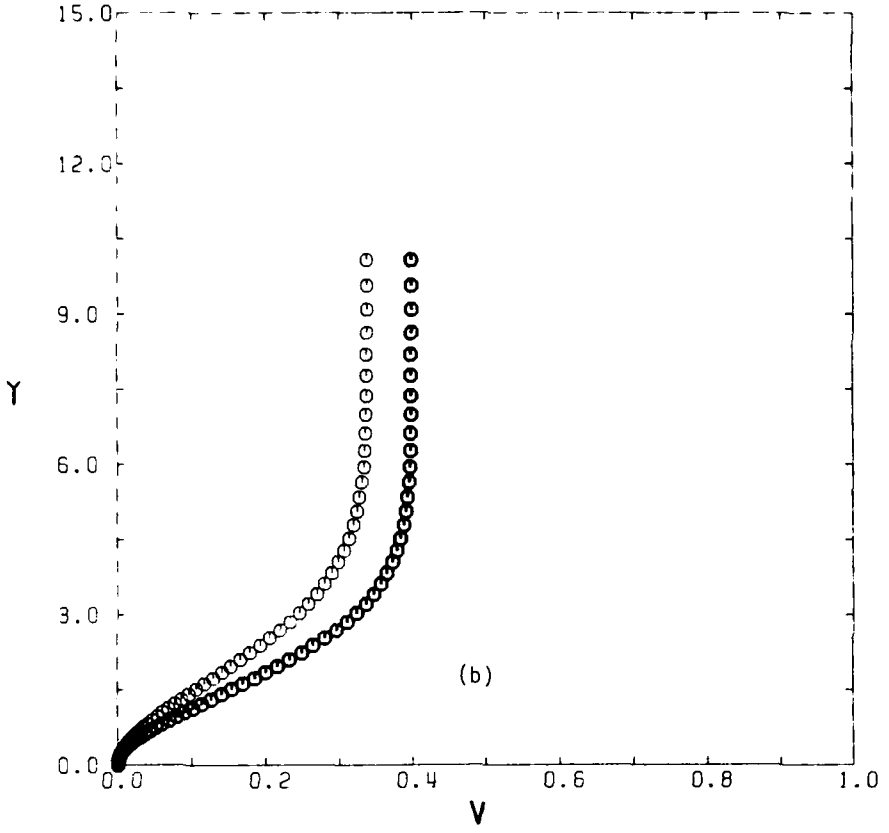
15.0
12.0
9.0
6.0
3.0
0.0
Y
0.0
0.2
0.4
0.6
0.8
1.0
V
(b)

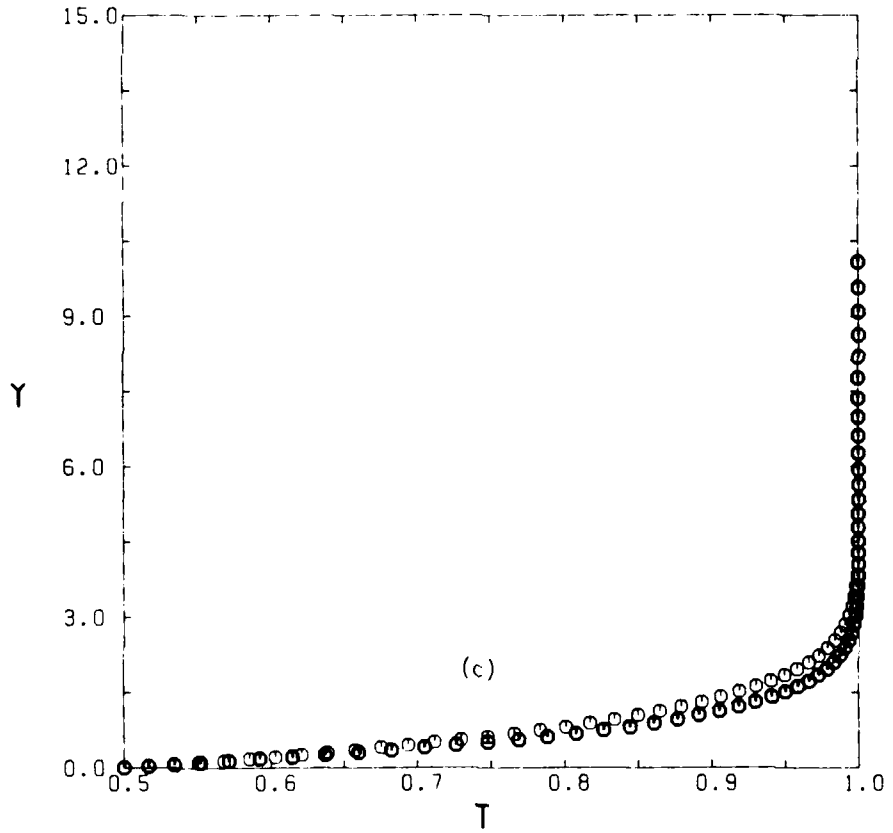
15.0
12.0
9.0
6.0
3.0
0.0
Y
0.5
0.6
0.7
0.8
0.9
1.0
T
(c)

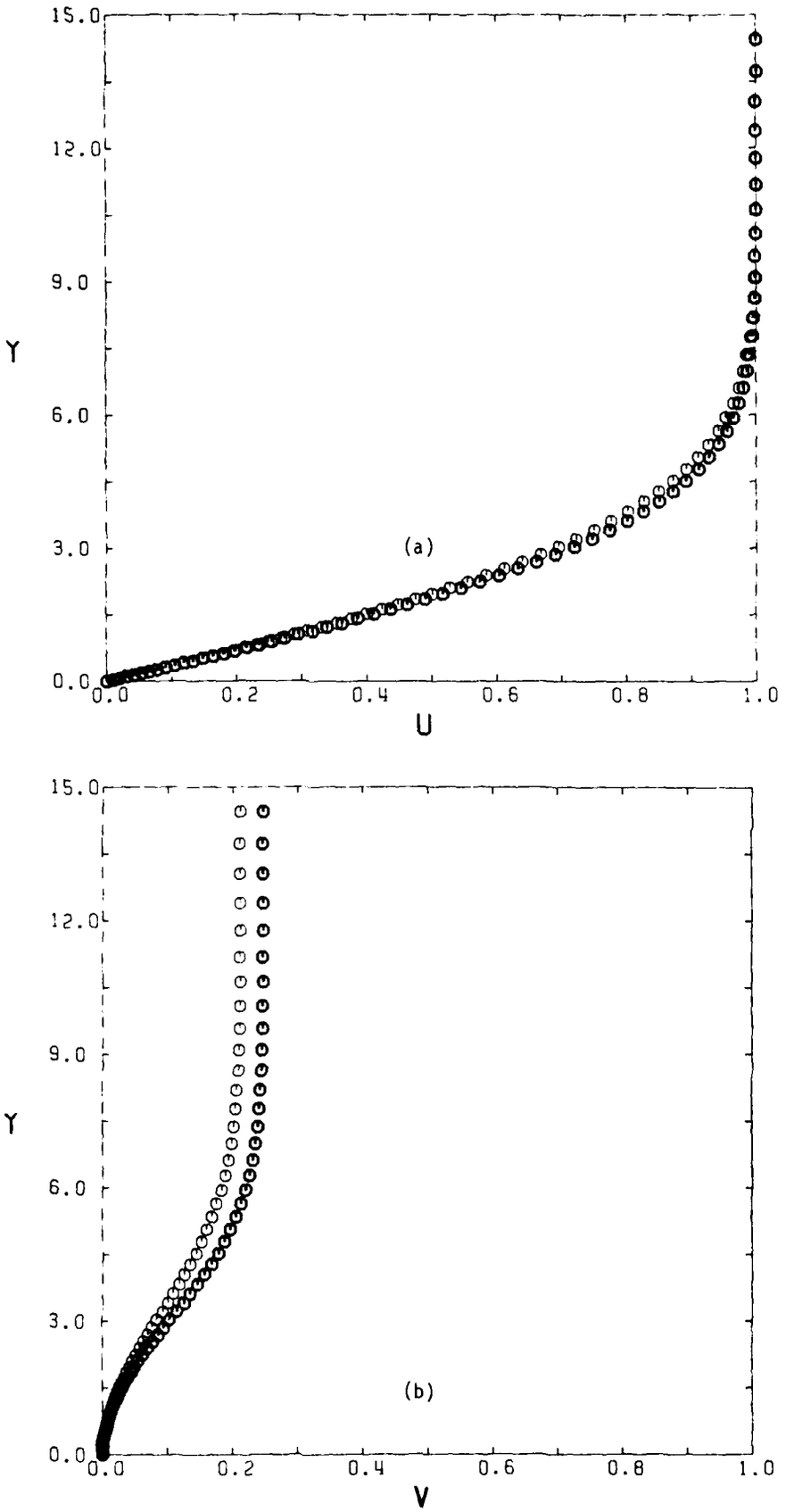

FIG. 10 FLOW PROFILES IN THE MODERATE-SLIP REGION (x = 5.05).

(a) TANGENTIAL VELOCITY; (b) NORMAL VELOCITY; (c) TEMPERATURE.

O GAS; O PARTICLES.

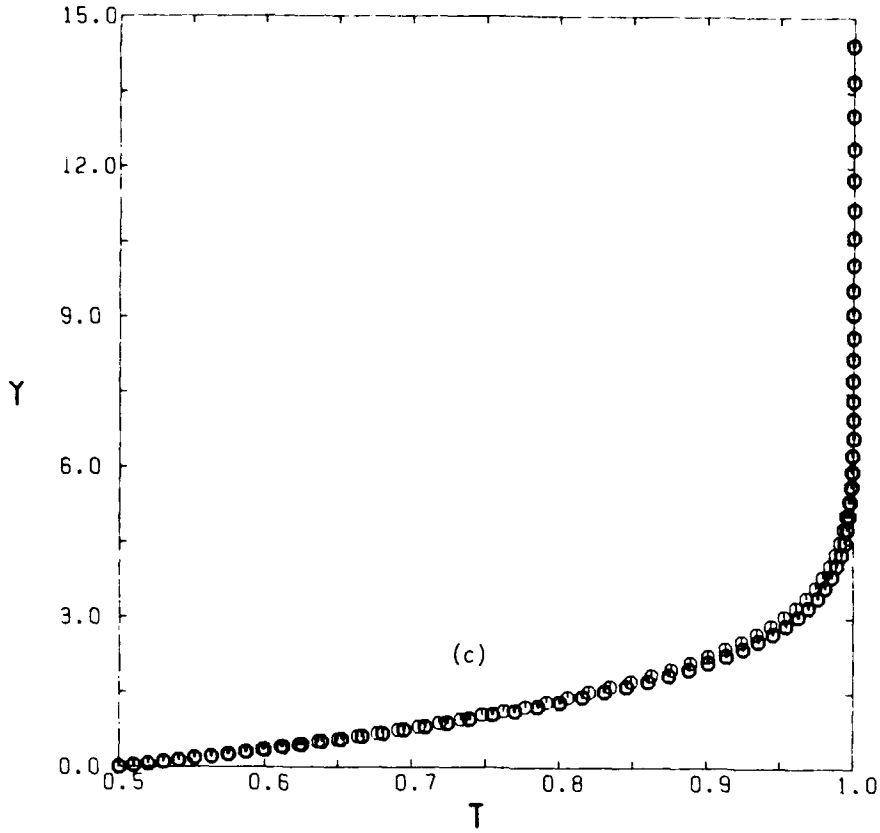

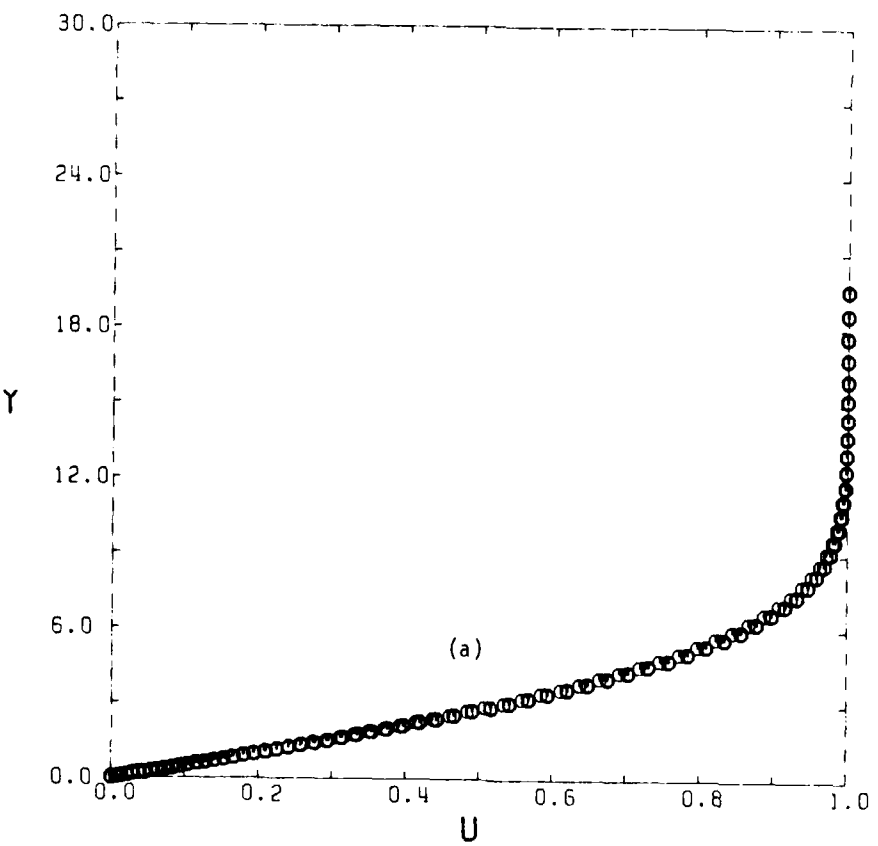

FIG. 11 FLOW PROFILES IN SMALL-SLIP REGION (x ≈ 10.05).

(a) TANGENTIAL VELOCITY; (b) NORMAL VELOCITY; (c) TEMPERATURE.

O GAS; O PARTICLES.

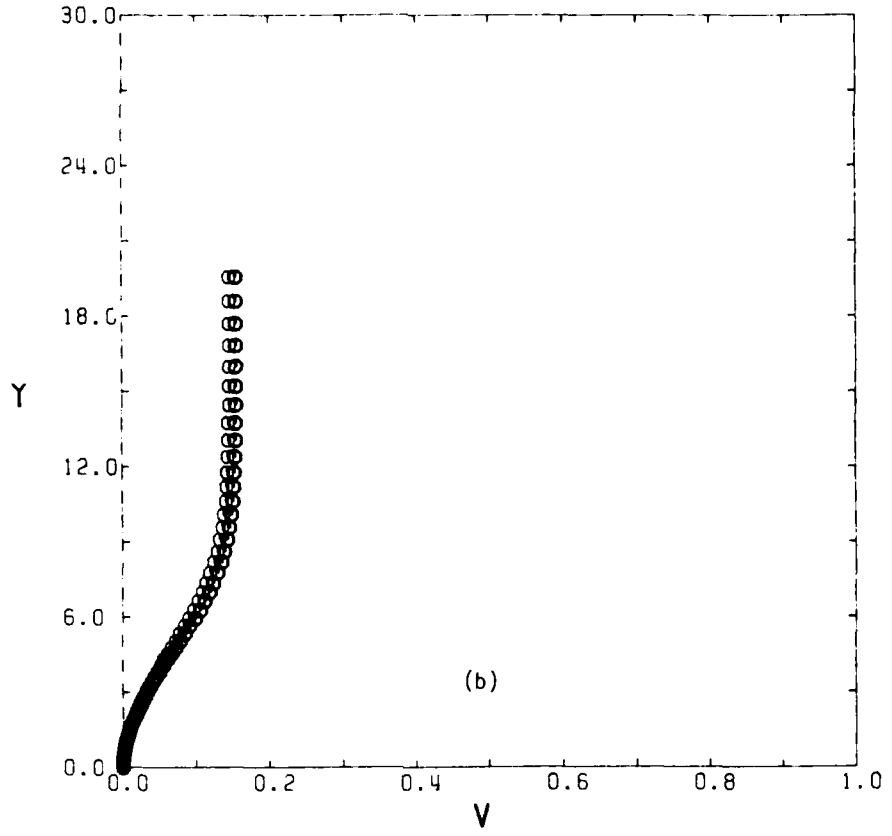
30.0
24.0
18.0
12.0
6.0
0.0
Y
0.0
0.2
0.4
0.6
0.8
1.0
V
(b)

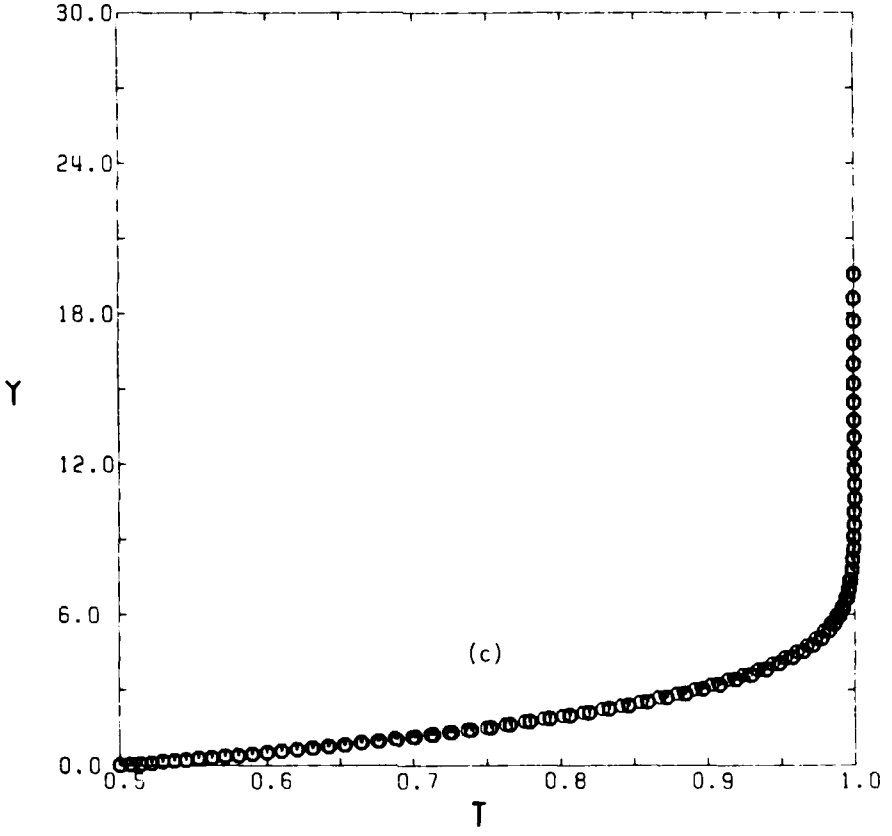
30.0
24.0
18.0
12.0
6.0
0.0
Y
0.5
0.6
0.7
0.8
0.9
1.0
T
(c)

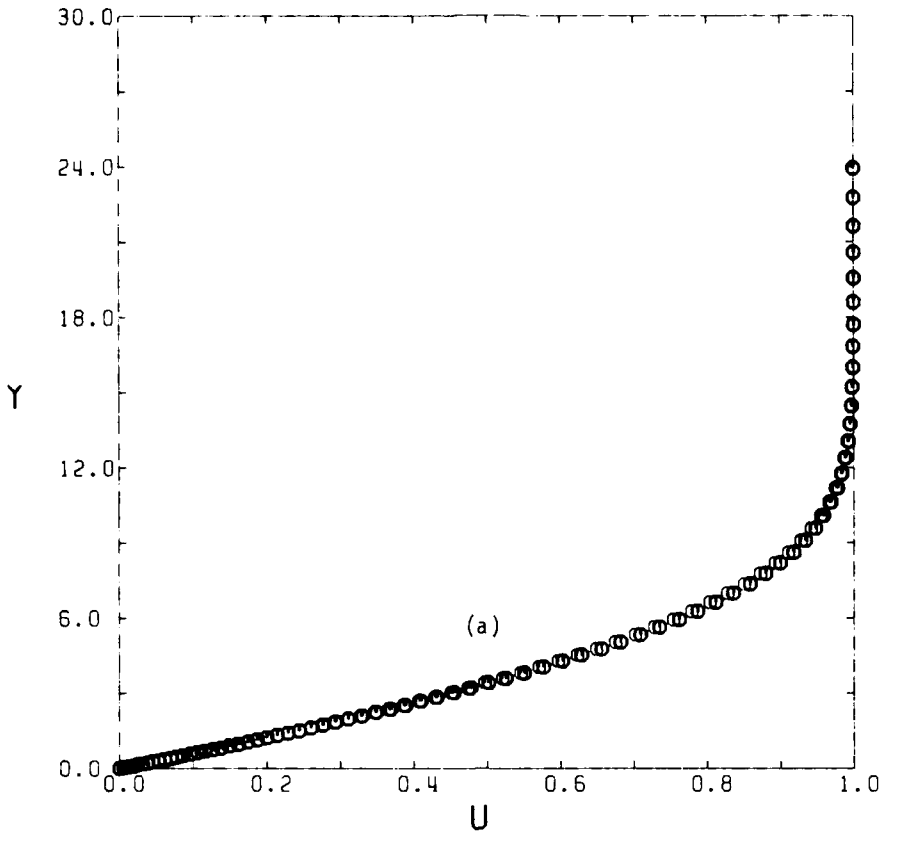

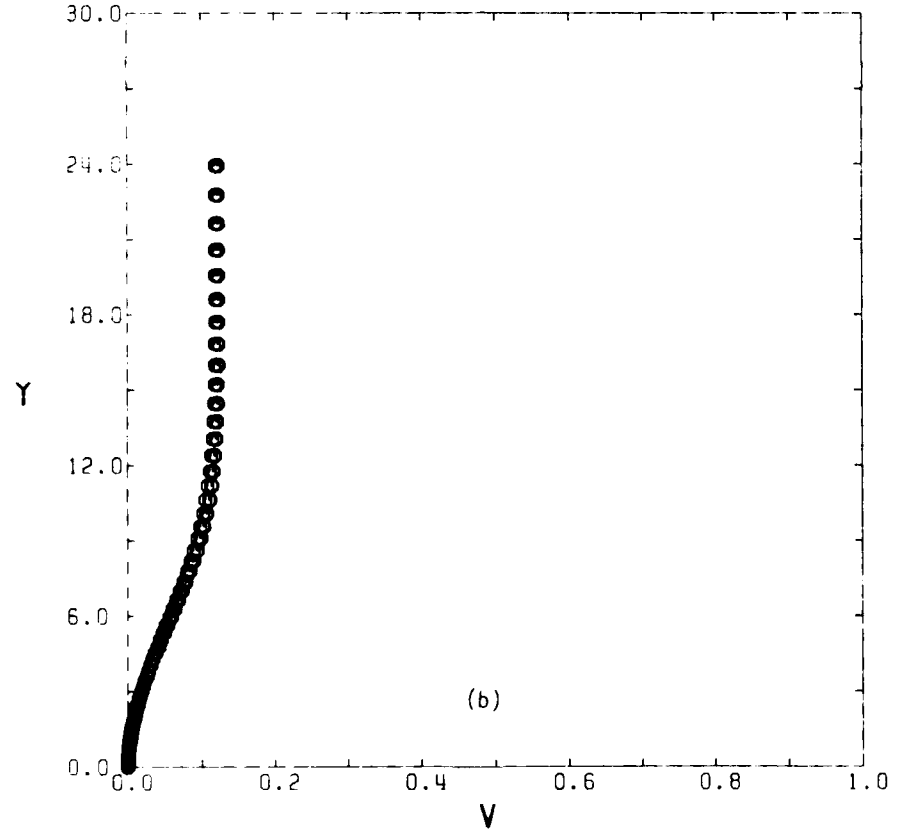

FIG. 12 FLOW PROFILES IN SMALL-SLIP REGION (x = 15.05).

(a) TANGENTIAL VELOCITY; (b) NORMAL VELOCITY; (c) TEMPERATURE.

○ GAS; ● PARTICLES.

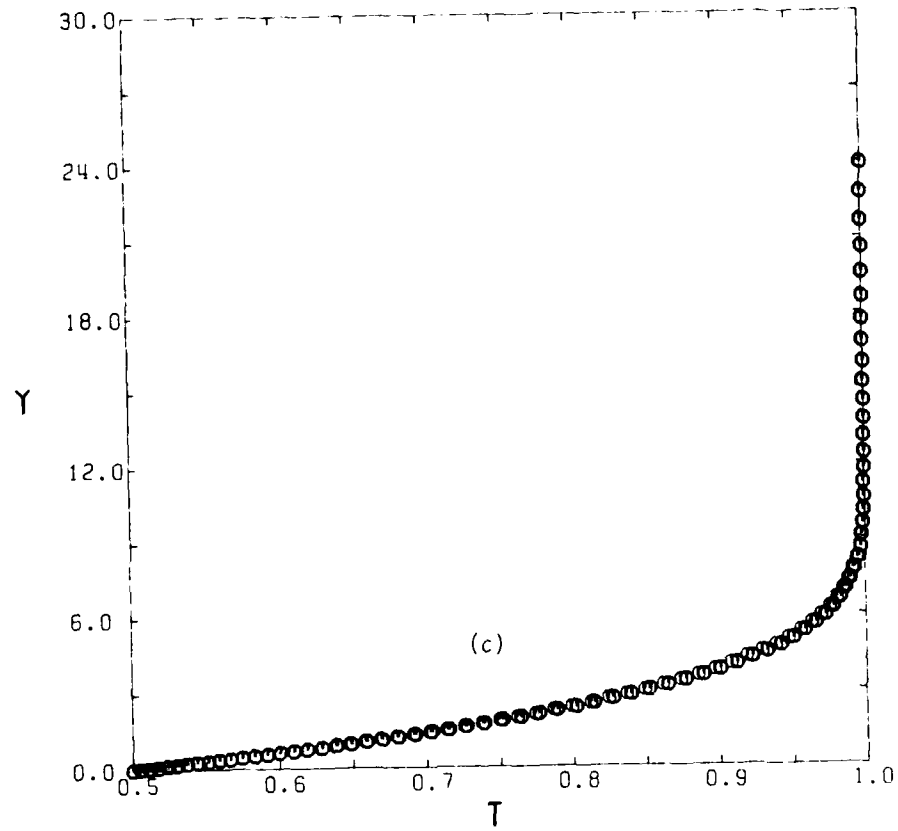

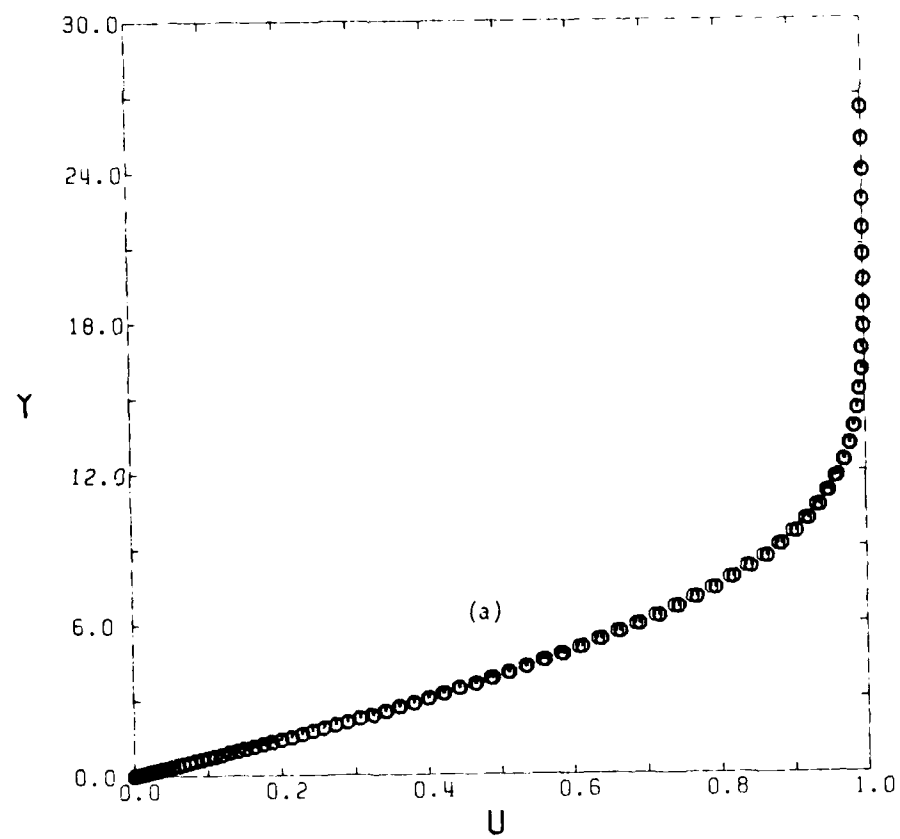

FIG. 13 FLOW PROFILES IN SMALL-SLIP REGION (x = 20.05).

(a) TANGENTIAL VELOCITY; (b) NORMAL VELOCITY; (c) TEMPERATURE.

○ GAS; ● PARTICLES.

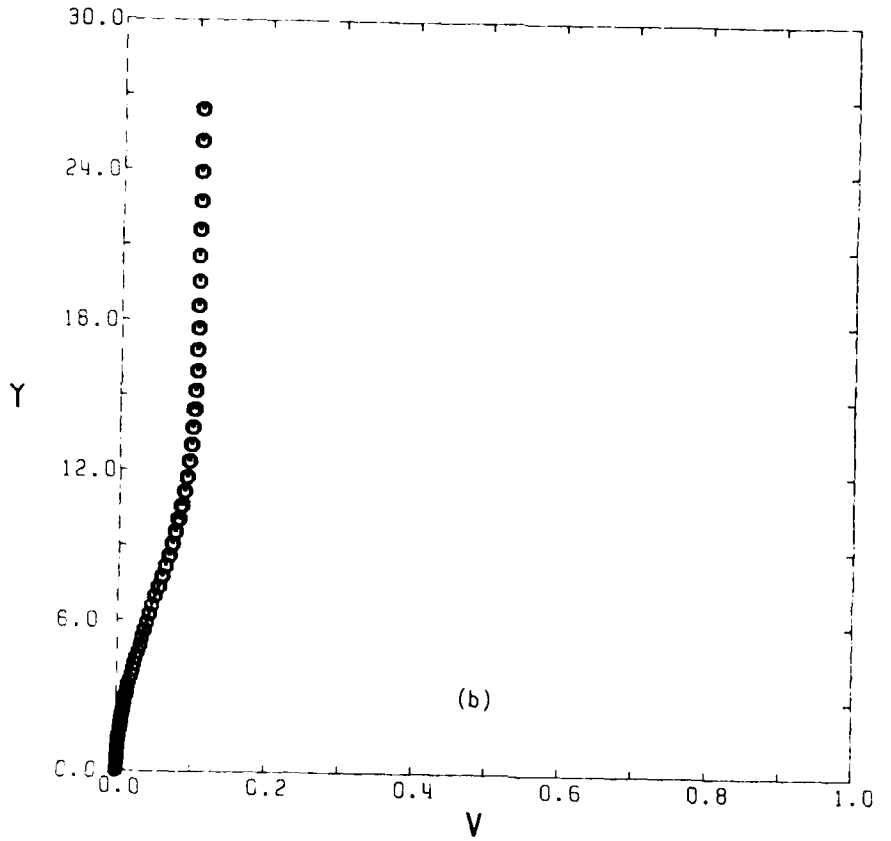
30.0
24.0
18.0
12.0
6.0
0.0
Y
0.0
0.2
0.4
0.6
0.8
1.0
V
(b)

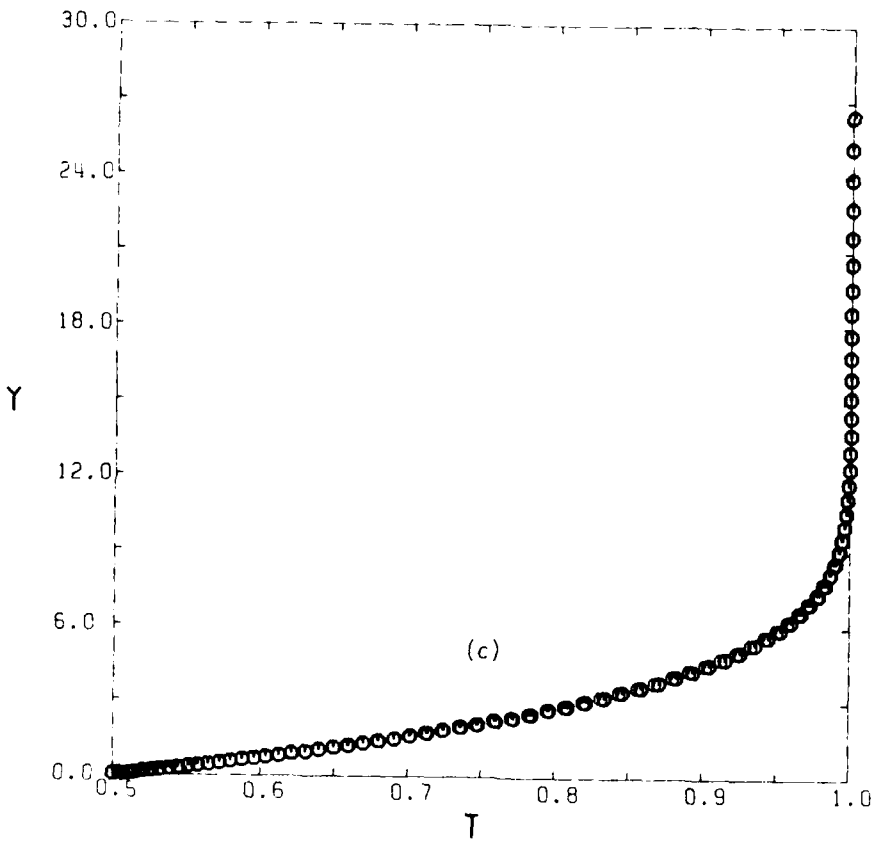
30.0
24.0
18.0
12.0
6.0
0.0
Y
0.5
0.6
0.7
0.8
0.9
1.0
T
(c)

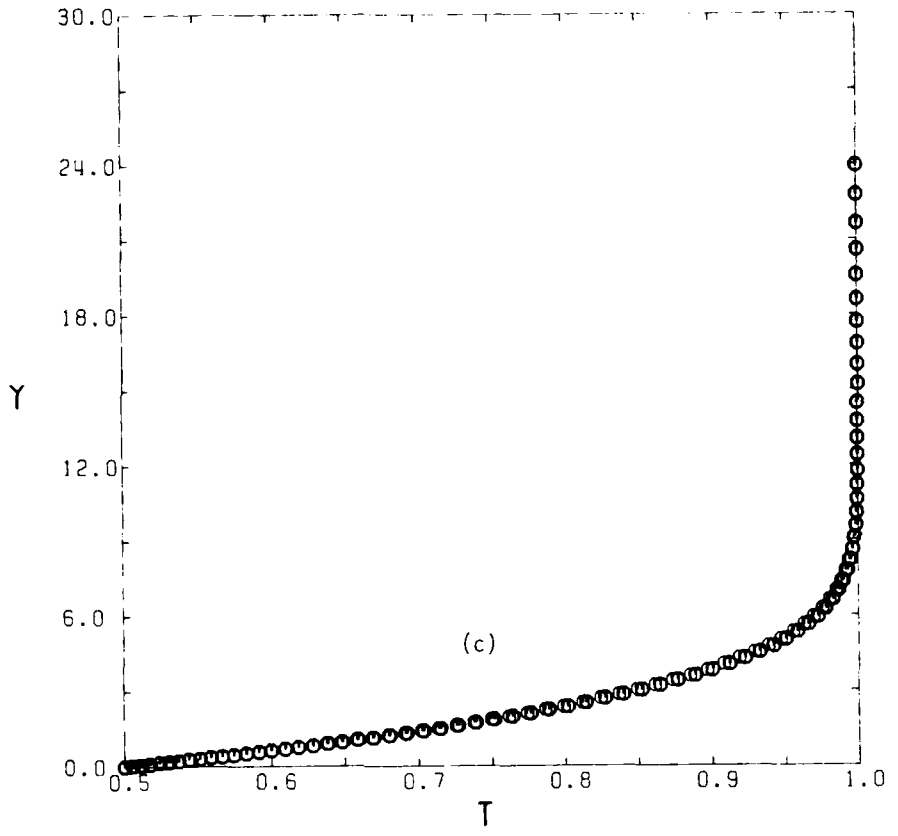

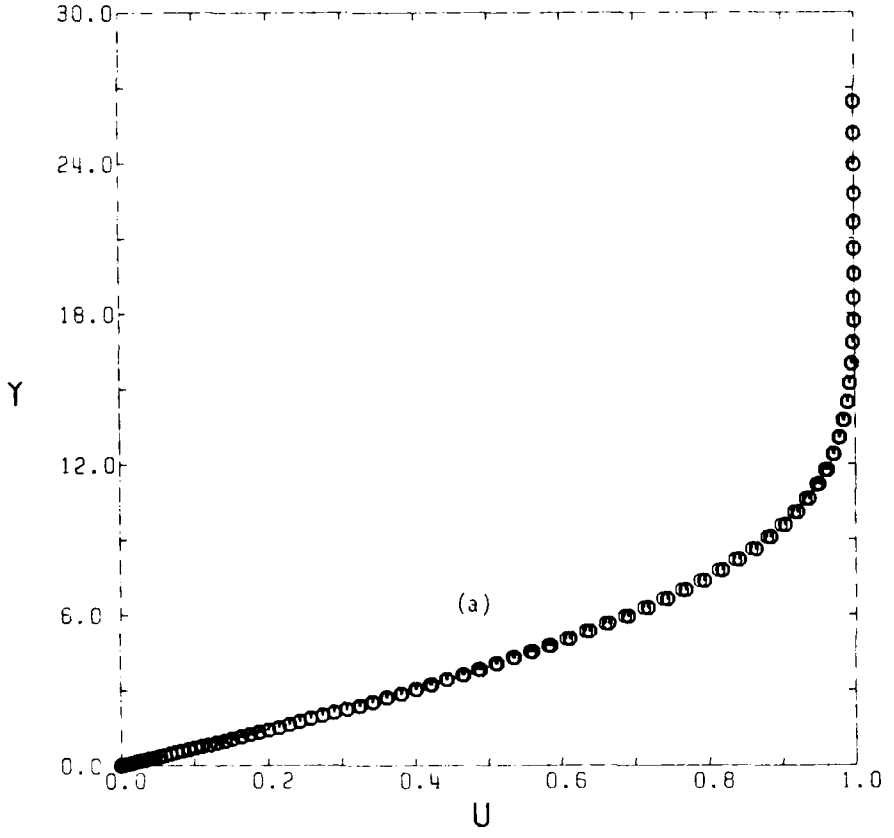

FIG. 13 FLOW PROFILES IN SMALL-SLIP REGION (x = 20.05).

(a) TANGENTIAL VELOCITY; (b) NORMAL VELOCITY; (c) TEMPERATURE.

○ GAS; ● PARTICLES.

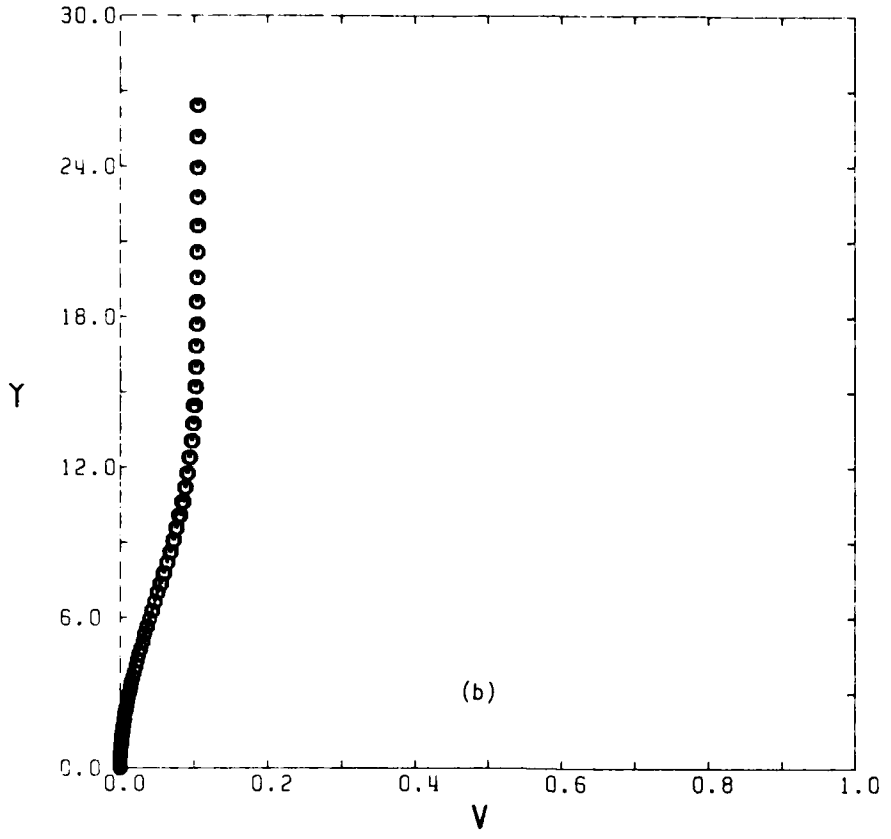
30.0
24.0
18.0
12.0
6.0
0.0
Y
0.0
0.2
0.4
0.6
0.8
1.0
V
(b)

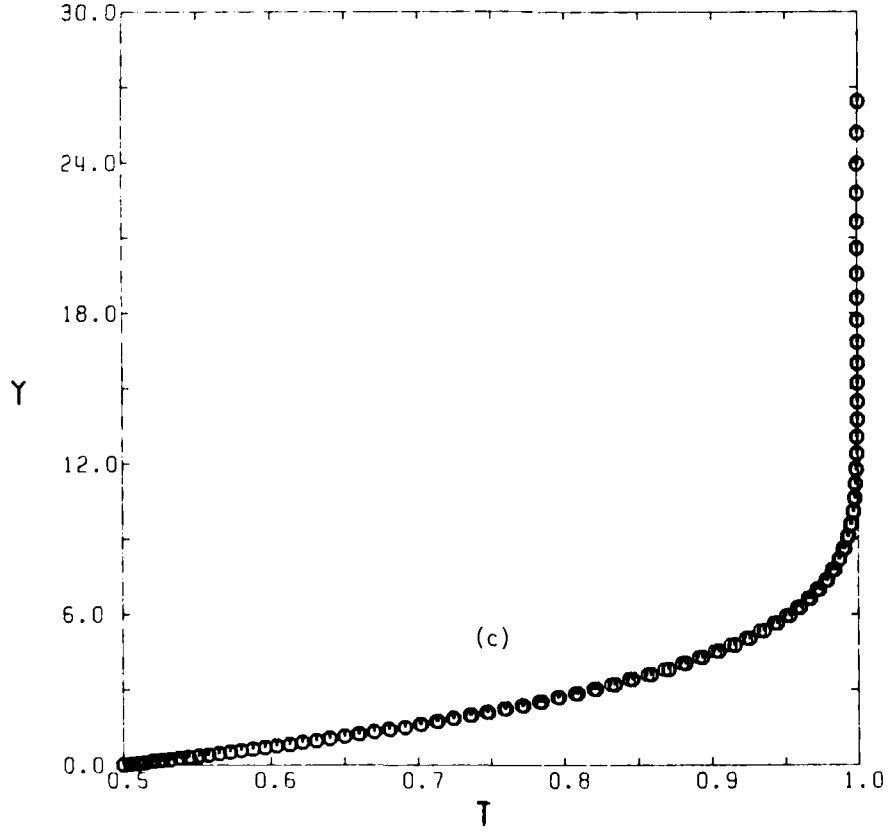
30.0
24.0
18.0
12.0
6.0
0.0
Y
0.5
0.6
0.7
0.8
0.9
1.0
T
(c)

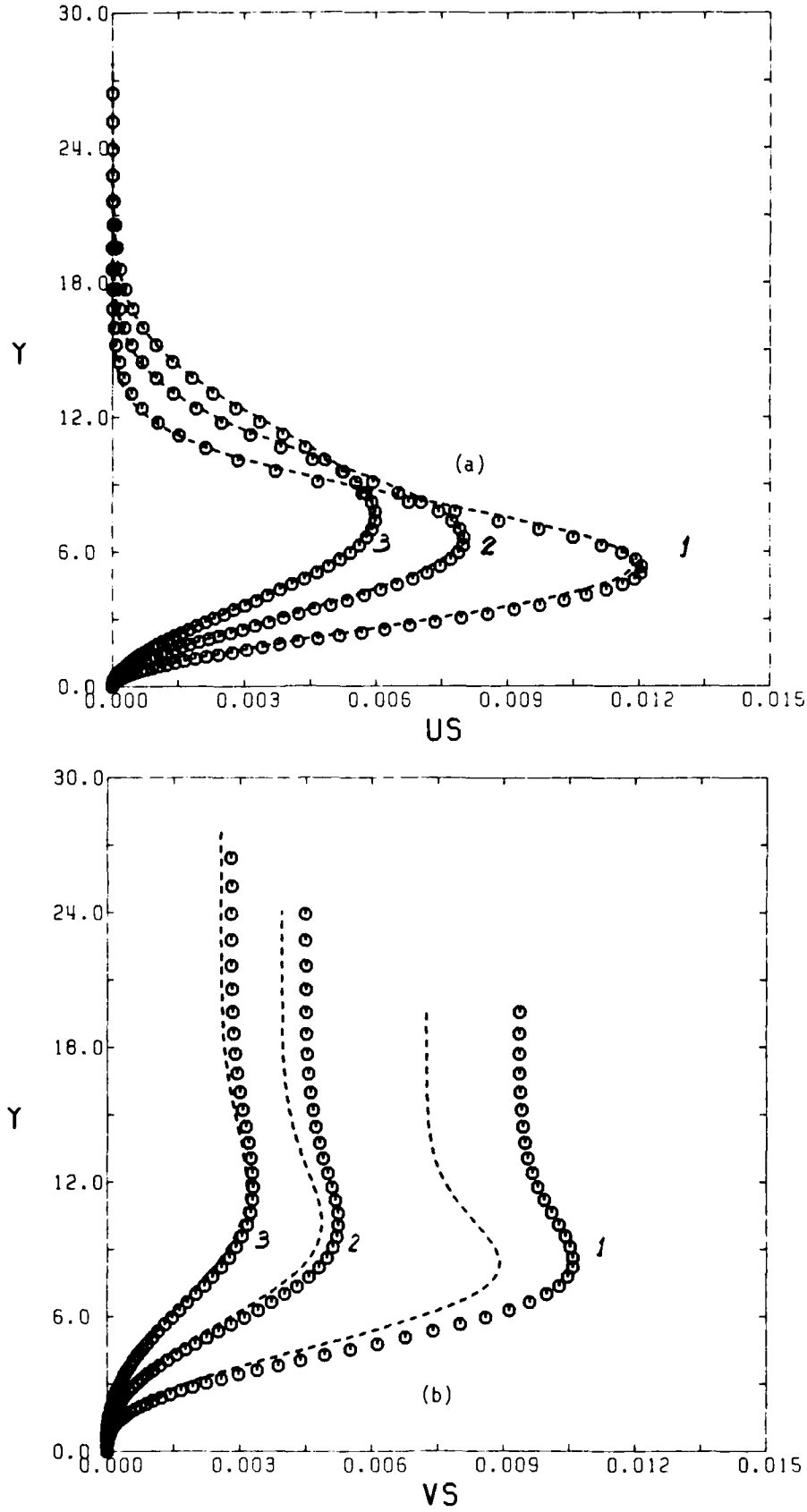

FIG. 14 SLIP FLOW QUANTITIES IN SMALL-SLIP REGION.

(a) TANGENTIAL SLIP VELOCITY; (b) NORMAL SLIP VELOCITY; (c) TEMPERATURE DEFECT.

O FINITE-DIFFERENCE SOLUTION; --- ASYMPTOTIC SOLUTION, 1: x = 10.05; 2: x = 15.05; 3: x = 20.05.

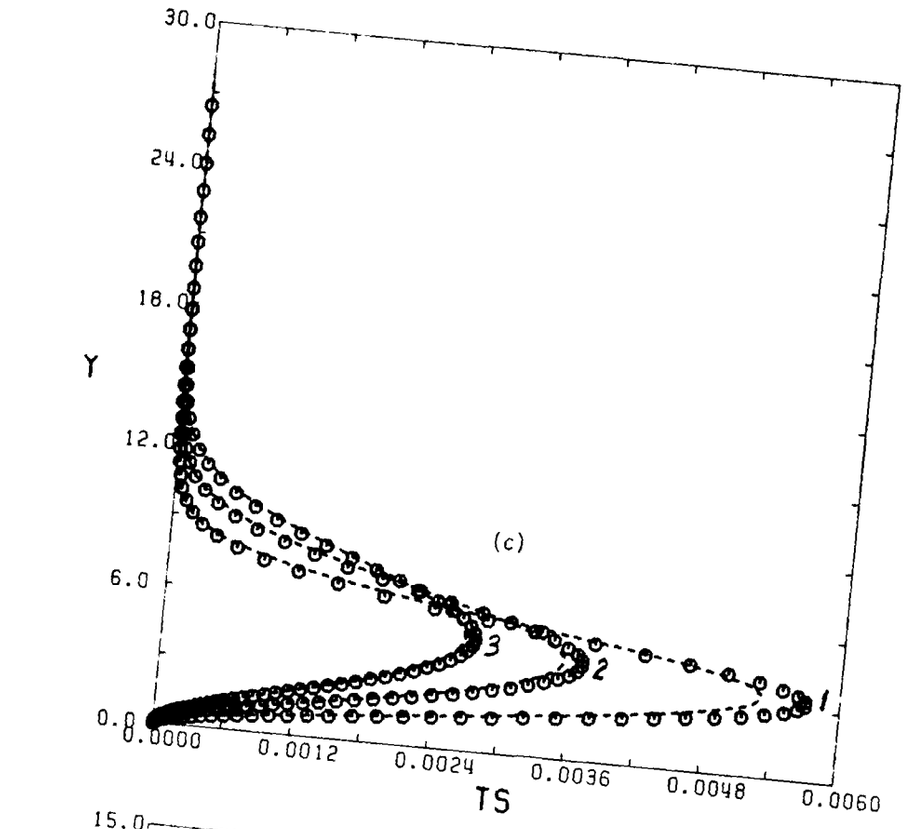

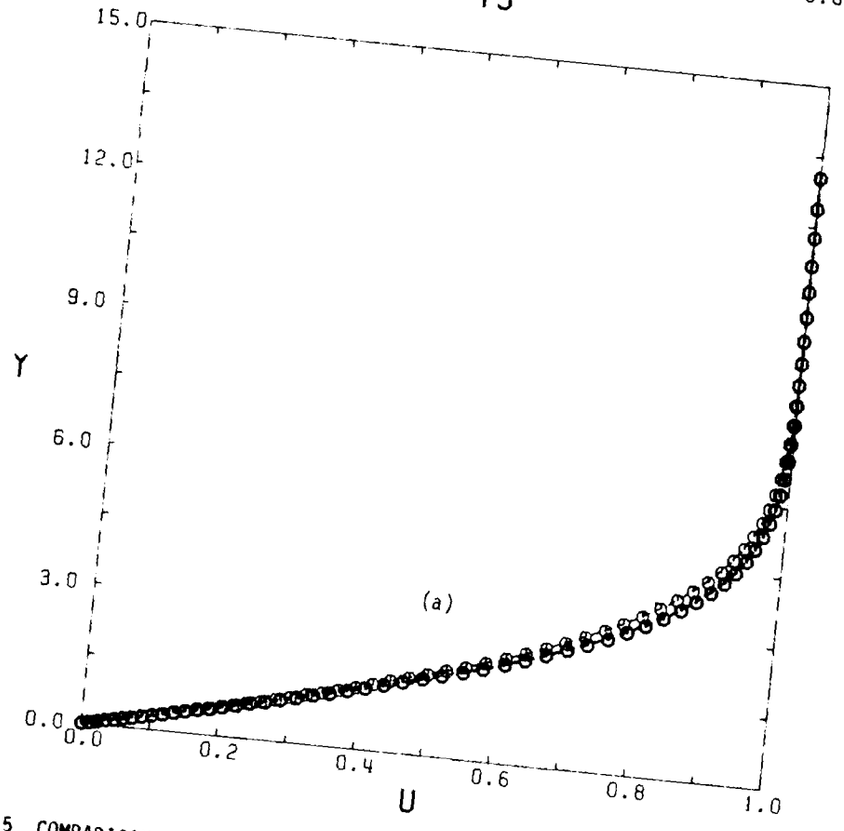

FIG. 15 COMPARISON BETWEEN FLOW PROFILES RESULTING FROM FOUR-POINT AND SIX-POINT SCHEMES IN NONEQUILIBRIUM REGION (x = 4.05).

(a) TANGENTIAL VELOCITY; (b) NORMAL VELOCITY; (c) TEMPERATURE.

FOUR-POINT SCHEME: ○ GAS; ● PARTICLE;
SIX-POINT SCHEME: --- GAS; ▬▬ PARTICLE.

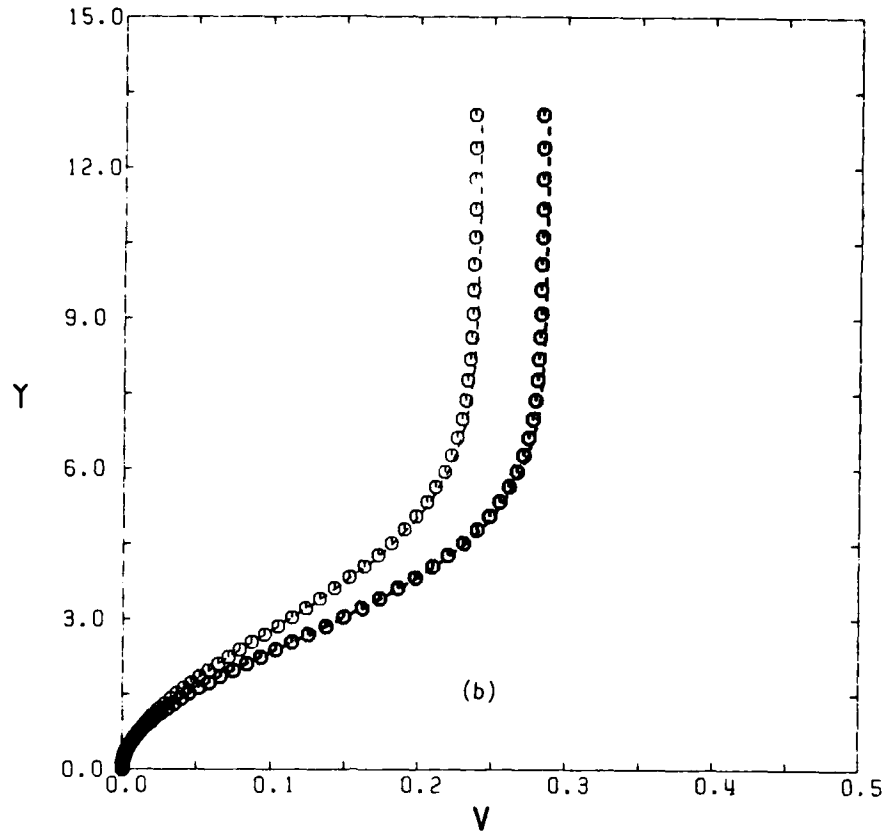
15.0
12.0
9.0
6.0
3.0
0.0
Y
0.0
0.1
0.2
0.3
0.4
0.5
V
(b)

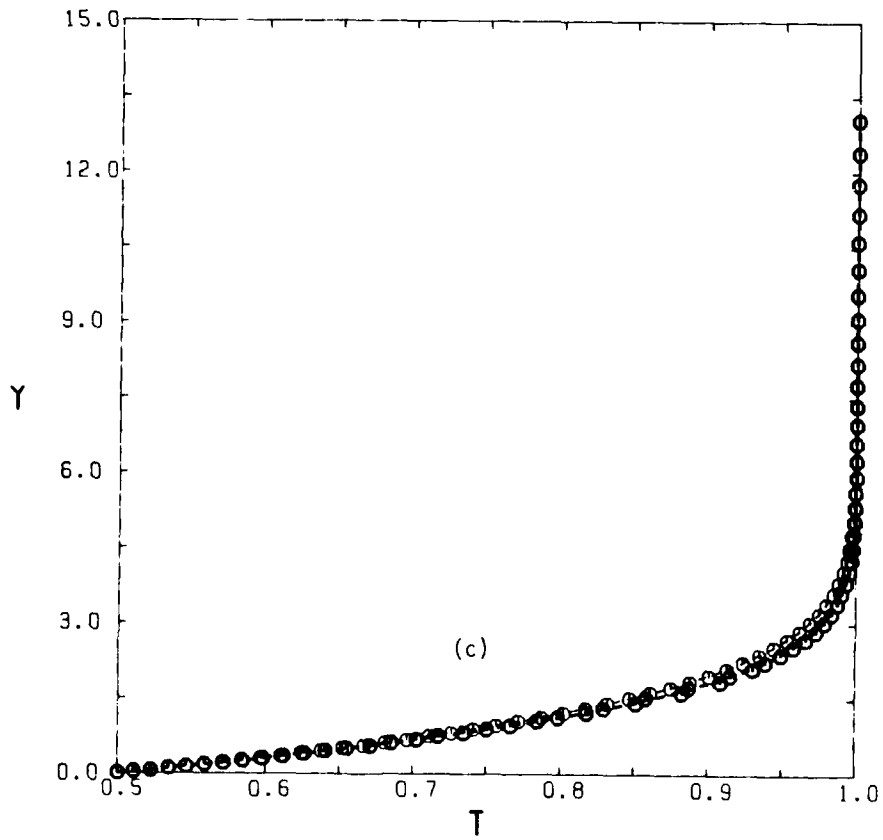
15.0
12.0
9.0
6.0
3.0
0.0
Y
0.5
0.6
0.7
0.8
0.9
1.0
T
(c)

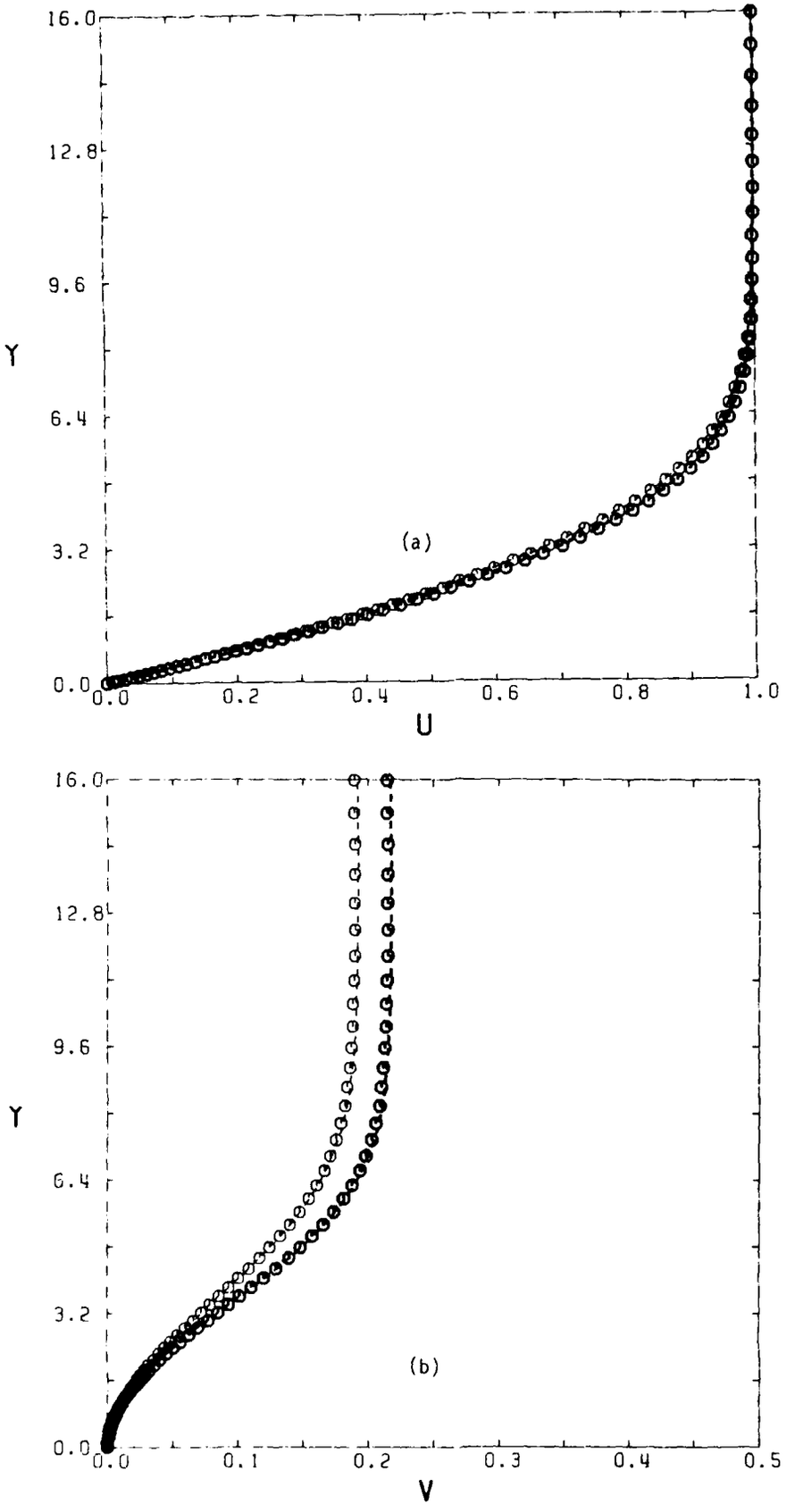

FIG. 16 COMPARISON BETWEEN FLOW PROFILES RESULTING FROM FOUR-POINT AND SIX-POINT SCHEMES IN NONEQUILIBRIUM REGION (x = 6.05).

(a) TANGENTIAL VELOCITY; (b) NORMAL VELOCITY; (c) TEMPERATURE.

FOUR-POINT SCHEME: ○ GAS; ● PARTICLE;
SIX-POINT SCHEME: --- GAS; ▬▬ PARTICLE.

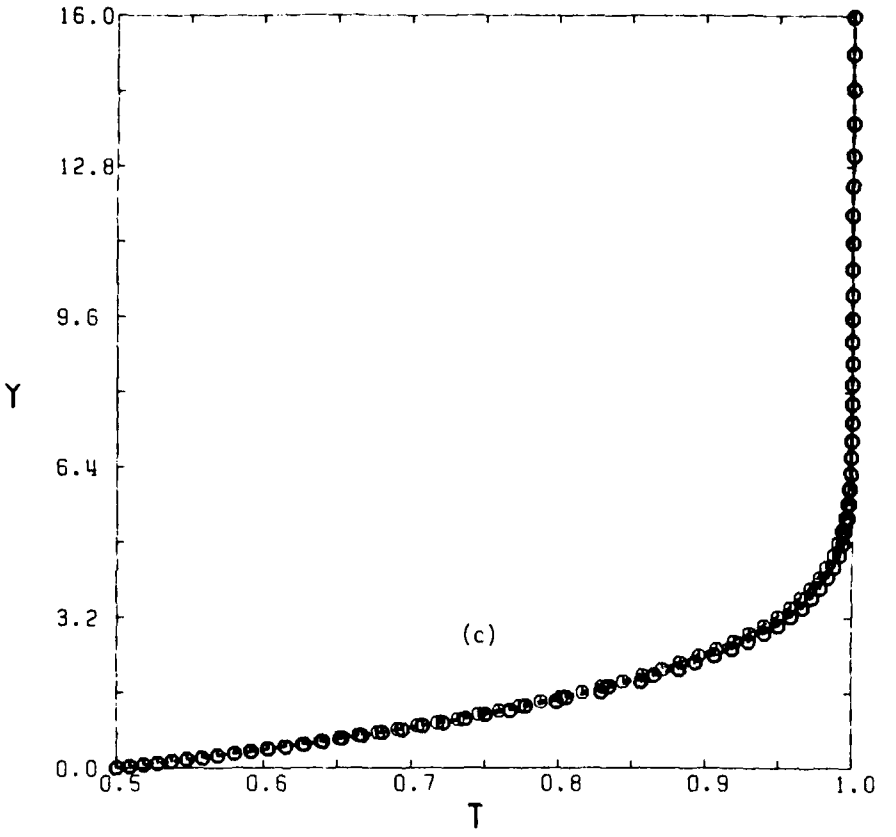

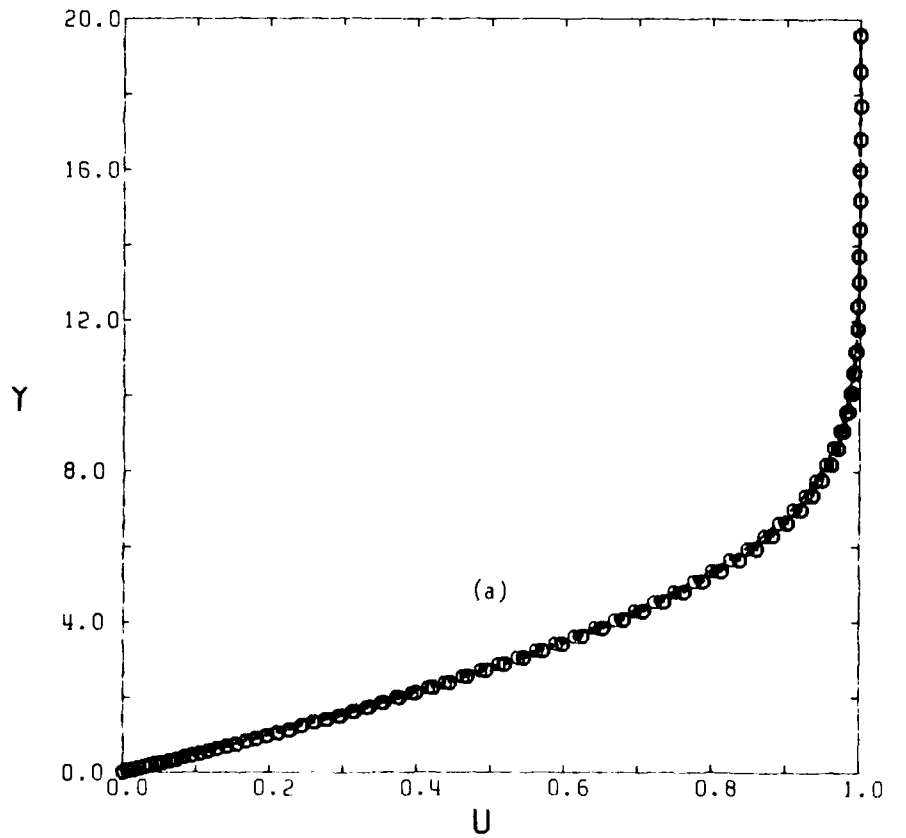

FIG. 17 COMPARISON BETWEEN FLOW PROFILES RESULTING FROM FOUR-POINT AND SIX-POINT SCHEMES IN SMALL-SLIP REGION (x = 10.05).

(a) TANGENTIAL VELOCITY; (b) NORMAL VELOCITY; (c) TEMPERATURE.

FOUR-POINT SCHEME: O GAS; O PARTICLE;
SIX-POINT SCHEME: --- GAS; --- PARTICLE.

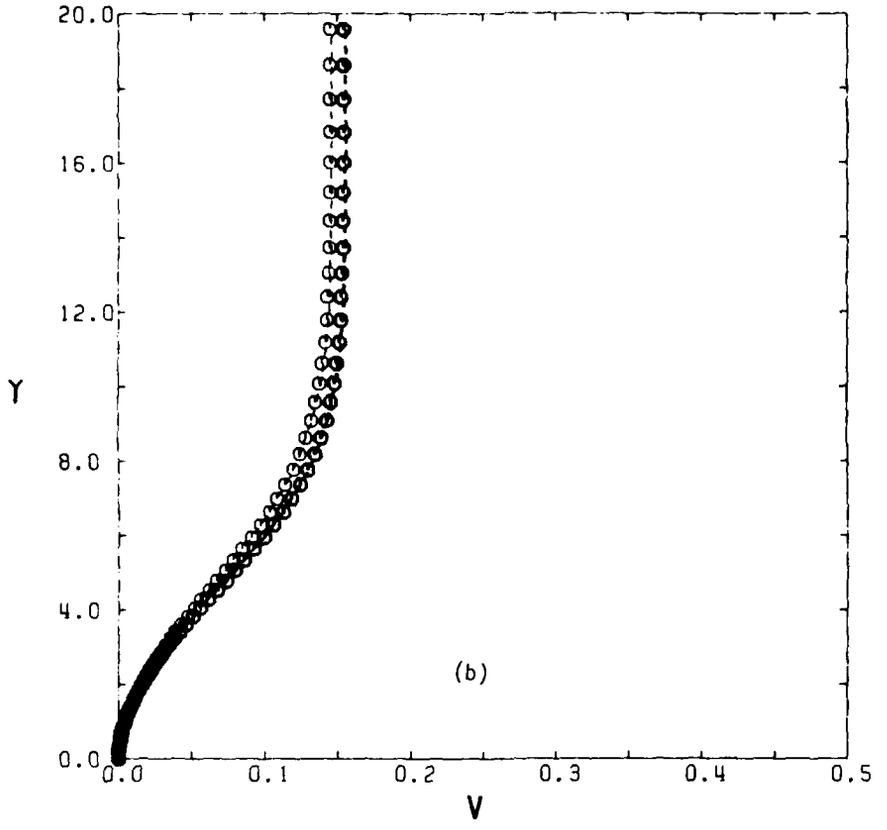
20.0
16.0
12.0
8.0
4.0
0.0
Y
0.0
0.1
0.2
0.3
0.4
0.5
V
(b)

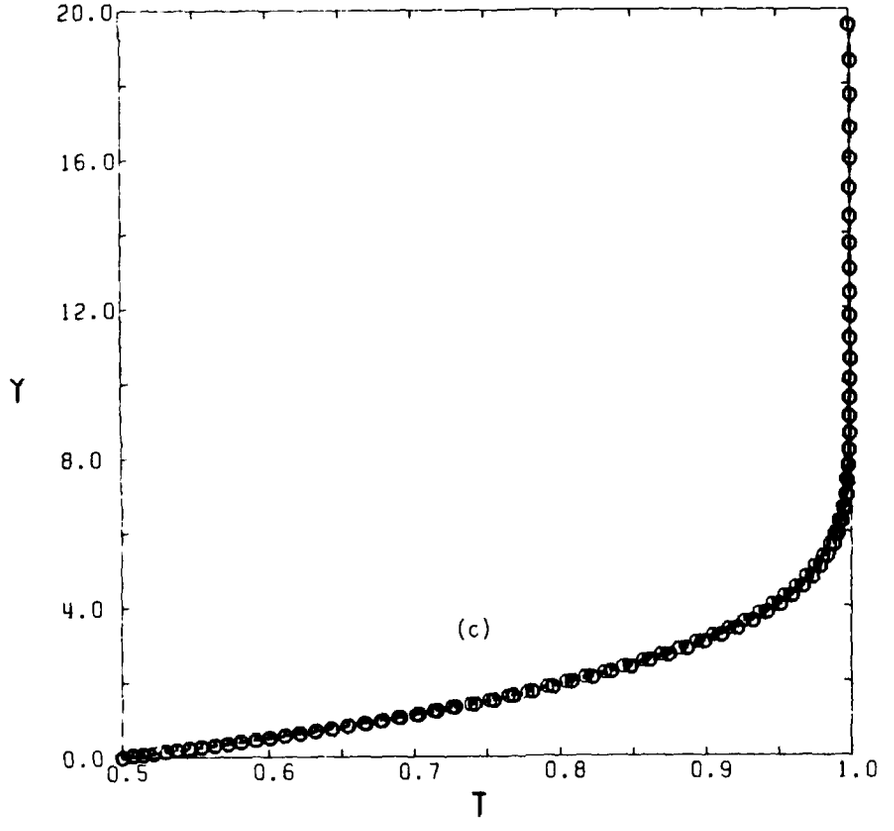
20.0
16.0
12.0
8.0
4.0
0.0
Y
0.5
0.6
0.7
0.8
0.9
1.0
T
(c)

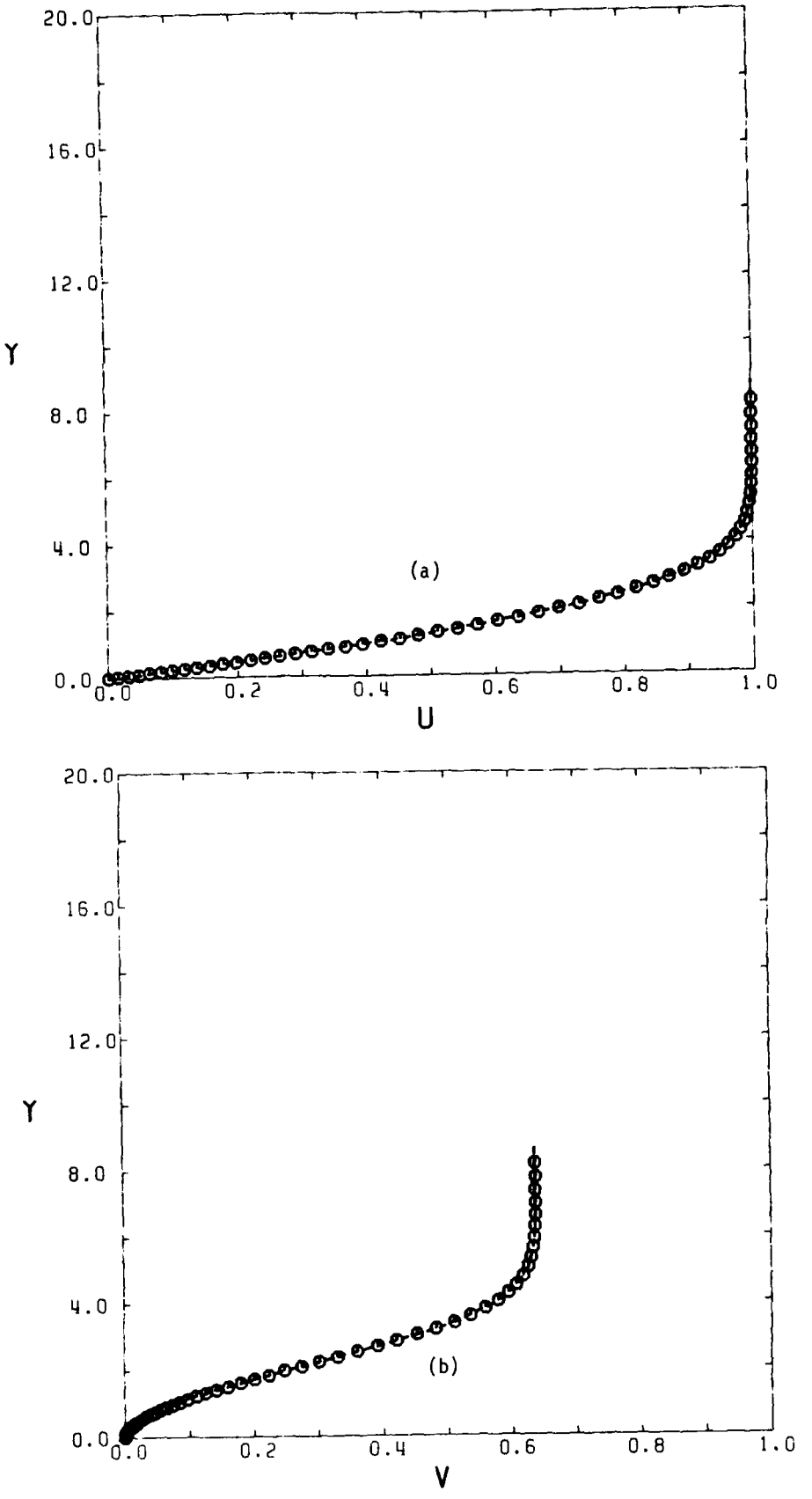

FIG. 18 COMPARISON BETWEEN FLOW PROFILES RESULTING FROM FINITE-DIFFERENCE SOLUTION WITH $\beta = 0$ AND SIMILARITY SOLUTION AT $x = 1.05$.

(a) TANGENTIAL VELOCITY; (b) NORMAL VELOCITY; (c) TEMPERATURE.

O FINITE-DIFFERENCE SOLUTION WITHOUT PARTICLES; —— PURE-GAS SIMILARITY SOLUTION.

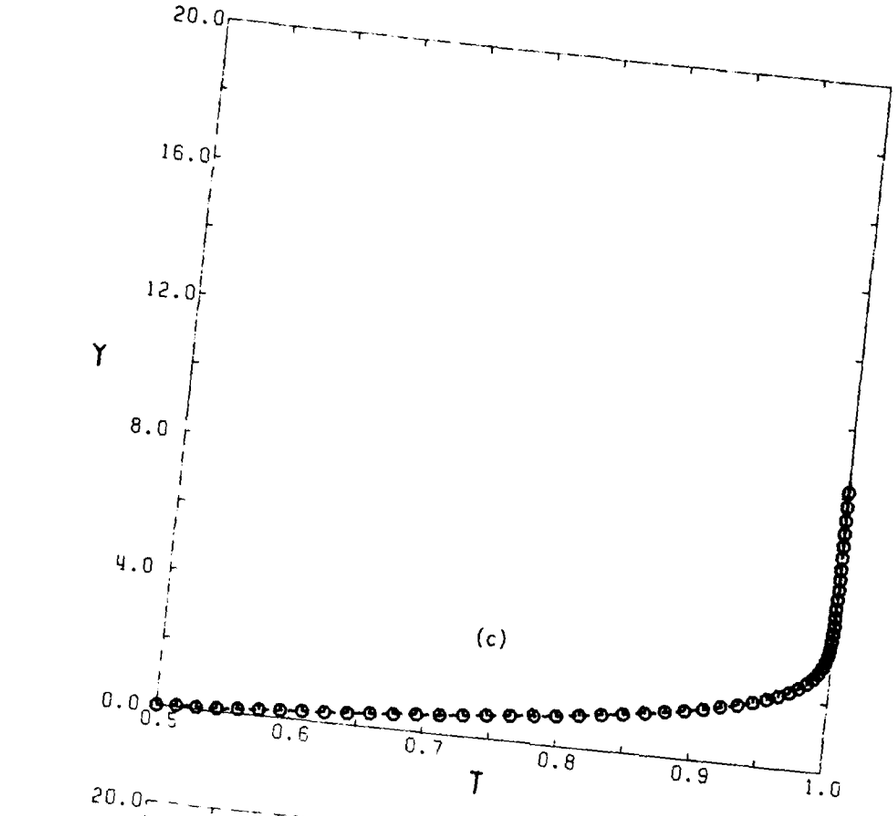

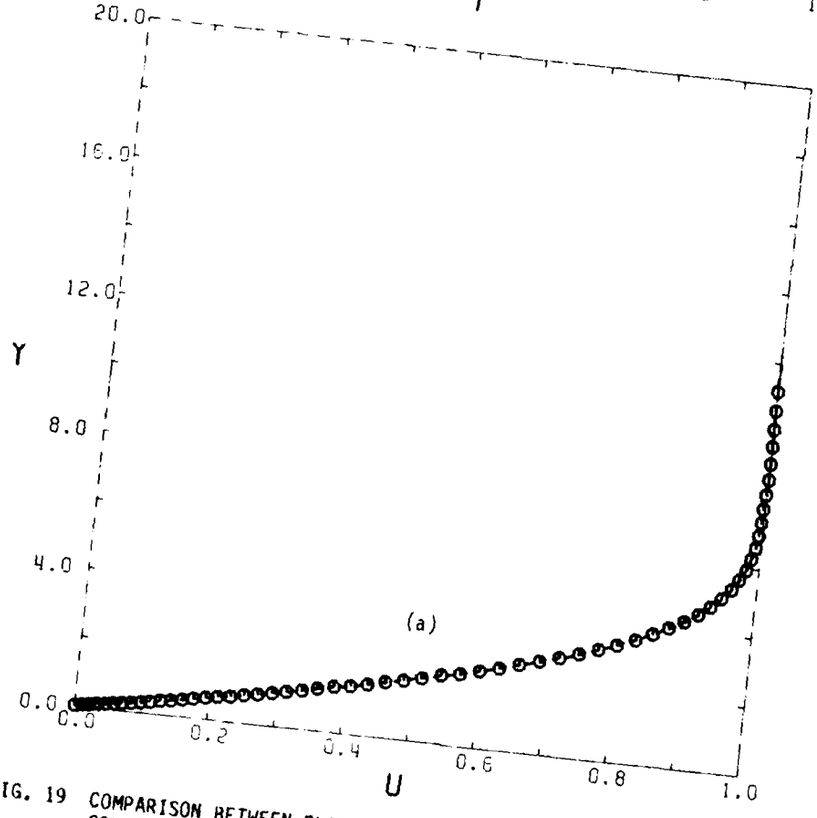

FIG. 19 COMPARISON BETWEEN FLOW PROFILES RESULTING FROM FINITE-DIFFERENCE SOLUTION WITH $\beta = 0$ AND SIMILARITY SOLUTION AT $x = 2.05$.

(a) TANGENTIAL VELOCITY; (b) NORMAL VELOCITY; (c) TEMPERATURE.

O FINITE-DIFFERENCE SOLUTION WITHOUT PARTICLES; --- PURE-GAS SIMILARITY SOLUTION.

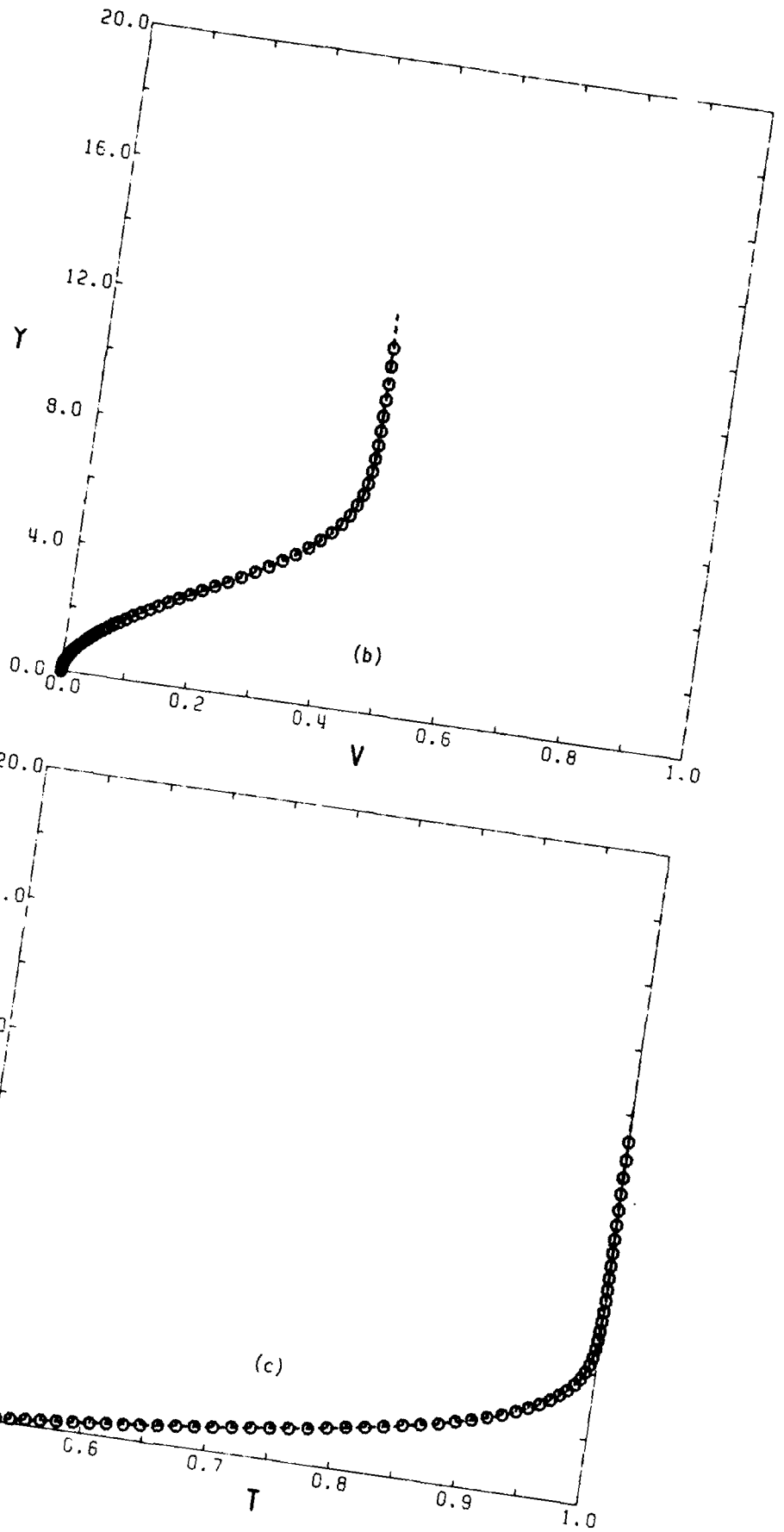
20.0
16.0
12.0
8.0
4.0
0.0
Y
0.0
0.2
0.4
0.6
0.8
1.0
V
(b)
20.0
16.0
12.0
8.0
4.0
0.0
Y
0.5
0.6
0.7
0.8
0.9
1.0
T
(c)

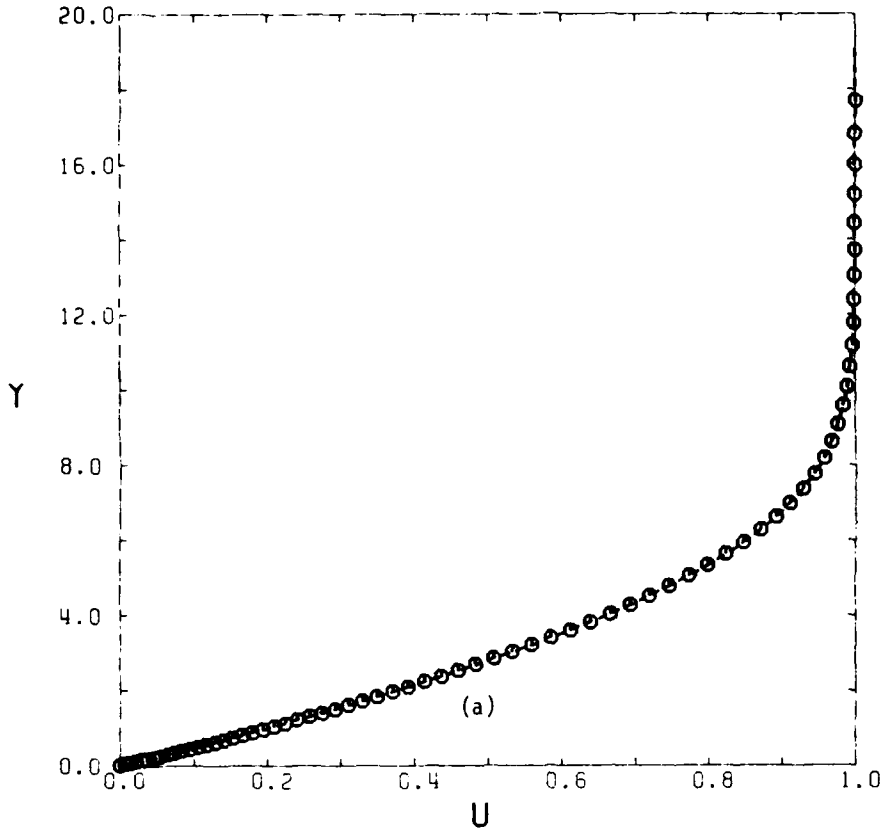

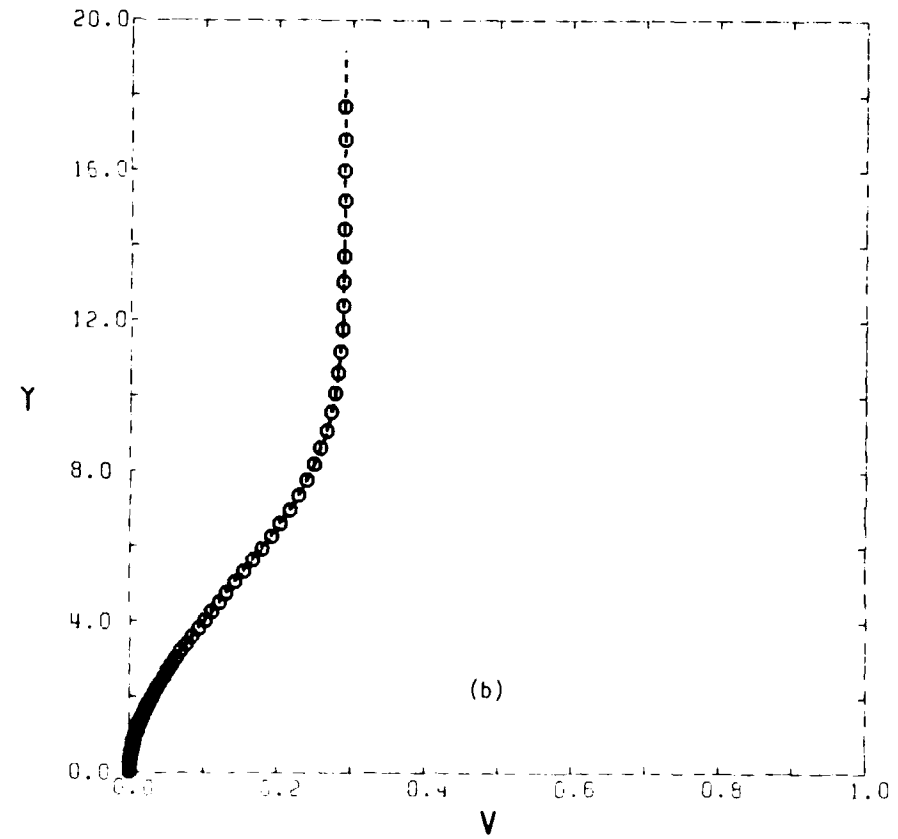

FIG. 20 COMPARISON BETWEEN FLOW PROFILES RESULTING FROM FINITE-DIFFERENCE SOLUTION WITH $\beta = 0$ AND SIMILARITY SOLUTION AT $x = 5.05$.

(a) TANGENTIAL VELOCITY; (b) NORMAL VELOCITY; (c) TEMPERATURE.

O FINITE-DIFFERENCE SOLUTION WITHOUT PARTICLES; ---- PURE-GAS SIMILARITY SOLUTION.

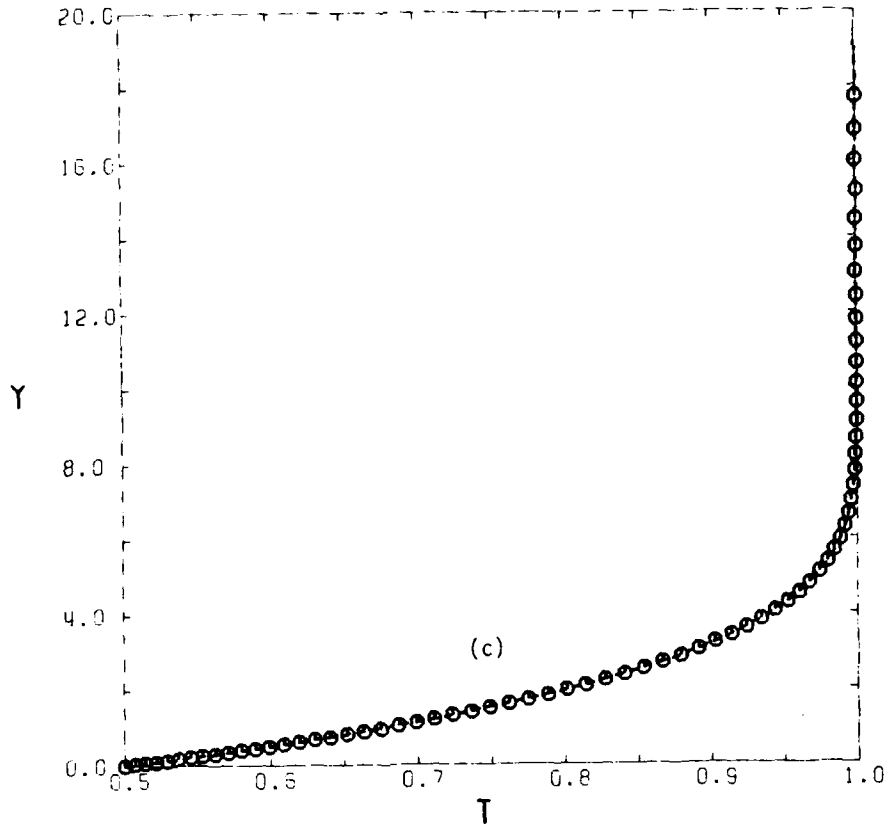

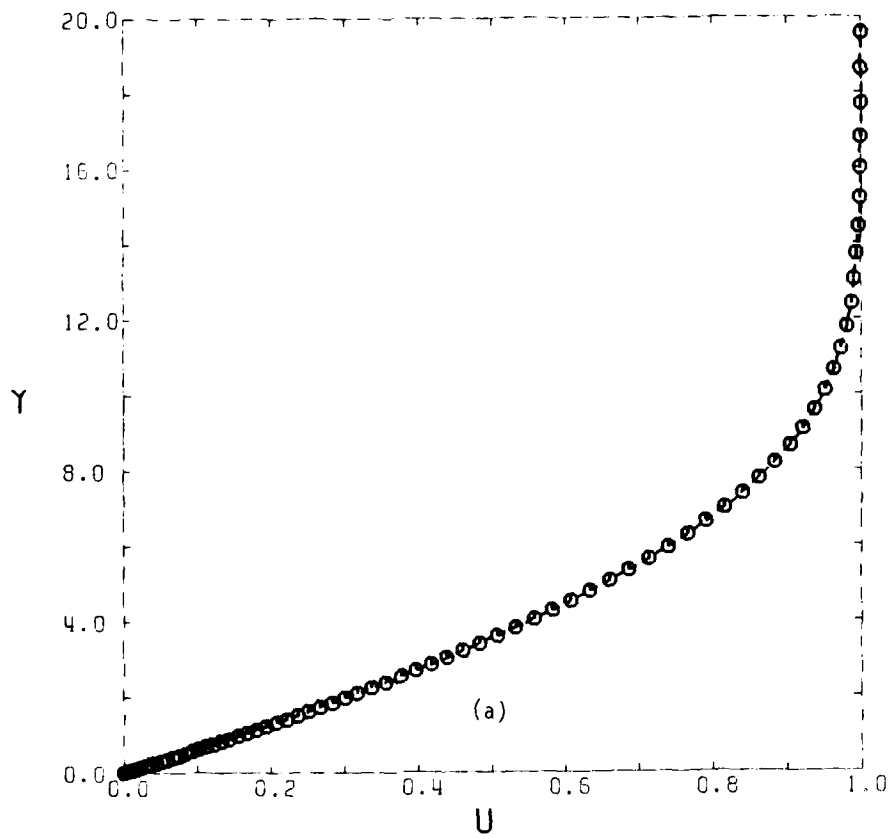

FIG. 21 COMPARISON BETWEEN FLOW PROFILES RESULTING FROM FINITE-DIFFERENCE SOLUTION WITH $\beta = 0$ AND SIMILARITY SOLUTION AT $x = 8.05$.

(a) TANGENTIAL VELOCITY; (b) NORMAL VELOCITY; (c) TEMPERATURE.

O FINITE-DIFFERENCE SOLUTION WITHOUT PARTICLES; ---- PURE-GAS SIMILARITY SOLUTION.

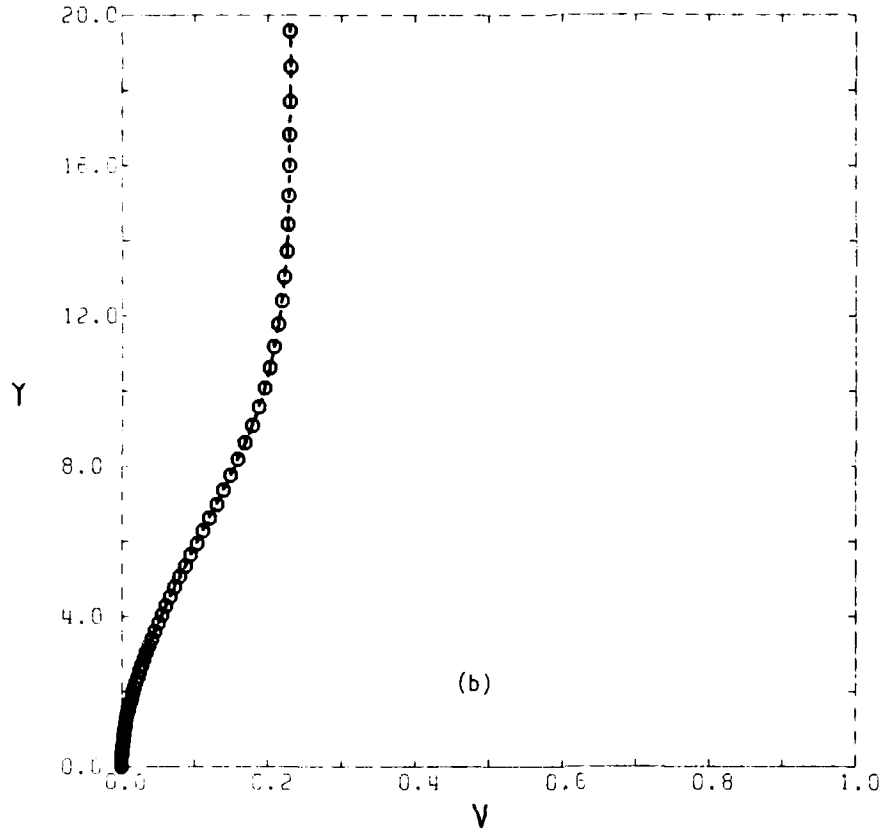
20.0
16.0
12.0
8.0
4.0
0.0
Y
0.0
0.2
0.4
0.6
0.8
1.0
V
(b)

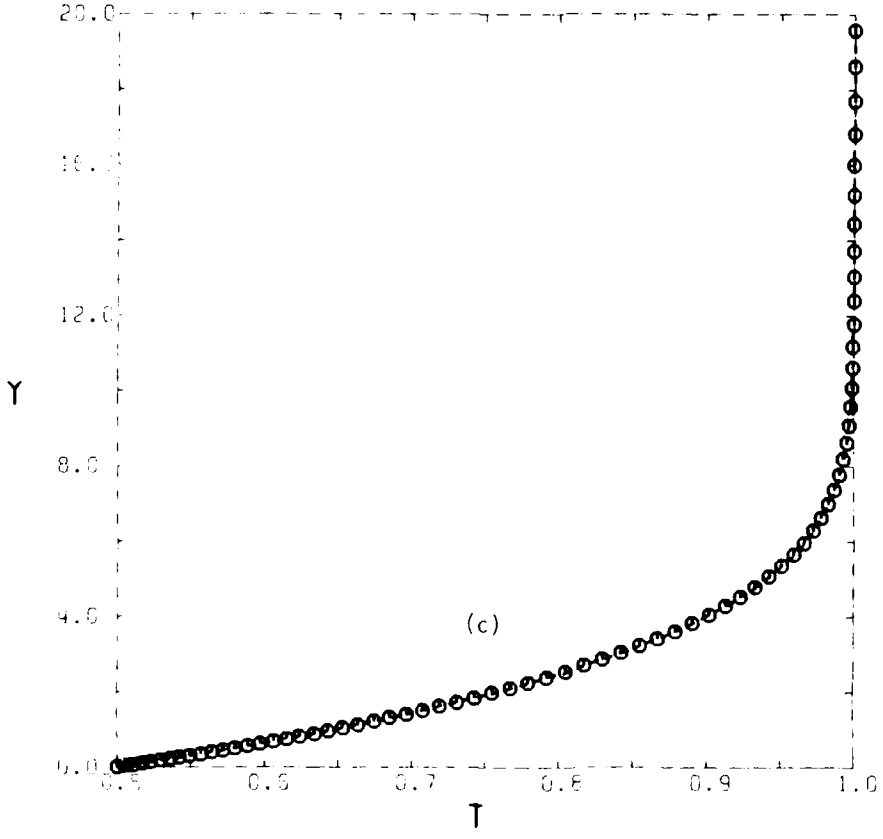
20.0
12.0
8.0
4.0
Y
0.5
0.6
0.7
0.8
0.9
1.0
T
(c)

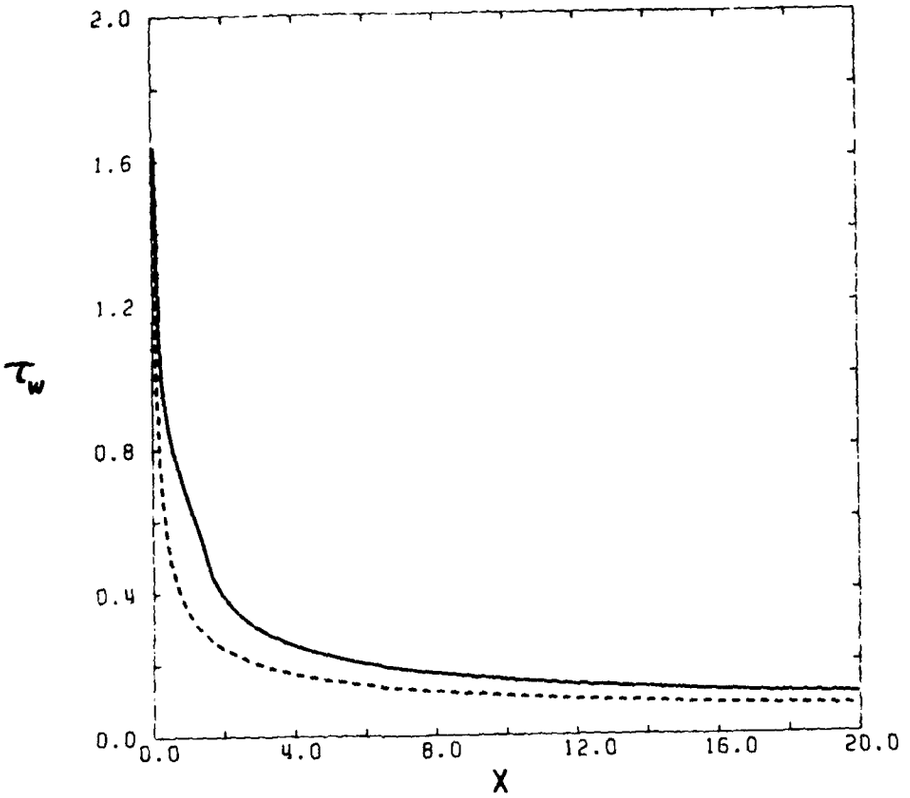

FIG. 22 SHEAR STRESS AT THE WALL AS A FUNCTION OF DISTANCE x: ——— WITH PARTICLES; ---- WITHOUT PARTICLES.

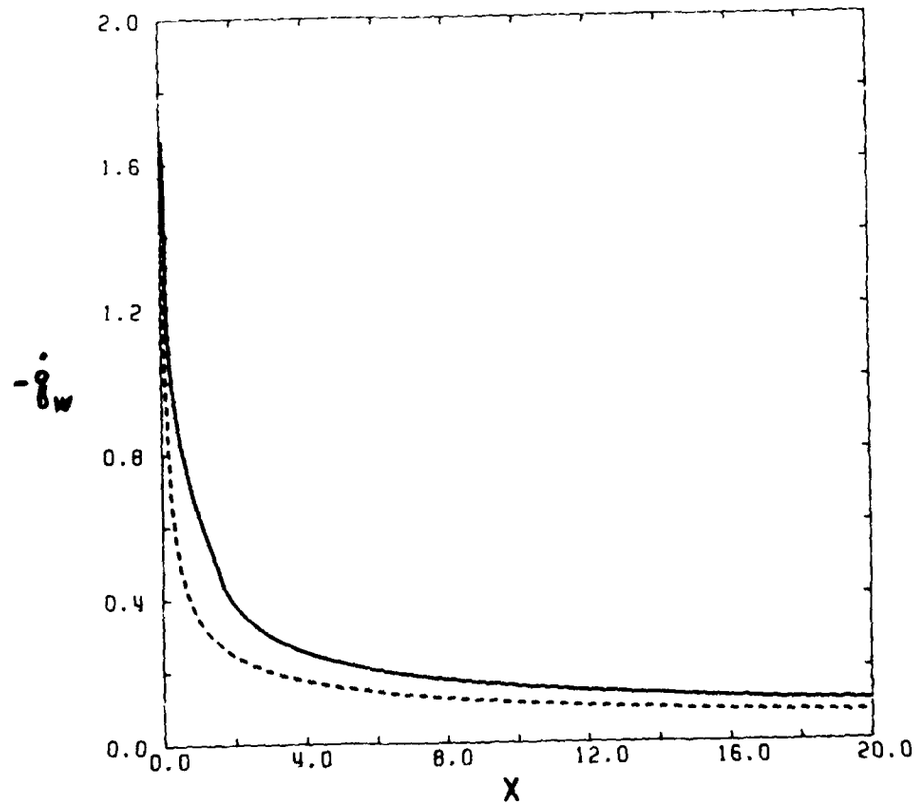

FIG. 23 WALL HEAT-TRANSFER RATE AS A FUNCTION OF DISTANCE x: ——— WITH PARTICLES; ---- WITHOUT PARTICLES.

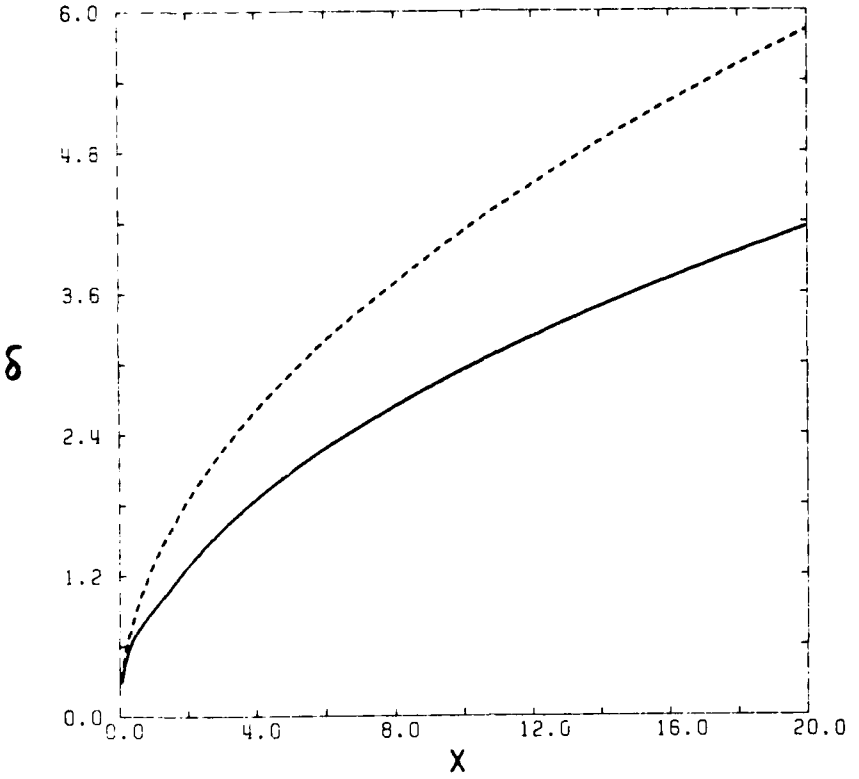

FIG. 24 NONDIMENSIONAL DISPLACEMENT THICKNESS AS A FUNCTION OF DISTANCE x: ——— WITH PARTICLES; ---- WITHOUT PARTICLES.

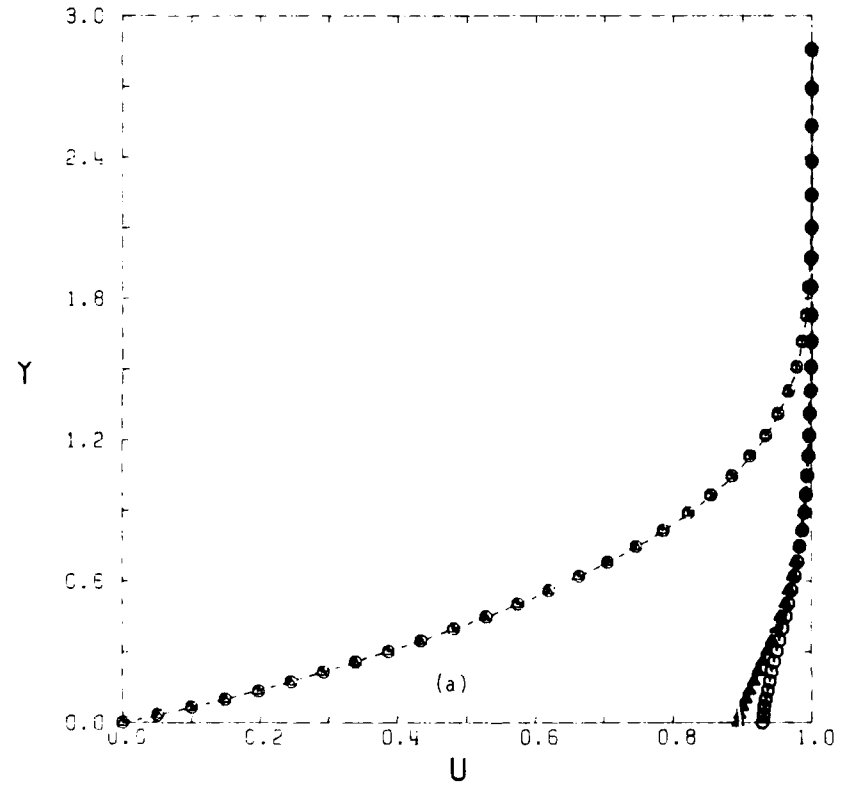

FIG. 25 FLOW PROFILES WITH THREE DIFFERENT TYPES OF INITIAL PROFILES IN QUASI-FROZEN FLOW REGION (x = 0.15).

(a) TANGENTIAL VELOCITY; (b) NORMAL VELOCITY; (c) TEMPERATURE.

ZEROTH-ORDER ASYMPTOTIC PROFILES: ○ GAS; ● PARTICLES;
EXTENDED WU-TYPE PROFILES: △ GAS; ▲ PARTICLES;
FIRST-ORDER ASYMPTOTIC PROFILES: --- GAS; ——— PARTICLES.

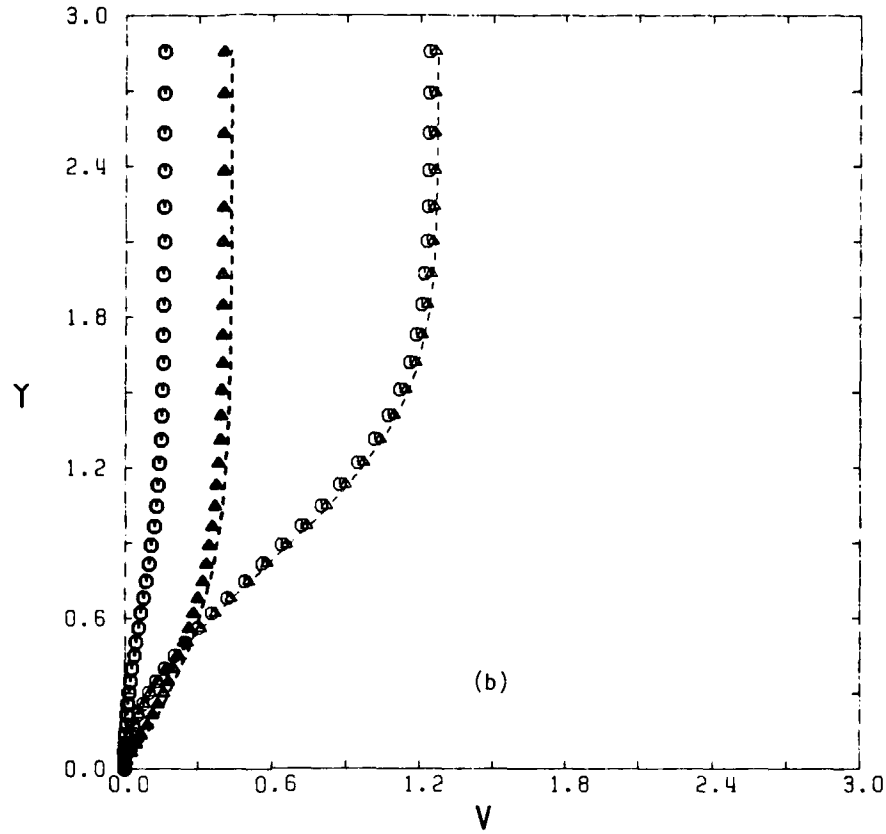
3.0
2.4
1.8
1.2
0.6
0.0
Y
0.0
0.6
1.2
1.8
2.4
3.0
V
(b)

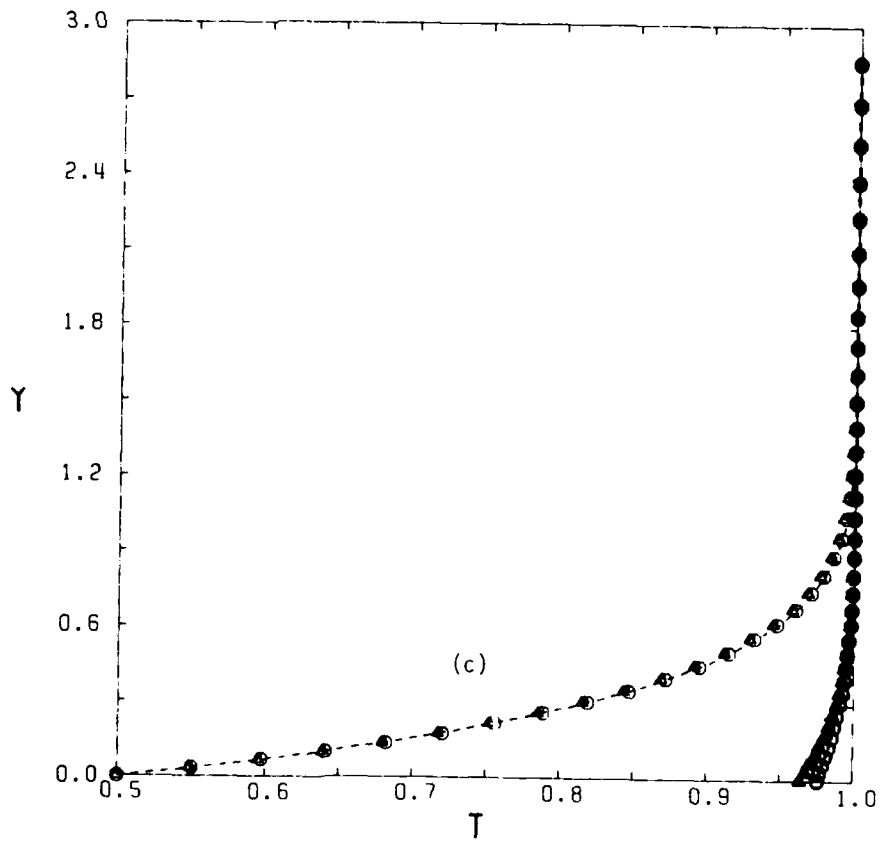
3.0
2.4
1.8
1.2
0.6
0.0
Y
0.5
0.6
0.7
0.8
0.9
1.0
T
(c)

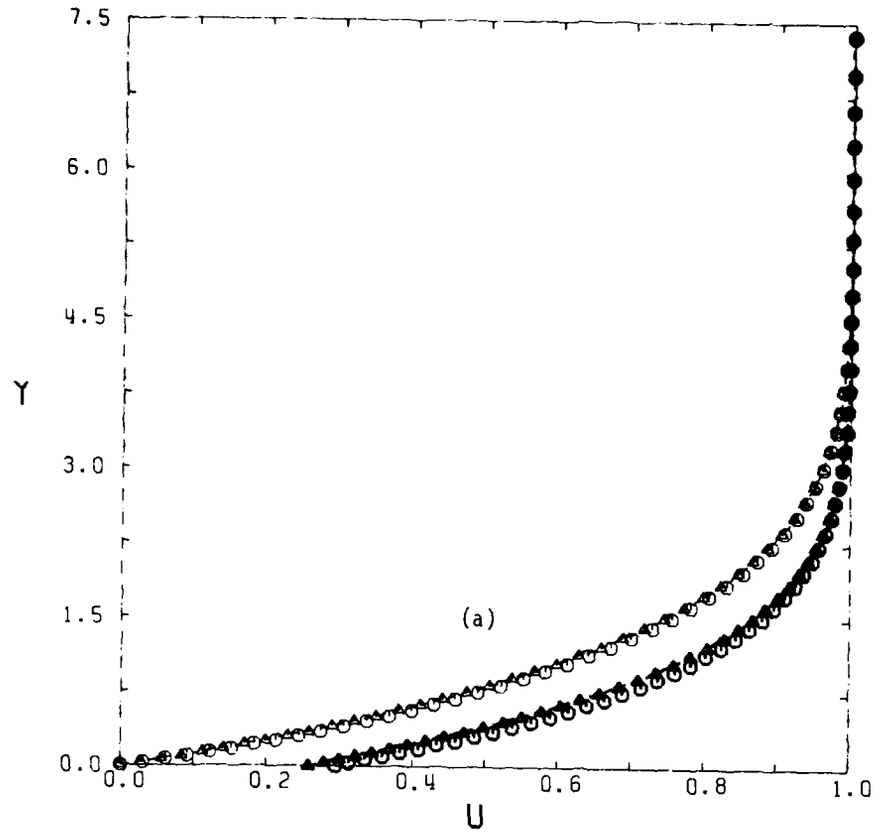

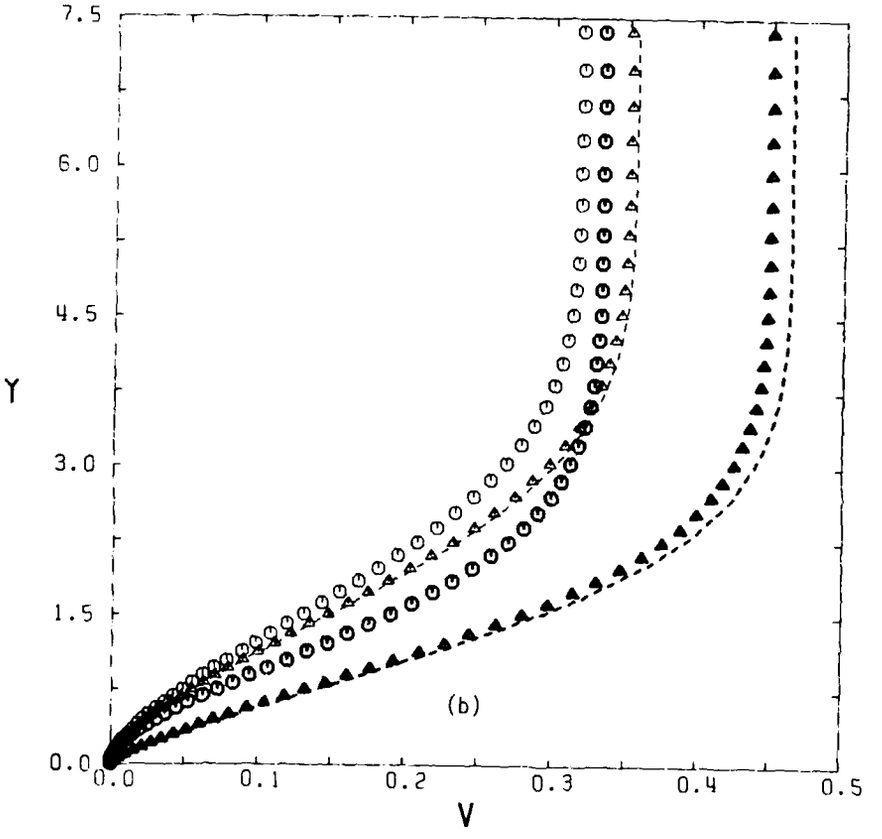

FIG. 26 FLOW PROFILES WITH THREE DIFFERENT TYPES OF INITIAL PROFILES IN NONEQUILIBRIUM FLOW REGION (x = 1.05).

(a) TANGENTIAL VELOCITY; (b) NORMAL VELOCITY; (c) TEMPERATURE.

ZEROTH-ORDER ASYMPTOTIC PROFILES: ○ GAS; ● PARTICLES;
EXTENDED WU-TYPE PROFILES: △ GAS; ▲ PARTICLES;
FIRST-ORDER ASYMPTOTIC PROFILES: ---GAS; ▬▬ PARTICLES.

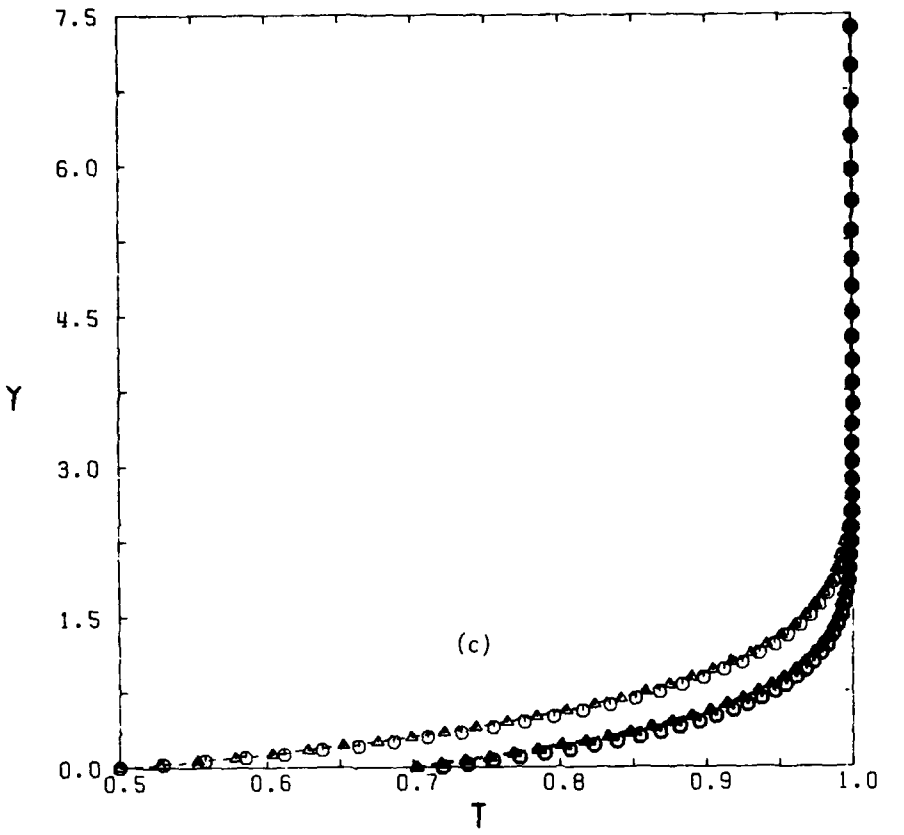

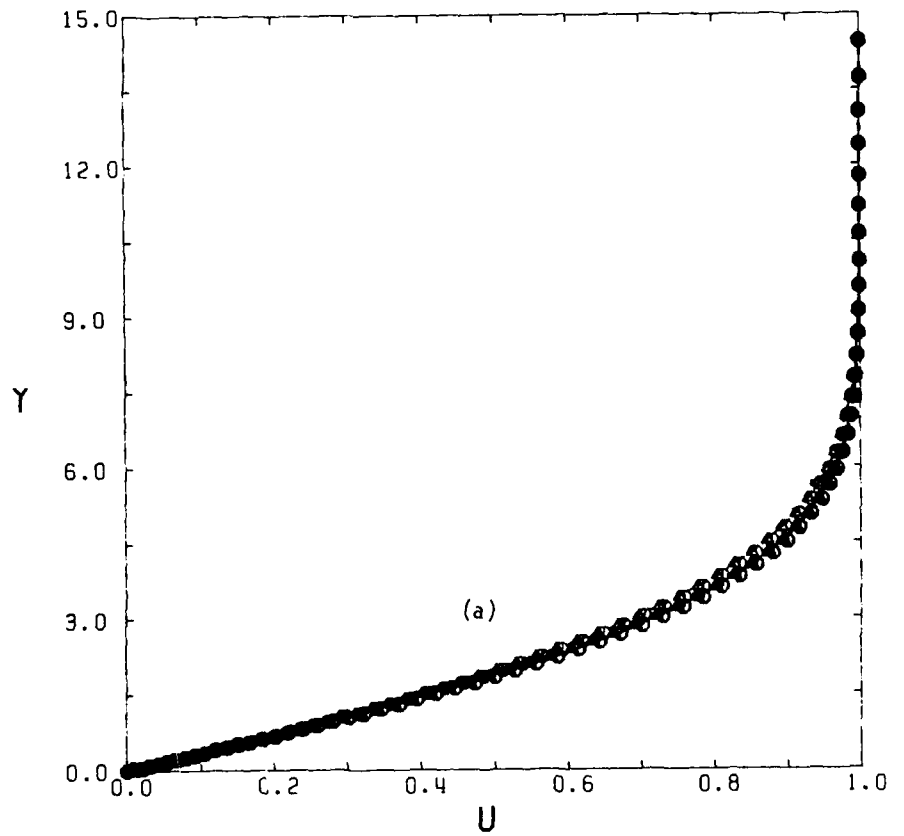

FIG. 27 FLOW PROFILES WITH THREE DIFFERENT TYPES OF INITIAL PROFILES IN NEAR-EQUILIBRIUM FLOW REGION (x = 5.05).

(a) TANGENTIAL VELOCITY; (b) NORMAL VELOCITY; (c) TEMPERATURE.

ZEROTH-ORDER ASYMPTOTIC PROFILES: ○ GAS; ● PARTICLES;
EXTENDED WU-TYPE PROFILES: △ GAS; ▲ PARTICLES;
FIRST-ORDER ASYMPTOTIC PROFILES: --- GAS; ▬▬ PARTICLES.

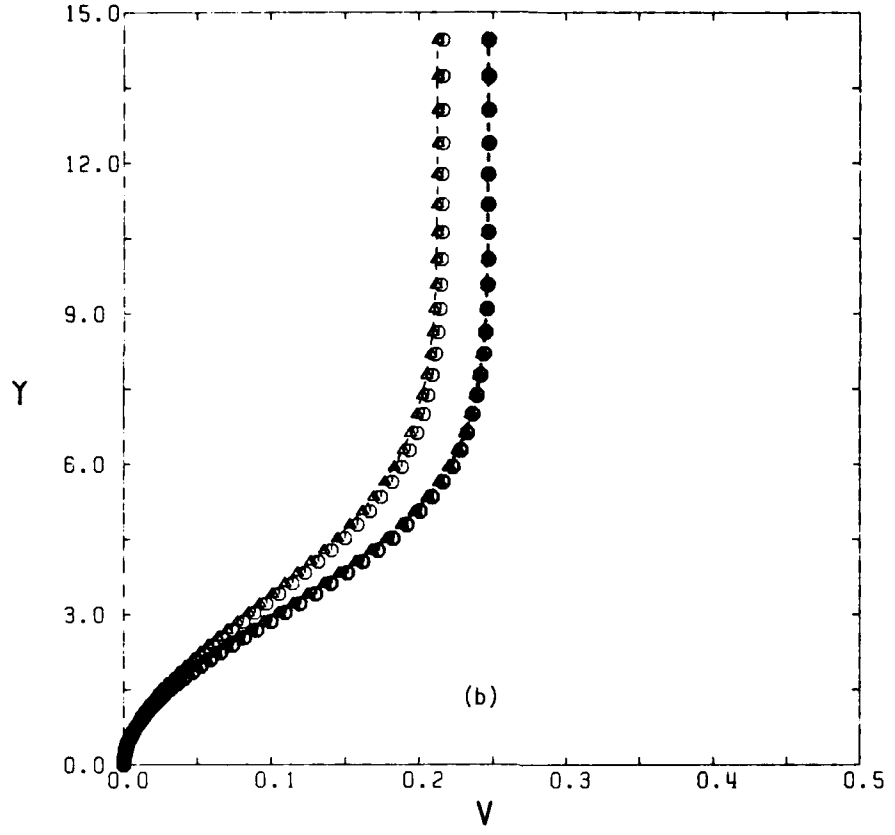
15.0
12.0
9.0
6.0
3.0
0.0
Y
0.0
0.1
0.2
0.3
0.4
0.5
V
(b)

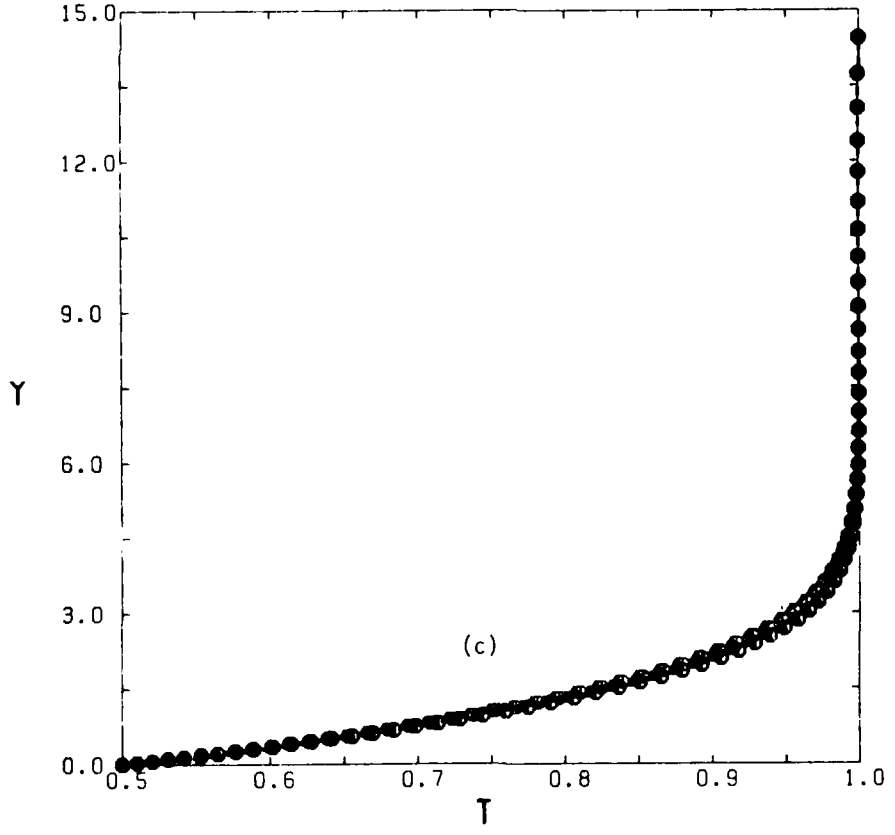
15.0
12.0
9.0
6.0
3.0
0.0
Y
0.5
0.6
0.7
0.8
0.9
1.0
T
(c)

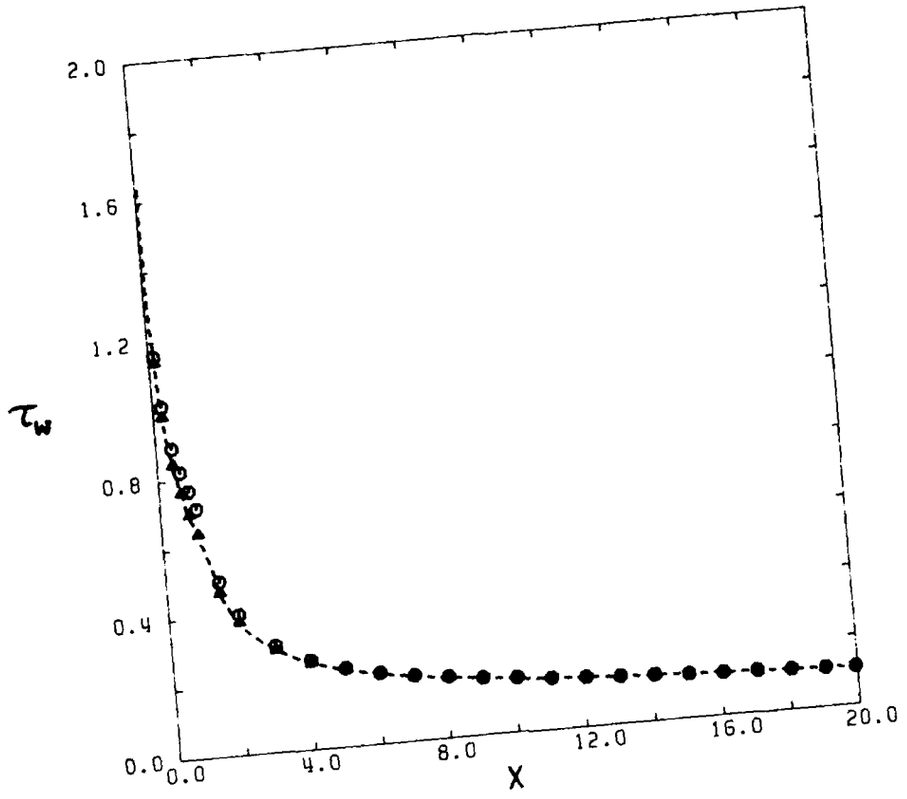

FIG. 28 SHEAR STRESS AT THE WALL WITH THREE DIFFERENT TYPES OF INITIAL PROFILES.

○ ZEROTH-ORDER ASYMPTOTIC PROFILES; △ EXTENDED WU-TYPE PROFILES;
---FIRST-ORDER ASYMPTOTIC PROFILES.

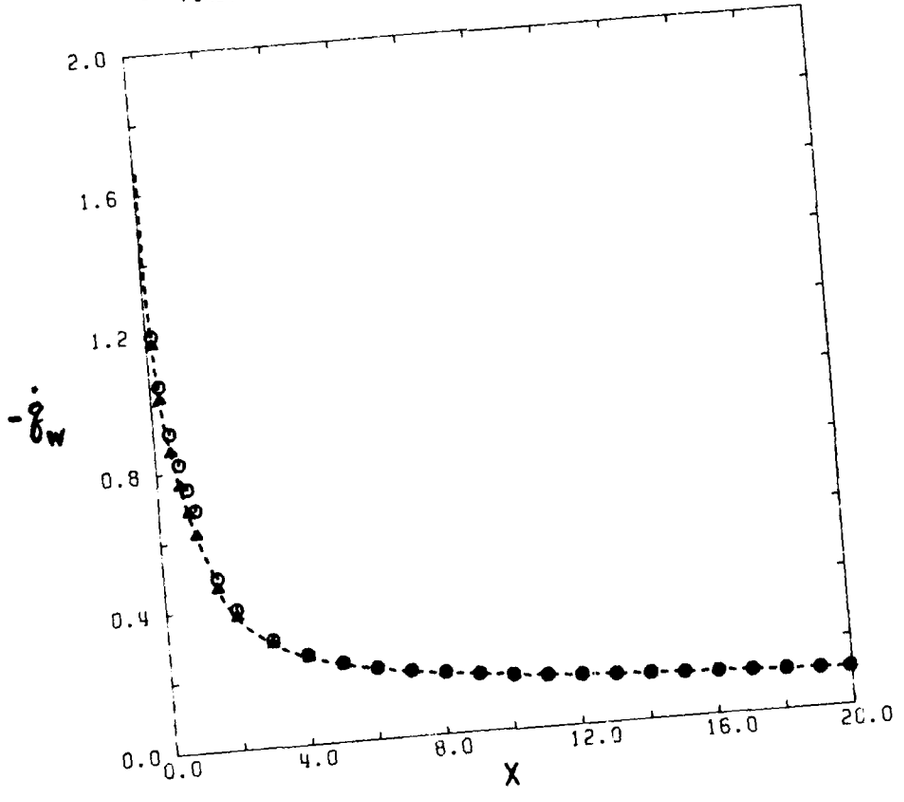

FIG. 29 WALL HEAT-TRANSFER RATE WITH THREE DIFFERENT TYPES OF INITIAL PROFILES.

○ ZEROTH-ORDER ASYMPTOTIC PROFILES; △ EXTENDED WU-TYPE PROFILES;
---FIRST-ORDER ASYMPTOTIC PROFILES.

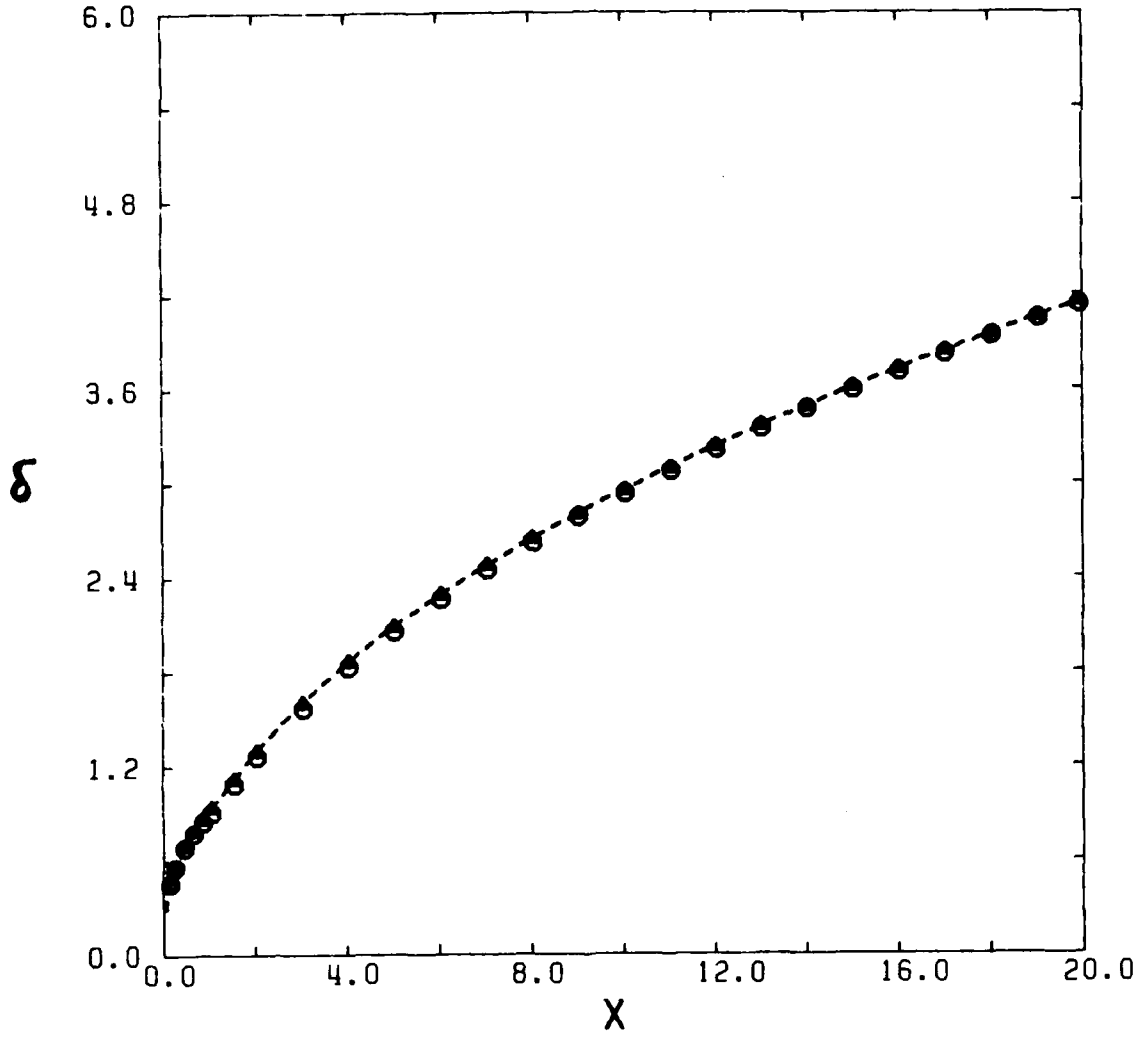

FIG. 30 NONDIMENSIONAL DISPLACEMENT THICKNESS WITH THREE DIFFERENT TYPES OF INITIAL PROFILES.

O ZEROTH-ORDER ASYMPTOTIC PROFILES; Δ EXTENDED WU-TYPE PROFILES;
---FIRST-ORDER ASYMPTOTIC PROFILES.

APPENDIX A

DERIVATION OF THE FINITE-DIFFERENCE EQUATIONS WITH A SIX-POINT SCHEME

The momentum equation of the gas phase is

$$\rho u \frac{\partial u}{\partial x} + \rho v \frac{\partial u}{\partial y} = \mu \frac{\partial^2 u}{\partial y^2} + \frac{d\mu}{dT} \frac{\partial T}{\partial y} \frac{\partial u}{\partial y} + \rho_p (u_p - u) \mu D \tag{A-1}$$

or

$$\rho u \frac{\partial u}{\partial x} + (\rho v - \mu' T_y) \frac{\partial u}{\partial y} - \mu \frac{\partial^2 u}{\partial y^2} = \rho_p u_p \mu D - \rho_p u \mu D \tag{A-2}$$

where

$$\mu' = \frac{d\mu}{dT}, \qquad T_y = \frac{\partial T}{\partial y} = \frac{T_{n+1} + (K^2-1)T_n - K^2 T_{n-1}}{(1+K)\Delta y_n}$$

Substituting the expressions for difference quotients (3.1)-(3.4), Eq. (A-2) becomes

$$(\rho u)_{m+\theta,n} \frac{1}{\Delta x} (u_{m+1,n} - u_{m,n}) + (\rho v - \mu' T_y)_{m+\theta,n} \{ \frac{\theta}{(1+K)\Delta y_n} [u_{m+1,n+1}$$

$$+ (K^2-1) u_{m+1,n} - K^2 u_{m+1,n-1}] + \frac{1-\theta}{(1+K)\Delta y_n} \Delta u_{m,n} \}$$

$$- \mu_{m+\theta,n} \{ \frac{2\theta K}{(1+K)\Delta y_n^2} [u_{m+1,n+1} - (K+1) u_{m+1,n} + K u_{m+1,n-1}]$$

$$+ \frac{2(1-\theta)K}{(1+K)\Delta y_n^2} \Delta^2 u_{m,n} \}$$

$$= (\rho_p u_p \mu D)_{m+\theta,n} - [\theta (\rho_p \mu D)_{m+1,n} u_{m+1,n} + (1-\theta)(\rho_p \mu D)_{m,n} u_{m,n}] \tag{A-3}$$

Multiplying by Δx and rearranging Eq. (A-3), the finite-difference form of the momentum equation can be obtained:

$$A_n^1 u_{m+1,n+1} + B_n^1 u_{m+1,n} + C_n^1 u_{m+1,n-1} = D_n^1 \qquad \text{(A-4)}$$

where the coefficients have the following expressions:

$$A_n^1 = a_n(\rho v - \mu' T_y)_{m+\theta,n} - c_n \mu_{m+\theta,n}$$

$$B_n^1 = (\rho u)_{m+\theta,n} + a_n(K^2-1)(\rho v - \mu' T_y)_{m+\theta,n} + c_n(K+1)\mu_{m+\theta,n} + \theta\Delta x(\rho_p \mu D)_{m+1,n}$$

$$C_n^1 = -a_n K^2(\rho v - \mu' T_y)_{m+\theta,n} - c_n K \mu_{m+\theta,n} \qquad \text{(A-5)}$$

$$D_n^1 = [(\rho u)_{m+\theta,n} - (1-\theta)\Delta x(\rho_p \mu D)_{m,n}]u_{m,n} - b_n(\rho v - \mu' T_y)_{m+\theta,n}\Delta u_{m,n}$$

$$+ d_n \mu_{m+\theta,n} \Delta^2 u_{m,n} + \Delta x(\rho_p u_p \mu D)_{m+\theta,n}$$

The energy equation of the gas phase is

$$\rho u \frac{\partial T}{\partial x} + \rho v \frac{\partial T}{\partial y} = \frac{\mu}{Pr} \frac{\partial^2 T}{\partial y^2} + \frac{1}{Pr} \frac{d\mu}{dT} \left(\frac{\partial T}{\partial y}\right)^2 + Ec\ \mu\left(\frac{\partial u}{\partial y}\right)^2 + Ec\ \rho_p[(u_p - u)^2$$

$$+ \frac{1}{Re_\infty}(v_p - v)^2]\mu D + \frac{1}{3Pr}\rho_p(T_p - T)\mu Nu \qquad \text{(A-6)}$$

or

$$\rho u \frac{\partial T}{\partial x} + \left(\rho v - \frac{\mu'}{Pr} T_y\right) \frac{\partial T}{\partial y} - \frac{\mu}{Pr} \frac{\partial^2 T}{\partial y^2} = Ec\ \mu\left(\frac{\partial u}{\partial y}\right)^2 + Ec\ \rho_p[(u_p - u)^2$$

$$+ \frac{1}{Re_\infty}(v_p - v)^2]\mu D + \frac{1}{3Pr}\rho_p T_p \mu Nu - \frac{1}{3Pr}\rho_p T \mu Nu \qquad \text{(A-7)}$$

Using a similar procedure, Eq. (A-7) is discretized as

$$(\rho u)_{m+\theta,n} \frac{1}{\Delta x}(T_{m+1,n} - T_{m,n}) + \left(\rho v - \frac{\mu'}{Pr} T_y\right)_{m+\theta,n} \left\{\frac{\theta}{(1+K)\Delta y_n}[T_{m+1,n+1}\right.$$

Continued

$$+ (K^2-1)T_{m+1,n} - K^2T_{m+1,n-1}] + \frac{1-\theta}{(1+K)\Delta y_n}\Delta T_{m,n}\}$$

$$- \left(\frac{\mu}{Pr}\right)_{m+\theta,n}\{\frac{2\theta K}{(1+K)\Delta y_n{}^2}[T_{m+1,n+1} - (K+1)T_{m+1,n} + KT_{m+1,n-1}]$$

$$+ \frac{2(1-\theta)K}{(1+K)\Delta y_n{}^2}\Delta^2 T_{m,n}\}$$

$$= \{Ec\ \mu\ u_y{}^2 + Ec\ \rho_p[(u_p - u)^2 + \frac{1}{Re_\infty}(v_p - v)^2]\mu D + \frac{1}{3Pr}\rho_p T_p \mu Nu\}_{m+\theta,n}$$

$$- [\theta(\frac{1}{3Pr}\rho_p \mu Nu)_{m+1,n}T_{m+1,n} + (1-\theta)(\frac{1}{3Pr}\rho_p \mu Nu)_{m,n}T_{m,n}] \qquad (A\text{-}8)$$

The difference equation for the energy conservation of the gas is

$$A_n^2\ T_{m+1,n+1} + B_n^2\ T_{m+1,n} + C_n^2\ T_{m+1,n-1} = D_n^2 \qquad (A\text{-}9)$$

where

$$A_n^2 = a_n(\rho v - \frac{\mu'}{Pr}T_y)_{m+\theta,n} - c_n(\frac{\mu}{Pr})_{m+\theta,n}$$

$$B_n^2 = (\rho u)_{m+\theta,n} + a_n(K^2-1)(\rho v - \frac{\mu'}{Pr}T_y)_{m+\theta,n} + c_n(K+1)(\frac{\mu}{Pr})_{m+\theta,n}$$

$$+ \theta\Delta x(\frac{1}{3Pr}\rho_p \mu Nu)_{m+1,n} \qquad (A\text{-}10)$$

$$C_n^2 = -a_nK^2(\rho v - \frac{\mu'}{Pr}T_y)_{m+\theta,n} - c_nK(\frac{\mu}{Pr})_{m+\theta,n}$$

$$D_n^2 = [(\rho u)_{m+\theta,n} - (1-\theta)\Delta x(\frac{1}{3Pr}\rho_p \mu Nu)_{m,n}]T_{m,n} - b_n(\rho v - \frac{\mu'}{Pr}T_y)_{m+\theta,n}\Delta T_{m,n}$$

$$+ d_n(\frac{\mu}{Pr})_{m+\theta,n}\Delta^2 T_{m,n} + \Delta x\{Ec\ \mu u_y{}^2 + Ec\rho_p[u_p - u)^2 + \frac{1}{Re_\infty}(v_p - v)^2]\mu D$$

Continued

$$+ \frac{1}{3Pr} \rho_p \bar{\rho} \mu Nu \}_{m+\theta,n}$$

The x-momentum equation of the particle phase is

$$u_p \frac{\partial u_p}{\partial x} + v_p \frac{\partial u_p}{\partial y} = -(u_p - u)\mu D = u\mu D - u_p \mu D \qquad \text{(A-11)}$$

Discretizing Eq. (A-11) yields

$$u_{p_{m+\theta,n}} \frac{1}{\Delta x} (u_{p_{m+1,n}} - u_{p_{m,n}}) + v_{p_{m+\theta,n}} \{\frac{\theta}{(1+K)\Delta y_n} [u_{p_{m+1,n+1}}$$

$$+ (K^2-1)u_{p_{m+1,n}} - K^2 u_{p_{m+1,n-1}}] + \frac{1-\theta}{(1+K)\Delta y_n} \Delta u_{p_{m,n}}\}$$

$$= (u\mu D)_{m+\theta,n} - [\theta(\mu D)_{m+1,n} u_{p_{m+1,n}} + (1-\theta)(\mu D)_{m,n} u_{p_{m,n}}] \qquad \text{(A-12)}$$

Therefore

$$A_n^7 \, u_{p_{m+1,n+1}} + B_n^7 \, u_{p_{m+1,n}} + C_n^7 \, u_{p_{m+1,n-1}} = D_n^7 \qquad \text{(A-13)}$$

where

$$A_n^7 = a_n \, v_{p_{m+\theta,n}}$$

$$B_n^7 = u_{p_{m+\theta,n}} + a_n(K^2-1)v_{p_{m+\theta,n}} + \theta\Delta x(\mu D)_{m+1,n} \qquad \text{(A-14)}$$

$$C_n^7 = -a_n K^2 v_{p_{m+\theta,n}}$$

$$D_n^7 = [u_{p_{m+\theta,n}} - (1-\theta)\Delta x(\mu D)_{m,n}] u_{p_{m,n}} - b_n v_{p_{m+\theta,n}} \Delta u_{p_{m,n}} + \Delta x(u\mu D)_{m+\theta,n}$$

The energy equation of the particle phase is

$$u_p \frac{\partial T_p}{\partial x} + v_p \frac{\partial T_p}{\partial y} = -\frac{\alpha}{3Pr}(T_p - T)\mu Nu = \frac{\alpha}{3Pr} T\mu Nu - \frac{\alpha}{3Pr} T_p \mu Nu \qquad (A\text{-}15)$$

Then

$$u_{p_{m+\theta,n}} \frac{1}{\Delta x}(T_{p_{m+1,n}} - T_{p_{m,n}}) + v_{p_{m+\theta,n}} \{\frac{\theta}{(1+K)\Delta y_n}[T_{p_{m+1,n+1}} + (K^2-1)T_{p_{m+1,n}}$$

$$- K^2 T_{p_{m+1,n-1}}] + \frac{1-\theta}{(1+K)\Delta y_n} \Delta T_{p_{m,n}}\}$$

$$= (\frac{\alpha}{3Pr} T\mu Nu)_{m+\theta,n} - [\theta(\frac{\alpha}{3Pr} \mu Nu)_{m+1,n} T_{p_{m+1,n}} + (1-\theta)(\frac{\alpha}{3Pr} \mu Nu)_{m,n} T_{p_{m,n}}] \qquad (A\text{-}16)$$

Consequently,

$$A_n^8 T_{p_{m+1,n+1}} + B_n^8 T_{p_{m+1,n}} + C_n^8 T_{p_{m+1,n-1}} = D_n^8 \qquad (A\text{-}17)$$

where

$$A_n^8 = a_n v_{p_{m+\theta,n}}$$

$$B_n^8 = u_{p_{m+\theta,n}} + a_n(K^2\ 1)v_{p_{m+\theta,n}} + \theta\Delta x(\frac{\alpha}{3Pr} \mu Nu)_{m+1,n}$$

$$C_n^8 = -a_n K^2 v_{p_{m+\theta,n}} \qquad (A\text{-}18)$$

$$D_n^8 = [u_{p_{m+\theta,n}} - (1-\theta)\Delta x(\frac{\alpha}{3Pr} \mu Nu)_{m,n}]T_{p_{m,n}} - b_n v_{p_{m+\theta,n}} \Delta T_{p_{m,n}}$$

$$+ \Delta x(\frac{\alpha}{3Pr} T\mu Nu)_{m+\theta,n}$$

The continuity equation of the particle phase can be written in the different forms as follows:

$$\frac{\partial}{\partial x} \rho_p u_p + \frac{\partial}{\partial y} \rho_p v_p = 0$$

$$u_p \frac{\partial \rho_p}{\partial x} + v_p \frac{\partial \rho_p}{\partial y} + \rho_p \left(\frac{\partial u_p}{\partial x} + \frac{\partial v_p}{\partial y}\right) = 0 \qquad \text{(A-19)}$$

$$u_p \frac{\partial}{\partial x}\left(\frac{1}{\rho_p}\right) + v_p \frac{\partial}{\partial y}\left(\frac{1}{\rho_p}\right) - \left(\frac{1}{\rho_p}\right)\left(\frac{\partial u_p}{\partial x} + \frac{\partial v_p}{\partial y}\right) = 0$$

The third form can be discretized as

$$u_{p_{m+\theta,n}} \frac{1}{\Delta x}\left[\left(\frac{1}{\rho_p}\right)_{m+1,n} - \left(\frac{1}{\rho_p}\right)_{m,n}\right] + v_{p_{m+\theta,n}} \left\{\frac{\theta}{(1+K)\Delta y_n}\left[\left(\frac{1}{\rho_p}\right)_{m+1,n+1}\right.\right.$$

$$\left. + (K^2-1)\left(\frac{1}{\rho_p}\right)_{m+1,n} - K^2\left(\frac{1}{\rho_p}\right)_{m+1,n-1}\right] + \frac{1-\theta}{(1+K)\Delta y_n}\Delta\left(\frac{1}{\rho_p}\right)_{m,n}\Big\}$$

$$- \left[\theta\left(\frac{1}{\rho_p}\right)_{m+1,n} + (1-\theta)\left(\frac{1}{\rho_p}\right)_{m,n}\right]\left\{\frac{1}{\Delta x}\left(u_{p_{m+1,n}} - u_{p_{m,n}}\right) + \frac{\theta}{(1+K)\Delta y_n}\Delta v_{p_{m+1,n}}\right.$$

$$\left. + \frac{1-\theta}{(1+K)\Delta y_n}\Delta v_{p_{m,n}}\right\} = 0 \qquad \text{(A-20)}$$

Then the difference equation becomes

$$A_n^9\left(\frac{1}{\rho_p}\right)_{m+1,n+1} + B_n^9\left(\frac{1}{\rho_p}\right)_{m+1,n} + C_n^9\left(\frac{1}{\rho_p}\right)_{m+1,n-1} = D_n^9 \qquad \text{(A-21)}$$

The coefficients in Eq. (A-21) are:

$$A_n^9 = a_n v_{p_{m+\theta,n}}$$

$$B_n^9 = u_{p_{m+\theta,n}} + a_n(K^2-1)v_{p_{m+\theta,n}} - \theta\left(u_{p_{m+1,n}} - u_{p_{m,n}}\right) - a_n \Delta v_{p_{m+\theta,n}}$$

$$C_n^9 = -a_n K^2 v_{p_{m+\theta,n}} \qquad \text{(A-22)}$$

$$D_n^9 = \left[u_{p_{m+\theta,n}} + (1-\theta)\left(u_{p_{m+1,n}} - u_{p_{m,n}}\right) + b_n \Delta v_{p_{m+\theta,n}}\right]\left(\frac{1}{\rho_p}\right)_{m,n}$$

$$- b_n v_{p_{m+\theta,n}} \Delta\left(\frac{1}{\rho_p}\right)_{m,n}$$

where

$$\Delta v_{p_{m+\theta,n}} = \theta \Delta v_{p_{m+1,n}} + (1-\theta)\Delta v_{p_{m,n}} \qquad \text{(A-23)}$$

AD-A174 952 FINITE-DIFFERENCE SOLUTIONS FOR COMPRESSIBLE LAMINAR BOUNDARY-LAYER FLOWS (U) TORONTO UNIV DOWNSVIEW (ONTARIO) INST FOR AEROSPACE STUDIES B Y WANG ET AL. 2/2

UNCLASSIFIED AUG 86 UTIAS-311 AFOSR-TR-86-2151 F/G 20/4 NL

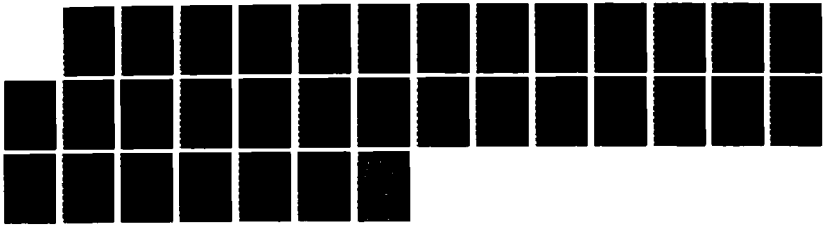

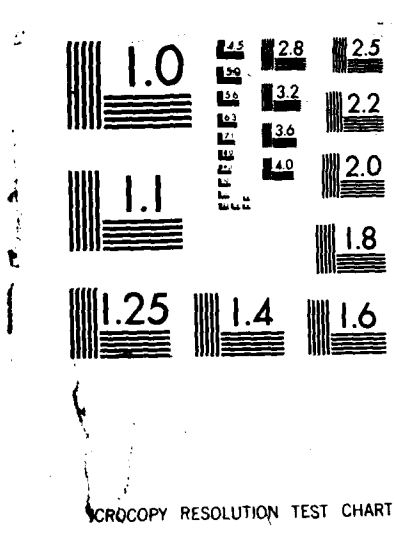

CROCOPY RESOLUTION TEST CHART

APPENDIX B

DERIVATION OF THE FINITE-DIFFERENCE EQUATIONS WITH A FOUR-POINT SCHEME

The continuity equation of the gas phase is

$$\frac{\partial}{\partial x}\rho u + \frac{\partial}{\partial y}\rho v = 0 \tag{B-1}$$

Using the expressions for the finite-difference quotients (3.5)-(3.7), Eq. (B-1) becomes

$$\frac{1}{2\Delta x}\left[(\rho u)_{m+1,n} - (\rho u)_{m,n} + (\rho u)_{m+1,n-1} - (\rho u)_{m,n-1}\right]$$

$$+ \frac{\theta}{\Delta y_{n-1}}\left[(\rho v)_{m+1,n} - (\rho v)_{m+1,n-1}\right] + \frac{1-\theta}{\Delta y_{n-1}}\left[(\rho v)_{m,n} - (\rho v)_{m,n-1}\right] = 0 \tag{B-2}$$

Therefore

$$(\rho v)_{m+1,n} = (\rho v)_{m+1,n-1} - \frac{1-\theta}{\theta}\left[(\rho v)_{m,n} - (\rho v)_{m,n-1}\right]$$

$$- \frac{\Delta y_{n-1}}{2\theta\Delta x}\left[(\rho u)_{m+1,n} - (\rho u)_{m,n} + (\rho u)_{m+1,n-1} - (\rho u)_{m,n-1}\right] \tag{B-3}$$

The x-momentum equation of the particle phase is

$$u_p \frac{\partial u_p}{\partial x} + v_p \frac{\partial u_p}{\partial y} = -(u_p - u)\mu D \tag{B-4}$$

With the quotient expressions (3.8)-(3.10), Eq. (B-4) becomes

$$u_{p_{m+\theta,n}} \frac{1}{\Delta x}\left(u_{p_{m+1,n}} - u_{p_{m,n}}\right) + v_{p_{m+\theta,n}}\left\{\frac{\theta}{\Delta y_n}\left(u_{p_{m+1,n+1}} - u_{p_{m+1,n}}\right)\right.$$

Continued

$$+ \frac{(1-\theta)}{\Delta y_n} \left(u_{p_{m,n+1}} - u_{p_{m,n}}\right)\}$$

$$= -[\theta(\mu D)_{m+1,n}\, u_{p_{m+1,n}} + (1-\theta)(\mu D)_{m,n}\, u_{p_{m,n}}] + (u\mu D)_{m+\theta,n} \qquad \text{(B-5)}$$

Therefore, the difference equation can be written as

$$A_n^3\, u_{p_{m+1,n+1}} + B_n^3\, u_{p_{m+1,n}} = C_n^3 \qquad \text{(B-6)}$$

where

$$A_n^3 = \frac{\theta\Delta x}{\Delta y_n}\, v_{p_{m+\theta,n}}$$

$$B_n^3 = u_{p_{m+\theta,n}} - \frac{\theta\Delta x}{\Delta y_n}\, v_{p_{m+\theta,n}} + \theta\Delta x(\mu D)_{m+1,n} \qquad \text{(B-7)}$$

$$C_n^3 = -\left[\frac{(1-\theta)\,\Delta x}{\Delta y_n}\, v_{p_{m+\theta,n}}\right] u_{p_{m,n+1}} + \left[u_{p_{m+\theta,n}} + \frac{(1-\theta)\,\Delta x}{\Delta y_n}\, v_{p_{m+\theta,n}}\right.$$

$$\left. - (1-\theta)\Delta x(\mu D)_{m,n}\right] u_{p_{m,n}} + \Delta x(u\mu D)_{m+\theta,n}$$

The y-momentum equation of the particle phase is

$$u_p \frac{\partial v_p}{\partial x} + v_p \frac{\partial v_p}{\partial y} = -(v_p - v)\mu D \qquad \text{(B-8)}$$

Substituting expressions (3.8), (3.9) and (3.11) into Eq. (B-8),

$$u_{p_{m+\theta,n}} \frac{1}{\Delta x}\left(v_{p_{m+1,n}} - v_{p_{m,n}}\right) + v_{p_{m+\theta,n}} \left\{\frac{\theta}{\Delta y_{n-1}}\left(v_{p_{m+1,n}} - v_{p_{m+1,n-1}}\right)\right.$$

$$\left. + \frac{1-\theta}{\Delta y_{n-1}}\left(v_{p_{m,n}} - v_{p_{m,n-1}}\right)\right\}$$

$$= -[\theta(\mu D)_{m+1,n}\, v_{p_{m+1,n}} + (1-\theta)(\mu D)_{m,n}\, v_{p_{m,n}}] + (v\mu D)_{m+\theta,n} \qquad \text{(B-9)}$$

Then, the finite-difference form for the y-momentum equation becomes

$$A_n^4 \, v_{p_{m+1,n}} + B_n^4 \, v_{p_{m+1,n-1}} = C_n^4 \tag{B-10}$$

$$A_n^4 = u_{p_{m+\theta,n}} + \frac{\theta\Delta x}{\Delta y_{n-1}} v_{p_{m+\theta,n}} + \theta\Delta x(\mu D)_{m+1,n}$$

$$B_n^4 = -\frac{\theta\Delta x}{\Delta y_{n-1}} v_{p_{m+\theta,n}} \tag{B-11}$$

$$C_n^4 = \left[u_{p_{m+\theta,n}} - \frac{(1-\theta)\Delta x}{\Delta y_{n-1}} v_{p_{m+\theta,n}} - (1-\theta)\Delta x(\mu D)_{m,n}\right] v_{p_{m,n}}$$

$$+ \left[\frac{(1-\theta)\Delta x}{\Delta y_{n-1}} v_{p_{m+\theta,n}}\right] v_{p_{m,n-1}} + \Delta x(v\mu D)_{m+\theta,n}$$

The energy equation of the particle phase is

$$u_p \frac{\partial T_p}{\partial x} + v_p \frac{\partial T_p}{\partial y} = -\frac{\alpha}{3Pr}(T_p - T)\mu Nu \tag{B-12}$$

Using a procedure similar to the x-momentum equation, the finite-difference equation for particle energy conservation can be derived as follows:

$$u_{p_{m+\theta,n}} \frac{1}{\Delta x}(T_{p_{m+1,n}} - T_{p_{m,n}}) + v_{p_{m+\theta,n}} \left\{\frac{\theta}{\Delta y_n}(T_{p_{m+1,n+1}} - T_{p_{m+1,n}})\right.$$

$$\left. + \frac{1-\theta}{\Delta y_n}(T_{p_{m,n+1}} - T_{p_{m,n}})\right\}$$

$$= -\left[\theta\left(\frac{\alpha}{3Pr}\mu Nu\right)_{m+1,n} T_{p_{m+1,n}} + (1-\theta)\left(\frac{\alpha}{3Pr}\mu Nu\right)_{m,n} T_{p_{m,n}}\right] + \left(\frac{\alpha}{3Pr} T\mu Nu\right)_{m+\theta,n} \tag{B-13}$$

$$A_n^5 \, T_{p_{m+1,n+1}} + B_n^5 \, T_{p_{m+1,n}} = C_n^5 \tag{B-14}$$

$$A_n^5 = \frac{\theta\Delta x}{\Delta y_n} v_{p_{m+\theta,n}}$$

$$B_n^5 = u_{p_{m+\theta,n}} - \frac{\theta\Delta x}{\Delta y_n} v_{p_{m+\theta,n}} + \theta\Delta x \left(\frac{\alpha}{3Pr} \mu Nu\right)_{m+1,n} \tag{B-15}$$

$$C_n^5 = -\left[\frac{(1-\theta)\Delta x}{\Delta y_n} v_{p_{m+\theta,n}}\right] T_{p_{m,n+1}} + \left[u_{p_{m+\theta,n}} + \frac{(1-\theta)\Delta x}{\Delta y_n} v_{p_{m+\theta,n}}\right.$$

$$\left. - (1-\theta)\Delta x \left(\frac{\alpha}{3Pr} \mu Nu\right)_{m,n}\right] T_{p_{m,n}} + \Delta x \left(\frac{\alpha}{3Pr} T\mu Nu\right)_{m+\theta,n}$$

The continuity equation of the particle phase is

$$\frac{\partial}{\partial x} \rho_p u_p + \frac{\partial}{\partial y} \rho_p v_p = 0 \tag{B-16}$$

or

$$u_p \frac{\partial \rho_p}{\partial x} + v_p \frac{\partial \rho_p}{\partial y} + \rho_p \left(\frac{\partial u_p}{\partial x} + \frac{\partial v_p}{\partial y}\right) = 0 \tag{B-17}$$

Using the quotient expressions (3.8)-(3.10), Eq. (B-17) becomes

$$u_{p_{m+\theta,n}} \frac{1}{\Delta x} \left(\rho_{p_{m+1,n}} - \rho_{p_{m,n}}\right) + v_{p_{m+\theta,n}} \left[\frac{\theta}{\Delta y_n} \left(\rho_{p_{m+1,n+1}} - \rho_{p_{m+1,n}}\right)\right.$$

$$\left. + \frac{(1-\theta)}{\Delta y_n} \left(\rho_{p_{m,n+1}} - \rho_{p_{m,n}}\right)\right] + \left[\theta\rho_{p_{m+1,n}} + (1-\theta)\rho_{p_{m,n}}\right]\left[\frac{1}{\Delta x} \left(u_{p_{m+1,n}} - u_{p_{m,n}}\right)\right.$$

$$\left. + \frac{\theta}{\Delta y_n} \left(v_{p_{m+1,n+1}} - v_{p_{m+1,n}}\right) + \frac{1-\theta}{\Delta y_n} \left(v_{p_{m,n+1}} - v_{p_{m,n}}\right)\right] = 0 \tag{B-18}$$

Then, the finite-difference equation can be written in the following form:

$$A_n^6 \rho_{p_{m+1,n+1}} + B_n^6 \rho_{p_{m+1,n}} = C_n^6 \tag{B-19}$$

where

$$A_n^6 = \frac{\theta \Delta x}{\Delta y_n} v_{p_{m+\theta,n}}$$

$$B_n^6 = 2\theta u_{p_{m+1,n}} + (1-2\theta) u_{p_{m,n}} + \frac{\theta^2 \Delta x}{\Delta y_n} (v_{p_{m+1,n+1}} - 2v_{p_{m+1,n}})$$

$$+ \frac{\theta(1-\theta)\Delta x}{\Delta y_n} (v_{p_{m,n+1}} - 2v_{p_{m,n}}) \qquad \text{(B-20)}$$

$$C_n^6 = -[\frac{(1-\theta)\Delta x}{\Delta y_n} v_{p_{m+\theta,n}}] \rho_{p_{m,n+1}} + [(2\theta-1) u_{p_{m+1,n}} + 2(1-\theta) u_{p_{m,n}}$$

$$- \frac{\theta(1-\theta)\Delta x}{\Delta y_n} (v_{p_{m+1,n+1}} - 2v_{p_{m+1,n}}) - \frac{(1-\theta)^2 \Delta x}{\Delta y_n} (v_{p_{m,n+1}} - 2v_{p_{m,n}})] \rho_{p_{m,n}}$$

APPENDIX C

DERIVATION OF THE RELATIONS FOR SHEAR STRESS, HEAT TRANSFER AND DISPLACEMENT THICKNESS

Characteristic quantities of boundary-layer flows are defined as

$$\tau_w^* = \mu_w^* \left(\frac{\partial u^*}{\partial y^*}\right)_w \tag{C-1}$$

$$\dot{q}_w^* = -k_w^* \left(\frac{\partial T^*}{\partial y^*}\right)_w \tag{C-2}$$

$$\delta^* = \int_0^\infty \left(1 - \frac{\rho^* u^*}{\rho_\infty^* u_\infty^*}\right) dy^* \tag{C-3}$$

Correspondingly, the nondimensional parameters take the following form:

$$\tau_w = \frac{\tau_w^*}{\rho_\infty^* u_\infty^{*2}} \sqrt{Re_\infty} \tag{C-4}$$

$$\dot{q}_w = \frac{\dot{q}_w^*}{\rho_\infty^* u_\infty^{*3}} \sqrt{Re_\infty} \tag{C-5}$$

$$\delta = \frac{\delta^*}{\lambda_\infty^*} \sqrt{Re_\infty} \tag{C-6}$$

where

$$Re_\infty = \frac{\rho_\infty^* u_\infty^* \lambda_\infty^*}{\mu_\infty^*}$$

From the definition of the nondimensional parameters, Eq. (2.11), the derivatives of the gas velocity u* and temperature T* can be given as

$$\frac{\partial u^*}{\partial y^*} = \frac{u^*_\infty}{\lambda^*_\infty} \sqrt{Re_\infty} \left(\frac{\partial u}{\partial y}\right) \tag{C-7}$$

$$\frac{\partial T^*}{\partial y^*} = \frac{T^*_\infty}{\lambda^*_\infty} \sqrt{Re_\infty} \left(\frac{\partial T}{\partial y}\right) \tag{C-8}$$

and the integration (C-3) becomes

$$\int_o^\infty \left(1 - \frac{\rho^* u^*}{\rho^*_\infty u^*_\infty}\right) dy^* = \frac{\lambda^*_\infty}{\sqrt{Re_\infty}} \int_o^\infty (1 - \rho u) dy \tag{C-9}$$

Therefore, the nondimensional characteristics of the boundary-layer flows can be expressed as,

$$\tau_w = \mu_w \left(\frac{\partial u}{\partial y}\right)_w \tag{C-10}$$

$$\dot{q}_w = - \frac{\mu_w}{Pr\ Ec} \left(\frac{\partial T}{\partial y}\right)_w \tag{C-11}$$

$$\delta = \int_o^\infty (1 - \rho u) dy \tag{C-12}$$

where

$$\mu_w = \frac{\mu^*_w}{\mu^*_\infty}, \qquad Pr = \frac{c^*_p\ \mu^*}{k^*} \qquad \text{and} \qquad Ec = \frac{u^{*2}_\infty}{c^*_p\ T^*_\infty}$$

In order to calculate the derivatives at the wall with the finite-difference solutions, the gas velocity u near the wall can be approximated by a cubic polynomial:

$$u = a_u + b_u y + c_u y^2 + d_u y^3 \tag{C-13}$$

At the four grid points nearest the wall, the values of gas velocity are known and are equal to u_1, u_2, u_3 and u_4, respectively. Then, there are four equations which can be used to obtain the coefficients a_u, b_u, c_u and d_u:

$$y_1 = 0: \qquad u_1 = a_u \tag{C-14}$$

$$y_2 = \Delta y_1: \qquad u_2 = a_u + b_u \Delta y_1 + c_u \Delta y_1^{\,2} + d_u \Delta y_1^{\,3} \tag{C-15}$$

$$y_3 = (K+1)\Delta y_1: \qquad u_3 = a_u + b_u (K+1)\Delta y_1 + c_u (K+1)^2 \Delta y_1^{\,2} + d_u (K+1)^3 \Delta y_1^{\,3} \tag{C-16}$$

$$y_4 = (K^2+K+1)\Delta y_1: \qquad u_4 = a_u + b_u (K^2+K+1)\Delta y_1 + c_u (K^2+K+1)^2 \Delta y_1^{\,2} + d_u (K^2+K+1)^3 \Delta y_1^{\,3} \tag{C-17}$$

Solving the system of simultaneous equations (C-14) - (C-17) by an elimination method, the value of coefficient b_u is obtained:

$$b_u = \frac{K^2+K+1}{K^2 \Delta y_1} \left[(u_2 - u_1) - \frac{u_3 - u_1}{K(K+1)} + \frac{u_4 - u_1}{K(K^2+K+1)^2} \right] \tag{C-18}$$

For the gas temperature T, there is a similar relation for coefficient b_T:

$$b_T = \frac{K^2+K+1}{K^2 \Delta y_1} \left[(T_2 - T_1) - \frac{T_3 - T_1}{K(K+1)} + \frac{T_4 - T_1}{K(K^2+K+1)^2} \right] \tag{C-19}$$

Since the gas velocity at the wall vanishes, $u_1 = 0$ in the expression (C-18), therefore, the nondimensional shear stress at the wall can be determined:

$$\tau_w = \mu_w \frac{(K^2+K+1)}{K^2 \Delta y_1} \left[u_2 - \frac{u_3}{K(K+1)} + \frac{u_4}{K(K^2+K+1)^2} \right] \tag{C-20}$$

and the corresponding heat transfer is

$$\dot{q}_w = - \frac{\mu_w}{Pr\ Ec} \frac{(K^2+K+1)}{K^2 \Delta y_1} \left[(T_2 - T_1) - \frac{T_3 - T_1}{K(K+1)} + \frac{T_4 - T_1}{K(K^2+K+1)^2} \right] \qquad (C\text{-}21)$$

As for the three-point difference formula, the integration I is calculated by

$$I = \int_o^{y_N} F(y)dy \qquad (C\text{-}22)$$

Within every small integration region, the integrated function F(y) can be approximated by a quadratic parabola p(y) through three consecutive grid points (m+1, n-1), (m+1, n) and (m+1, n+1):

$$p(y) = A_n \left(\frac{y - y_n}{\Delta y_n} \right)^2 + B_n \left(\frac{y - y_n}{\Delta y_n} \right) + C_n \qquad (C\text{-}23)$$

The quadratic polynomial p(y) satisfies the conditions:

$$p(y_{n-1}) = F_{m+1,n-1}, \quad p(y_n) = F_{m+1,n}, \quad p(y_{n+1}) = F_{m+1,n+1} \qquad (C\text{-}24)$$

Then a system of simultaneous algebraic equations for the coefficients A_n, B_n and C_n can be constructed:

$$A_n - KB_n + K^2 C_n = K^2 F_{m+1,n-1}, \quad C_n = F_{m+1,n}, \quad A_n + B_n + C_n = F_{m+1,n+1} \qquad (C\text{-}25)$$

Consequently, the solutions of the above equations can be found as

$$A_n = \frac{K}{K+1} F_{m+1,n+1} - K F_{m+1,n} + \frac{K^2}{K+1} F_{m+1,n-1}$$

$$B_n = \frac{1}{K+1} F_{m+1,n+1} + (K-1) F_{m+1,n} - \frac{K^2}{K+1} F_{m+1,n-1} \qquad (C\text{-}26)$$

$$C_n = F_{m+1,n}$$

Substituting the coefficient expression (C-26) into Eq. (C-23), replacing the integrated function F(y) by p(y), and integrating Eq. (C-22) in every small interval Δy_{n-1} and making the summation, the three-point difference formula for nonequal intervals is derived:

$$I = \sum_{2}^{N-1} \left[\frac{\Delta y_{n-1}}{3K^2} A_n - \frac{\Delta y_{n-1}}{2K} B_n + \Delta y_{n-1} C_n\right]$$

$$= \sum_{2}^{N-1} \frac{\Delta y_{n-1}}{6} \left[\frac{3K+2}{K+1} F_{m+1,n-1} + \frac{3K+1}{K} F_{m+1,n} - \frac{1}{K(K+1)} F_{m+1,n+1}\right] \qquad \text{(C-27)}$$

APPENDIX D

COMPUTER PROGRAM FDBLEP

The program FDBLEP for solving finite-difference boundary-layer equations over a flat plate for a dusty gas is written on the Perkin-Elmer 3250 system at UTIAS. The main notations used in the program are listed and explained below.

U(I) = u at grid point (m+1, n)

V(I) = v at grid point (m+1, n)

T(I) = T at grid point (m+1, n)

RO(I) = ρ at grid point (m+1, n)

UP(I) = u_p at grid point (m+1, n)

VP(I) = v_p at grid point (m+1, n)

TP(I) = T_p at grid point (m+1, n)

ROP(I) = ρ_p at grid point (m+1, n)

SHEAR = τ_w at grid line (m+1)

HEAT = $\dot{q}_w$ at grid line (m+1)

THICK = δ at grid line (m+1)

UW = u_w

TW = T_w

EC = Ec

PR = Pr

WN = ω

BETA = β

DX = Δx

DY = Δy_1

KE = K

CITA = θ

EPS = ε

N = maximum value of n

XSTA = initial value of x

XMAX = maximum value of x

XCRI = critical value of x

```
C - - - - - - - - - - - - - - - - - - - - - - - - - - - - - - - - - -
C     THIS PROGRAM SOLVES THE GAS AND PARTICLE PARAMETERS FOR
C     THE BOUNDARY LAYER EQUATIONS OF A DUSTY GAS OVER A SEMI-
C     INFINITE FLAT PLATE BY MEANS OF FINITE DIFFERENCE METHOD
C     AND GIVES CHARACTERISTIC QUANTITIES OF BOUNDARY LAYER FLOW
C     (IMPLICIT SCHEMES FOR TWO PHASES, NONITERATION PROCEDURE)
C - - - - - - - - - - - - - - - - - - - - - - - - - - - - - - - - - -
C - - - - - - - - - - - - - - - - - - - - - - - - - - - - - - - - - -
C     MAIN PROGRAM
C - - - - - - - - - - - - - - - - - - - - - - - - - - - - - - - - - -
C - - - - - - - - - - - - - - - - - - - - - - - - - - - - - - - - - -
      IMPLICIT REAL*8(A-H,O-Z)
      REAL*8 KE, KE1, KE2, KE3, KE4, MUI, MDR, MNU, MUW
      DIMENSION A(100), B(100), C(100), D(100)
      DIMENSION U(100), V(100), T(100), RO(100)
      DIMENSION UP(100), VP(100), TP(100), ROP(100)
      DIMENSION RUB(100), RVB(100)
      DIMENSION RU(100), CR(100), CRB(100)
      DIMENSION DMD(100), DMN(100), DMDB(100), DMNB(100)
      DIMENSION UD(100), VD(100), TD(100)
      COMMON /G/ PR, WN, EC
      COMMON /H1/ KE, KE1, KE2, KE3
      COMMON /H2/ CA, CB, CC, CD
C - - - - - - - - - - - - - - - - - - - - - - - - - - - - - - - - - -
1020  FORMAT (3E13.6)
1030  FORMAT (5E13.6)
1050  FORMAT (1X, 3E13.6)
1060  FORMAT (1X, 5E13.6)
1070  FORMAT (2I5, 2E13.6)
1080  FORMAT (1E16.8, 7E15.8)
1090  FORMAT (1X, 2I5, 2E13.6)
1100  FORMAT (1X, 8E15.8)
1110  FORMAT (1X, 2I5, 1E13.6, 3E15.8)
C - - - - - - - - - - - - - - - - - - - - - - - - - - - - - - - - - -
C     SET THE BASIC PARAMETERS
C - - - - - - - - - - - - - - - - - - - - - - - - - - - - - - - - - -
      READ (7,1020) UW, TW, BETA
      READ (7,1020) EC, PR, WN
      READ (7,1030) DX, DY, EPS, KE, CITA
      WRITE (8,1050) UW, TW, BETA
      WRITE (8,1050) EC, PR, WN
      WRITE (8,1060) DX, DY, EPS, KE, CITA
      READ (7,1070) MEND, N, XSTA, XMAX
      READ (7,1080) (U(I), V(I), T(I), RO(I),
     1               UP(I), VP(I), TP(I), ROP(I), I=1, N)
      WRITE (8,1090) MEND, N, XSTA, XMAX
      WRITE (8,1100) (U(I), V(I), T(I), RO(I), UP(I), VP(I), TP(I), ROP(I),
     1               I=1, 10)
```

```
C - - - - - - - - - - - - - - - - - - - - - - - - - - - - - - - - - -
C       SET THE NUMERICAL PARAMETERS
C - - - - - - - - - - - - - - - - - - - - - - - - - - - - - - - - - -
        KE1=KE+1. D+00
        KE2=KE*KE
        KE3=KE2-1. D+00
        KE4=KE1+KE2
        CITA1=1. D+00-CITA
        CITA2=CITA1/CITA
        CITA3=2. D+00*CITA
        CITA4=CITA3-1. D+00
        CITA5=2. D+00*CITA1
        CI1=CITA*DX
        CI2=CITA1*DX
        CI3=2. D+00*CI1
        CI4=2. D+00*CI2
        CK1=KE4/KE2
        CK2=KE*KE1
        CK3=KE*KE4*KE4
        CK4=(2. D+00+3. D+00*KE)/KE1
        CK5=(1. D+00+3. D+00*KE)/KE
        CK6=1. D+00/CK2
C - - - - - - - - - - - - - - - - - - - - - - - - - - - - - - - - - -
C       CALCULATE THE FLOW PROFILES AT THE NEXT GRID LINE (M+1)
C - - - - - - - - - - - - - - - - - - - - - - - - - - - - - - - - - -
        MUW=TW**WN
        XCRI=1. D+00/MUW
        X=XSTA
10      CONTINUE
        DO 950 L=1, 10
        DO 900 M=1, MEND
        N1=N-1
        N2=N-2
        X=X+DX
        IF (X. GT. XMAX) GO TO 999
C - - - - - - - - - - - - - - - - - - - - - - - - - - - - - - - - - -
C       STORE THE VALUES OF GAS VELOCITY AT THE PREVIOUS LINE (M)
C - - - - - - - - - - - - - - - - - - - - - - - - - - - - - - - - - -
        DO 20 I=1, N
20      RU(I)=U(I)
C - - - - - - - - - - - - - - - - - - - - - - - - - - - - - - - - - - -
C       SOLVE THE NEW GAS TANGENTIAL VELOCITY U AT THE NEXT
C       GRID LINE (M+1) USING SIX-POINT IMPLICIT SCHEME
C - - - - - - - - - - - - - - - - - - - - - - - - - - - - - - - - - -
C       SET THE BOUNDARY CONDITIONS AT THE LINE (M+1)
C - - - - - - - - - - - - - - - - - - - - - - - - - - - - - - - - - -
        U(1)=UW
        U(N)=1. OD+00
```

```
C - - - - - - - - - - - - - - - - - - - - - - - - - - - - - - - - - -
C     SET THE FLOW PARAMETERS AT THE GRID POINT (N+1) TO CALCULATE
C     THE FIRST AND SECOND ORDER DIFFERENCES AT THE GRID LINE (M)
C - - - - - - - - - - - - - - - - - - - - - - - - - - - - - - - - - -
      U(N+1)=U(N)
      T(N+1)=T(N)
C - - - - - - - - - - - - - - - - - - - - - - - - - - - - - - - - - -
C     CALCULATE THE INITIAL VALUE OF SOME COEFFICIENTS
C - - - - - - - - - - - - - - - - - - - - - - - - - - - - - - - - - -
      CALL VALU1(CI1,CI2,CI3,CI4,DY,DY1)
C - - - - - - - - - - - - - - - - - - - - - - - - - - - - - - - - - -
C     CALCULATE THE COEFFICIENT MATRIX ELEMENTS
C - - - - - - - - - - - - - - - - - - - - - - - - - - - - - - - - - -
      CALL PARA1(1,U,V,RO,RUI,RVI)
      RUB(1)=RUI
      RVB(1)=RVI
      CALL PARA2(1,T,MUI,DMUI,MDR,MNU)
      CALL PARA5(1,DX,MDR,MNU,DMDB,DMNB,U,V,T,UD,VD,TD)
      DO 110 I=2,N
      CALL PARA1(I,U,V,RO,RUI,RVI)
      RUB(I)=RUI
      RVB(I)=RVI
      CALL PARA3(I,KE2,KE3,U,DEUI)
      CALL PARA3(I,KE2,KE3,T,DETI)
      DY1=DY1*KE
      DTI=DETI/DY1
      CALL PARA4(I,KE,KE1,U,DDEUI)
      CALL PARA2(I,T,MUI,DMUI,MDR,MNU)
      CALL PARA5(I,DX,MDR,MNU,DMDB,DMNB,U,V,T,UD,VD,TD)
      ROMD=ROP(I)*DMDB(I)
      UDI=ROMD*UP(I)
      CR(I)=CITA*ROMD
      CRB(I)=CITA1*ROMD
      DMUI=DMUI*DTI
      CALL VALU2(KE,KE2)
110   CALL COEF1(I,U,RUI,RVI,MUI,DMUI,DEUI,DDEUI,UDI,CR,CRB,A,B,C,D)
      CALL COEF2(U,A,B,C,D)
C - - - - - - - - - - - - - - - - - - - - - - - - - - - - - - - - - -
C     SOLVE THE GAS TANGENTIAL VELOCITY PROFILE BY THOMAS ALGORITHM
C - - - - - - - - - - - - - - - - - - - - - - - - - - - - - - - - - -
      DO 120 I=2,N1
120   CALL THOM1(I,A,B,C,D)
      DO 130 I=1,N2
      J=N-I
130   CALL THOM2(J,U,A,B,D)
C - - - - - - - - - - - - - - - - - - - - - - - - - - - - - - - - - -
C     TEST FOR THE OUTER EDGE OF BOUNDARY LAYER
C - - - - - - - - - - - - - - - - - - - - - - - - - - - - - - - - - -
C     COMPARE THE DIFFERENCE OF FLOW PROPERTIES BETWEEN THE LAST
C     TWO CONSECUTIVE GRID POINTS WITH THE SPECIFIED TOLERANCE
C - - - - - - - - - - - - - - - - - - - - - - - - - - - - - - - - - -
      ITEST=0
140   ERROR=DABS(U(N)-U(N1))
      IF (ERROR.LT.EPS) GO TO 150
```

```
C - - - - - - - - - - - - - - - - - - - - - - - - - - - - - - - - - - -
C       ADD A NEW GRID POINT AT THE NEW GRID LINE (M+1)
C - - - - - - - - - - - - - - - - - - - - - - - - - - - - - - - - - - -
        ITEST=ITEST+1
        U(N+1)=U(N)
        V(N+1)=V(N)
        T(N+1)=T(N)
        RO(N+1)=RO(N)
        UP(N+1)=UP(N)
        VP(N+1)=VP(N)
        TP(N+1)=TP(N)
        ROP(N+1)=ROP(N)
C - - - - - - - - - - - - - - - - - - - - - - - - - - - - - - - - - - -
C       CALCULATE THE MATRIX COEFFICIENTS AT THE NEW GRID POINT
C - - - - - - - - - - - - - - - - - - - - - - - - - - - - - - - - - - -
        IF (ITEST.GT.1) GO TO 160
        CALL THOM1(N,A,B,C,D)
        CALL THOM2(N,U,A,B,D)
        GO TO 170
160     MUI=1.D+00
        DMUI=0.D+00
        DEUI=0.D+00
        DDEUI=0.D+00
        ROMD=ROP(N)*DMDB(N)
        UDI=ROMD*UP(N)
        CR(N)=CITA*ROMD
        CRB(N)=CITA1*ROMD
        CALL VALU2(KE,KE2)
        CALL COEF1(N,U,RUI,RVI,MUI,DMUI,DEUI,DDEUI,UDI,CR,CRB,A,B,C,D)
        CALL THOM1(N,A,B,C,D)
        CALL THOM2(N,U,A,B,D)
170     N=N+1
        N1=N1+1
        N2=N2+1
        RU(N)=RU(N1)
        RUB(N)=RUB(N1)
        RVB(N)=RVB(N1)
        DMDB(N)=DMDB(N1)
        DMNB(N)=DMNB(N1)
        UD(N)=UD(N1)
        VD(N)=VD(N1)
        TD(N)=TD(N1)
        IF (N.EQ.100) GO TO 999
        GO TO 140
150     IF (ITEST.EQ.0) GO TO 200
        DO 180 I=1,N2
        J=N-I
180     CALL THOM2(J,U,A,B,D)
```

```
C - - - - - - - - - - - - - - - - - - - - - - - - - - - - - - - - - - - -
C     SOLVE THE NEW GAS TEMPERATURE T AT THE NEXT GRID
C     LINE (M+1) USING SIX-POINT IMPLICIT SCHEME
C - - - - - - - - - - - - - - - - - - - - - - - - - - - - - - - - - - - -
C     SET THE BOUNDARY CONDITIONS AT THE LINE (M+1)
C - - - - - - - - - - - - - - - - - - - - - - - - - - - - - - - - - - - -
200   T(1)=TW
      T(N)=1.0D+00
C - - - - - - - - - - - - - - - - - - - - - - - - - - - - - - - - - - - -
C     CALCULATE THE INITIAL VALUE OF SOME COEFFICIENTS
C - - - - - - - - - - - - - - - - - - - - - - - - - - - - - - - - - - - -
      CALL VALU1(CI1,CI2,CI3,CI4,DY,DY1)
C - - - - - - - - - - - - - - - - - - - - - - - - - - - - - - - - - - - -
C     CALCULATE THE COEFFICIENT MATRIX ELEMENTS
C - - - - - - - - - - - - - - - - - - - - - - - - - - - - - - - - - - - -
      DO 210 I=2,N1
      CALL PARA1(I,U,V,RO,RUI,RVI)
      RUI=CITA*RUI+CITA1*RUB(I)
      CALL PARA3(I,KE2,KE3,U,DEUI)
      CALL PARA3(I,KE2,KE3,T,DETI)
      DY1=DY1*KE
      DUI=DEUI/DY1
      DTI=DETI/DY1
      CALL PARA3(I,KE2,KE3,RU,DEUI)
      DUI=CITA*DUI+CITA1*DEUI/DY1
      CALL PARA4(I,KE,KE1,T,DDETI)
      CALL PARA2(I,T,MUI,DMUI,MDR,MNU)
      UPU=CITA*(UP(I)-U(I))+CITA1*(UP(I)-RU(I))
      UDI=ROP(I)*UPU*DMDB(I)
      EDM=EC*DUI*DUI*MUI*DX
      ERD=EC*UDI*UPU
      ROMN=ROP(I)*DMNB(I)
      TPT=ROMN*TP(I)
      TDI=EDM+ERD+TPT
      CR(I)=CITA*ROMN
      CRB(I)=CITA1*ROMN
      CALL VALU2(KE,KE2)
      MUI=MUI/PR
      DMUI=DMUI*DTI/PR
210   CALL COEF1(I,T,RUI,RVI,MUI,DMUI,DETI,DDETI,TDI,CR,CRB,A,B,C,D)
      CALL COEF2(T,A,B,C,D)
C - - - - - - - - - - - - - - - - - - - - - - - - - - - - - - - - - - - -
C     SOLVE THE GAS TEMPERATURE PROFILE BY THOMAS ALGORITHM
C - - - - - - - - - - - - - - - - - - - - - - - - - - - - - - - - - - - -
      DO 220 I=2,N1
220   CALL THOM1(I,A,B,C,D)
      DO 230 I=1,N2
      J=N-I
230   CALL THOM2(J,T,A,B,D)
```

```
C - - - - - - - - - - - - - - - - - - - - - - - - - - - - - - - - - -
C     CALCULATE THE GAS DENSITY PROFILE AT THE GRID LINE (M+1)
C - - - - - - - - - - - - - - - - - - - - - - - - - - - - - - - - - -
      DO 240 I=1,N
240   RO(I)=1.D+00/T(I)
C - - - - - - - - - - - - - - - - - - - - - - - - - - - - - - - - - -
C     SOLVE THE GAS NORMAL VELOCITY PROFILE AT THE GRID LINE (M+1)
C - - - - - - - - - - - - - - - - - - - - - - - - - - - - - - - - - -
      DO 310 I=1,N
310   RU(I)=RO(I)*U(I)
      DO 320 I=2,N
      B(I)=RU(I)-RUB(I)+RU(I-1)-RUB(I-1)
320   C(I)=RVB(I)-RVB(I-1)
      CF=DY/(CI3*KE)
      D(1)=0.D+00
      DO 330 I=2,N
      CF=CF*KE
330   D(I)=D(I-1)-CITA2*C(I)-CF*B(I)
      DO 340 I=1,N
340   V(I)=D(I)*T(I)
C - - - - - - - - - - - - - - - - - - - - - - - - - - - - - - - - - -
C     SOLVE THE NEW PARTICLE PARAMETERS (UP,VP,TP,AND ROP) AT THE
C     GRID LINE (M+1) USING FOUR- OR SIX-POINT IMPLICIT SCHEME
C - - - - - - - - - - - - - - - - - - - - - - - - - - - - - - - - - -
C     CALCULATE SOME COEFFICIENTS OF THE FINITE DIFFERENCE EQUATION
C - - - - - - - - - - - - - - - - - - - - - - - - - - - - - - - - - -
      DO 410 I=1,N
      UDI=UD(I)
      VDI=VD(I)
      TDI=TD(I)
      CALL PARA2(I,T,MUI,DMUI,MDR,MNU)
      CALL PARA5(I,DX,MDR,MNU,DMD,DMN,U,V,T,UD,VD,TD)
      UD(I)=CITA*UD(I)+CITA1*UDI
      VD(I)=CITA*VD(I)+CITA1*VDI
      TD(I)=CITA*TD(I)+CITA1*TDI
      DMD(I)=CITA*DMD(I)
      DMN(I)=CITA*DMN(I)
      DMDB(I)=CITA1*DMDB(I)
410   DMNB(I)=CITA1*DMNB(I)
C - - - - - - - - - - - - - - - - - - - - - - - - - - - - - - - - - -
C     STORE THE VALUES OF PARTICLE VELOCITIES AT THE PREVIOUS LINE
C - - - - - - - - - - - - - - - - - - - - - - - - - - - - - - - - - -
      DO 420 I=1,N
      RUB(I)=UP(I)
420   RVB(I)=VP(I)
C - - - - - - - - - - - - - - - - - - - - - - - - - - - - - - - - - -
C     SOLVE THE PARTICLE TANGENTIAL VELOCITY UP AT THE LINE (M+1)
C - - - - - - - - - - - - - - - - - - - - - - - - - - - - - - - - - -
      IF (X.LT.XCRI) GO TO 530
```

```
C - - - - - - - - - - - - - - - - - - - - - - - - - - - - - - - - - -
C      SOLVE THE DIFFERENCE EQUATIONS USING SIX-POINT SCHEME
C - - - - - - - - - - - - - - - - - - - - - - - - - - - - - - - - - -
C      SET THE BOUNDARY CONDITIONS AT THE LINE (M+1)
C - - - - - - - - - - - - - - - - - - - - - - - - - - - - - - - - - -
       UP(1)=0.D+00
       UP(N)=1.D+00
C - - - - - - - - - - - - - - - - - - - - - - - - - - - - - - - - - -
C      CALCULATE THE INITIAL VALVE OF SOME COEFFICIENTS
C - - - - - - - - - - - - - - - - - - - - - - - - - - - - - - - - - -
       CALL VALU1(CI1,CI2,CI3,CI4,DY,DY1)
C - - - - - - - - - - - - - - - - - - - - - - - - - - - - - - - - - -
C      CALCULATE THE COEFFICIENT MATRIX ELEMENTS
C - - - - - - - - - - - - - - - - - - - - - - - - - - - - - - - - - -
       DO 510 I=2,N1
       RUI=UP(I)
       RVI=VP(I)
       CALL PARA3(I,KE2,KE3,UP,DEUPI)
       DDEUPI=0.D+00
       MUI=0.D+00
       DMUI=0.D+00
       UPDI=UD(I)
       CALL VALU2(KE,KE2)
510    CALL COEF1(I,UP,RUI,RVI,MUI,DMUI,DEUPI,DDEUPI,UPDI,DMD,DMDB,
     1           A,B,C,D)
       CALL COEF2(UP,A,B,C,D)
       DO 520 I=2,N1
520    CALL THOM1(I,A,B,C,D)
       DO 525 I=1,N2
       J=N-I
525    CALL THOM2(J,UP,A,B,D)
       GO TO 560
C - - - - - - - - - - - - - - - - - - - - - - - - - - - - - - - - - -
C      SOLVE THE DIFFERENCE EQUATIONS USING FOUR-POINT SCHEME
C - - - - - - - - - - - - - - - - - - - - - - - - - - - - - - - - - -
530    DX1=CI1*KE/DY
       DX2=CI2*KE/DY
       DO 540 I=1,N1
       DX1=DX1/KE
       DX2=DX2/KE
       A(I)=DX1*VP(I)
       B(I)=UP(I)-A(I)+DMD(I)
       DXVP=DX2*VP(I)
540    C(I)=-DXVP*UP(I+1)+(UP(I)+DXVP-DMDB(I))*UP(I)+UD(I)
       UP(N)=1.D+00
       DO 550 I=1,N1
       J=N-I
550    UP(J)=(C(J)-A(J)*UP(J+1))/B(J)
```

```
C - - - - - - - - - - - - - - - - - - - - - - - - - - - - - - - - - - -
C     CALCULATE THE VALUES OF UP AT THE HALF POINT (M+θ)
C - - - - - - - - - - - - - - - - - - - - - - - - - - - - - - - - - - -
560     DO 570 I=1,N
570     UD(I)=CITA*UP(I)+CITA1*RUB(I)
C - - - - - - - - - - - - - - - - - - - - - - - - - - - - - - - - - - -
C       SOLVE THE PARTICLE NORMAL VELOCITY VP  AT THE LINE (M+1)
C       BY MEANS OF THE FOUR-POINT SCHEME
C - - - - - - - - - - - - - - - - - - - - - - - - - - - - - - - - - - -
        DX1=CI1*KE/DY
        DX2=CI2*KE/DY
        DO 610 I=2,N
        DX1=DX1/KE
        DX2=DX2/KE
        B(I)=-DX1*VP(I)
        A(I)=UD(I)-B(I)+DMD(I)
        DXVP=DX2*VP(I)
610     C(I)=(UD(I)-DXVP-DMDB(I))*VP(I)+DXVP*VP(I-1)+VD(I)
        VP(1)=0.D+00
        DO 620 I=2,N
620     VP(I)=(C(I)-B(I)*VP(I-1))/A(I)
C - - - - - - - - - - - - - - - - - - - - - - - - - - - - - - - - - - -
C       CALCULATE THE VALUES OF VP AT THE HALF POINT (M+θ)
C - - - - - - - - - - - - - - - - - - - - - - - - - - - - - - - - - - -
        DO 630 I=1,N
630     VD(I)=CITA*VP(I)+CITA1*RVB(I)
C - - - - - - - - - - - - - - - - - - - - - - - - - - - - - - - - - - -
C       SOLVE THE PARTICLE TEMPERATURE TP AT THE LINE (M+1)
C - - - - - - - - - - - - - - - - - - - - - - - - - - - - - - - - - - -
        IF (X.LT.XCRI) GO TO 730
C - - - - - - - - - - - - - - - - - - - - - - - - - - - - - - - - - - -
C       SOLVE THE DIFFERENCE EQUATIONS USING SIX-POINT SCHEME
C - - - - - - - - - - - - - - - - - - - - - - - - - - - - - - - - - - -
C       SET THE BOUNDARY CONDITIONS AT THE LINE (M+1)
C - - - - - - - - - - - - - - - - - - - - - - - - - - - - - - - - - - -
        TP(1)=TW
        TP(N)=1.D+00
C - - - - - - - - - - - - - - - - - - - - - - - - - - - - - - - - - - -
C       CALCULATE THE INITIAL VALUE OF SOME COEFFICIENTS
C - - - - - - - - - - - - - - - - - - - - - - - - - - - - - - - - - - -
        CALL VALU1(CI1,CI2,CI3,CI4,DY,DY1)
C - - - - - - - - - - - - - - - - - - - - - - - - - - - - - - - - - - -
C       CALCULATE THE COEFFICIENT MATRIX ELEMENTS
C - - - - - - - - - - - - - - - - - - - - - - - - - - - - - - - - - - -
        DO 710 I=2,N1
        RUI=UD(I)
        RVI=VD(I)
        CALL PARA3(I,KE2,KE3,TP,DETPI)
        DDETPI=0.D+00
        MUI=0.D+00
        DMUI=0.D+00
        TPDI=TD(I)
```

```
      CALL VALU2(KE,KE2)
710   CALL COEF1(I,TP,RUI,RVI,MUI,DMUI,DETPI,DDETPI,TPDI,DMN,DMNB,
     1           A,B,C,D)
      CALL COEF2(TP,A,B,C,D)
      DO 720 I=2,N1
720   CALL THOM1(I,A,B,C,D)
      DO 725 I=1,N2
      J=N-I
725   CALL THOM2(J,TP,A,B,D)
      GO TO 805
C - - - - - - - - - - - - - - - - - - - - - - - - - - - - - - - - - -
C     SOLVE THE DIFFERENCE EQUATIONS USING FOUR-POINT SCHEME
C - - - - - - - - - - - - - - - - - - - - - - - - - - - - - - - - - -
730   DX1=CI1*KE/DY
      DX2=CI2*KE/DY
      DO 740 I=1,N1
      DX1=DX1/KE
      DX2=DX2/KE
      A(I)=DX1*VD(I)
      B(I)=UD(I)-A(I)+DMN(I)
      DXVP=DX2*VD(I)
740   C(I)=-DXVP*TP(I+1)+(UD(I)+DXVP-DMNB(I))*TP(I)+TD(I)
      TP(N)=1.D+00
      DO 750 I=1,N1
      J=N-I
750   TP(J)=(C(J)-A(J)*TP(J+1))/B(J)
C - - - - - - - - - - - - - - - - - - - - - - - - - - - - - - - - - -
C     SOLVE THE PARTICLE DENSITY ROP AT THE LINE (M+1)
C - - - - - - - - - - - - - - - - - - - - - - - - - - - - - - - - - -
805   IF (X.LT.XCRI) GO TO 830
C - - - - - - - - - - - - - - - - - - - - - - - - - - - - - - - - - -
C     GET THE PARTICLE DENSITY BY THE ASSUMPTION THAT THERE IS NO
C     DEPOSITION OF PARTICLES ON THE SURFACE OF THE PLATE
C - - - - - - - - - - - - - - - - - - - - - - - - - - - - - - - - - -
      DO 820 I=1,N
820   ROP(I)=BETA*RO(I)
      GO TO 900
C - - - - - - - - - - - - - - - - - - - - - - - - - - - - - - - - - -
C     SOLVE THE DIFFERENCE EQUATIONS USING FOUR-POINT SCHEME
C - - - - - - - - - - - - - - - - - - - - - - - - - - - - - - - - - -
830   DX1=CI1*KE/DY
      DX2=CI2*KE/DY
      DO 840 I=1,N1
      DX1=DX1/KE
      DX2=DX2/KE
      A(I)=DX1*VD(I)
      B(I)=CITA3*UP(I)-CITA4*RUB(I)
     1     +CITA*DX1*(VP(I+1)-2.D+00*VP(I))
     2     +CITA*DX2*(RVB(I+1)-2.D+00*RVB(I))
840   C(I)=-DX2*VD(I)*ROP(I+1)+(CITA4*UP(I)+CITA5*RUB(I)
     1     -CITA1*DX1*(VP(I+1)-2.D+00*VP(I))
     2     -CITA1*DX2*(RVB(I+1)-2.D+00*RVB(I)))*ROP(I)
```

```
      ROP(N)=BETA
      DO 850 I=1,N1
      J=N-I
850   ROP(J)=(C(J)-A(J)*ROP(J+1))/B(J)
900   CONTINUE
C - - - - - - - - - - - - - - - - - - - - - - - - - - - - - - - - - -
C     CALCULATE THE CHARACTERISTIC QUANTITIES OF BOUNDARY LAYER
C     FLOW: SHEAR STRESS, HEAT TRANSFER AND DISPLACEMENT THICKNESS
C - - - - - - - - - - - - - - - - - - - - - - - - - - - - - - - - - -
C     GET THE SHEAR STRESS AT THE WALL
C - - - - - - - - - - - - - - - - - - - - - - - - - - - - - - - - - -
      CMDY=CK1*MUW/DY
      SHEAR=(U(2)-U(1))-(U(3)-U(1))/CK2+(U(4)-U(1))/CK3
      SHEAR=SHEAR*CMDY
C - - - - - - - - - - - - - - - - - - - - - - - - - - - - - - - - - -
C     GET THE HEAT TRANSFER AT THE WALL
C - - - - - - - - - - - - - - - - - - - - - - - - - - - - - - - - - -
      CMDY=CMDY/(PR*EC)
      HEAT=(T(2)-T(1))-(T(3)-T(1))/CK2+(T(4)-T(1))/CK3
      HEAT=-HEAT*CMDY
C - - - - - - - - - - - - - - - - - - - - - - - - - - - - - - - - - -
C     GET THE DISPLACEMENT THICKNESS USING THREE-POINT DIFFERENCE
C     FORMULA
C - - - - - - - - - - - - - - - - - - - - - - - - - - - - - - - - - -
      DY1=DY/(6.D+00*KE)
      DO 910 I=1,N
910   RU(I)=1.D+00-RU(I)
      RU(N+1)=0.D+00
      THICK=0.D+00
      DO 920 I=2,N
      DY1=DY1*KE
      SUMI=CK4*RU(I-1)+CK5*RU(I)-CK6*RU(I+1)
      SUMI=SUMI*DY1
920   THICK=THICK+SUMI
C - - - - - - - - - - - - - - - - - - - - - - - - - - - - - - - - - -
C     OUTPUT THE COMPUTATION RESULTS AT THE GRID LINE (M+1)
C - - - - - - - - - - - - - - - - - - - - - - - - - - - - - - - - - -
950   WRITE(8,1110) M,N,X,SHEAR,HEAT,THICK
      WRITE(8,1100) (U(I),V(I),T(I),RO(I),
     1               UP(I),VP(I),TP(I),ROP(I),I=1,N)
      IF (X-XMAX) 10,10,999
999   STOP
      END
```

```
C - - - - - - - - - - - - - - - - - - - - - - - - - - - - - - - - - -
C - - - - - - - - - - - - - - - - - - - - - - - - - - - - - - - - - -
C - - - - - - - - - - - - - - - - - - - - - - - - - - - - - - - - - -
C     SUBROUTINE PROGRAMS
C - - - - - - - - - - - - - - - - - - - - - - - - - - - - - - - - - -
C - - - - - - - - - - - - - - - - - - - - - - - - - - - - - - - - - -
C - - - - - - - - - - - - - - - - - - - - - - - - - - - - - - - - - -
      SUBROUTINE PARA1(I,WU,WV,WR,RUI,RVI)
C - - - - - - - - - - - - - - - - - - - - - - - - - - - - - - - - - -
C     CALCULATE SOME PRODUCTS USED WHEN SOLVING THE FINITE
C     DIFFERENCE EQUATIONS
C - - - - - - - - - - - - - - - - - - - - - - - - - - - - - - - - - -
      IMPLICIT REAL*8(A-H,O-Z)
      DIMENSION WU(1),WV(1),WR(1)
C
      RUI=WR(I)*WU(I)
      RVI=WR(I)*WV(I)
C
      RETURN
      END
C - - - - - - - - - - - - - - - - - - - - - - - - - - - - - - - - - -
      SUBROUTINE PARA2(I,T,MUI,DMUI,MDR,MNU)
C - - - - - - - - - - - - - - - - - - - - - - - - - - - - - - - - - -
C     CALCULATE SOME PARAMETERS USED WHEN SOLVING THE FINITE
C     DIFFERENCE EQUATIONS
C - - - - - - - - - - - - - - - - - - - - - - - - - - - - - - - - - -
      IMPLICIT REAL*8(A-H,O-Z)
      REAL*8 MUI,MDR,MNU,NU
      DIMENSION T(1)
      COMMON /G/ PR,WN,S,REYP,EC
C
      MUI=T(I)**WN
      DMUI=WN*MUI/T(I)
      DR=1 D+00
      NU=2 D+00
      MDR=MUI*DR
      MNU=MUI*NU/(3 D+00*PR)
C
      RETURN
      END
C - - - - - - - - - - - - - - - - - - - - - - - - - - - - - - - - - -
      SUBROUTINE PARA3(I,KE2,KE3,W,DEWI)
C - - - - - - - - - - - - - - - - - - - - - - - - - - - - - - - - - -
C     CALCULATE THE FIRST ORDER DIFFERENCE USED WHEN SOLVING THE
C     FINITE DIFFERENCE EQUUATIONS
C - - - - - - - - - - - - - - - - - - - - - - - - - - - - - - - - - -
      IMPLICIT REAL*8(A-H,O-Z)
      REAL*8 KE2,KE3
      DIMENSION W(1)
C
      DEWI=W(I+1)+KE3*W(I)-KE2*W(I-1)
C
      RETURN
      END
```

```
C - - - - - - - - - - - - - - - - - - - - - - - - - - - - - - - - - - -
      SUBROUTINE PARA4(I,KE,KE1,W,DDEWI)
C - - - - - - - - - - - - - - - - - - - - - - - - - - - - - - - - - - -
C     CALCULATE THE SECOND ORDER DIFFERENCE USED WHEN SOLVING THE
C     FINITE DIFFERENCE EQUUATIONS
C - - - - - - - - - - - - - - - - - - - - - - - - - - - - - - - - - - -
      IMPLICIT REAL*8(A-H,O-Z)
      REAL*8 KE,KE1
      DIMENSION W(1)
C
      DDEWI=W(I+1)-KE1*W(I)+KE*W(I-1)
C
      RETURN
      END
C - - - - - - - - - - - - - - - - - - - - - - - - - - - - - - - - - - -
      SUBROUTINE PARA5(I,DX,MDR,MNU,DMD,DMN,U,V,T,UD,VD,TD)
C - - - - - - - - - - - - - - - - - - - - - - - - - - - - - - - - - - -
C     CALCULATE SOME PARAMETERS RELATED TO THE INTERACTION TERMS
C     BETWEEN GES AND PARTICLES
C - - - - - - - - - - - - - - - - - - - - - - - - - - - - - - - - - - -
      IMPLICIT REAL*8(A-H,O-Z)
      REAL*8 MDR,MNU
      DIMENSION DMD(1),DMN(1),U(1),V(1),T(1),UD(1),VD(1),TD(1)
C
      DMD(I)=DX*MDR
      DMN(I)=DX*MNU
      UD(I)=U(I)*DMD(I)
      VD(I)=V(I)*DMD(I)
      TD(I)=T(I)*DMN(I)
C
      RETURN
      END
C - - - - - - - - - - - - - - - - - - - - - - - - - - - - - - - - - - -
      SUBROUTINE VALU1(CI1,CI2,CI3,CI4,DY,DY1)
C - - - - - - - - - - - - - - - - - - - - - - - - - - - - - - - - - - -
C     GIVE THE INITIAL VALUES OF SOME COEFFICIENTS
C - - - - - - - - - - - - - - - - - - - - - - - - - - - - - - - - - - -
      IMPLICIT REAL*8(A-H,O-Z)
      REAL*8 KE,KE1
      COMMON /H1/ KE,KE1,KE2,KE3
      COMMON /H2/ CA,CB,CC,CD
C
      DY1=KE1*DY
      DY2=DY1*DY/KE
      CA=CI1/DY1
      CB=CI2/DY1
      CC=CI3/DY2
      CD=CI4/DY2
C
      RETURN
      END
```

```
C - - - - - - - - - - - - - - - - - - - - - - - - - - - - - - - - - -
      SUBROUTINE VALU2(KE,KE2)
C - - - - - - - - - - - - - - - - - - - - - - - - - - - - - - - - - -
C     CALCULATE THE VALUES OF SOME COEFFICIENTS AT THE GRID POINT
C - - - - - - - - - - - - - - - - - - - - - - - - - - - - - - - - - -
      IMPLICIT REAL*8(A-H,O-Z)
      REAL*8 KE,KE2
      COMMON /H2/ CA,CB,CC,CD
C
      CA=CA/KE
      CB=CB/KE
      CC=CC/KE2
      CD=CD/KE2
C
      RETURN
      END
C - - - - - - - - - - - - - - - - - - - - - - - - - - - - - - - - - -
      SUBROUTINE COEF1(I,W,RUI,RVI,MUI,DMUI,DEWI,DDEWI,WDI,CR,CRB,
     *                 A,B,C,D)
C - - - - - - - - - - - - - - - - - - - - - - - - - - - - - - - - - -
C     CALCULATE THE COEFFICIENT MATRIX ELEMENTS A,B,C, AND D FOR
C     THE CRANK-NICOLSON SCHEME
C - - - - - - - - - - - - - - - - - - - - - - - - - - - - - - - - - -
      IMPLICIT REAL*8(A-H,O-Z)
      REAL*8 KE,KE1,KE2,KE3,MUI
      DIMENSION W(1),CR(1),CRB(1),A(1),B(1),C(1),D(1)
      COMMON /H1/ KE,KE1,KE2,KE3
      COMMON /H2/ CA,CB,CC,CD
C
      RVT=RVI-DMUI
      CRVT=CA*RVT
      CMU=CC*MUI
      A(I)=CRVT-CMU
      B(I)=RUI+KE3*CRVT+KE1*CMU+CR(I)
      C(I)=-KE2*CRVT-KE*CMU
      DEWI=DEWI*CB
      DDEWI=DDEWI*CD
      D(I)=(RUI-CRB(I))*W(I)-RVT*DEWI+MUI*DDEWI+WDI
C
      RETURN
      END
```

```
C - - - - - - - - - - - - - - - - - - - - - - - - - - - - - - - - - -
      SUBROUTINE COEF2(W,A,B,C,D)
C - - - - - - - - - - - - - - - - - - - - - - - - - - - - - - - - - -
C     SPECIFY THE COEFFICIENT MATRIX ELEMENTS A(1),B(1),C(1),D(1)
C - - - - - - - - - - - - - - - - - - - - - - - - - - - - - - - - - -
      IMPLICIT REAL*8(A-H,O-Z)
      DIMENSION W(1),A(1),B(1),C(1),D(1)
C
      A(1)=0.D+00
      B(1)=1.D+00
      C(1)=0.D+00
      D(1)=W(1)
C
      RETURN
      END
C - - - - - - - - - - - - - - - - - - - - - - - - - - - - - - - - - -
      SUBROUTINE THOM1(I,A,B,C,D)
C - - - - - - - - - - - - - - - - - - - - - - - - - - - - - - - - - -
C     ESTABLISH UPPER TRIANGULAR MATRIX (FORWARD ELIMINATION) FOR
C     SOLVING THE TRI-DIAGONAL SYSTEM FOLLOWING THE THOMAS ALGORITHM
C - - - - - - - - - - - - - - - - - - - - - - - - - - - - - - - - - -
      IMPLICIT REAL*8(A-H,O-Z)
      DIMENSION A(1),B(1),C(1),D(1)
C
      BC=C(I)/B(I-1)
      B(I)=B(I)-BC*A(I-1)
      D(I)=D(I)-BC*D(I-1)
C
      RETURN
      END
C - - - - - - - - - - - - - - - - - - - - - - - - - - - - - - - - - -
      SUBROUTINE THOM2(I,W,A,B,D)
C - - - - - - - - - - - - - - - - - - - - - - - - - - - - - - - - - -
C     GET SOLUTION (BACK SUBSTITUTION) FOLLOWING THOMAS ALGORITHM
C - - - - - - - - - - - - - - - - - - - - - - - - - - - - - - - - - -
      IMPLICIT REAL*8(A-H,O-Z)
      DIMENSION W(1),A(1),B(1),D(1)
C
      W(I)=(D(I)-A(I)*W(I+1))/B(I)
C
      RETURN
      END
```

APPENDIX E

AN ADDITIONAL DISCUSSION REGARDING THE ASSUMPTION OF THE PARTICLE-DENSITY PROFILE AFTER THE CRITICAL POINT

In the foregoing analysis, it was pointed out that at the critical point, the particle velocity at the wall vanishes. Physically, $u_{pw} = 0$ means that the particles will stop and stay at the wall. Consequently, a lot of particles would gradually accumulate on the surface and it would result in a great increase of the particle density at the wall unless a diffusion mechanism is the predominant process. Therefore, contrary to a diffusion-controlled process (as assumed in the previous analysis), the accumulation of particles on the surface represents another extreme limiting case for a gas-particle system. It is not the purpose of this discussion to obtain information concerning particle deposition on the flat plate, although such data can be used in some practical problems (for example, retardation, accumulation and impingement of particles on solid surfaces have considerable effects on the erosion of the surfaces). The aim here is to attempt to gain more insight into the assumption of the particle-density profile when $x > x_{cri}$.

In the following, it is assumed that the accumulation of the particles at the wall is allowed and the thickness of the particle accumulation layer can be neglected compared with the boundary-layer thickness. The particle density will eventually become very large at the wall. So it is reasonable to specify the reciprocal of particle density at the wall to be zero. Then an additional boundary condition is obtained and the six-point scheme can be applied to the continuity equation of the particle phase. Using the reciprocal of the density as a new dependent variable, the continuity equation (2.16) can be written as

$$u_p \frac{\partial}{\partial x}\left(\frac{1}{\rho_p}\right) + v_p \frac{\partial}{\partial y}\left(\frac{1}{\rho_p}\right) - \left(\frac{1}{\rho_p}\right)\left(\frac{\partial u_p}{\partial x} + \frac{\partial v_p}{\partial y}\right) = 0 \qquad \text{(E-1)}$$

With the quotient expressions for the six-point scheme (3.1)-(3.4), its finite-difference form is

$$A_n^9\left(\frac{1}{\rho_p}\right)_{m+1,n+1} + B_n^9\left(\frac{1}{\rho_p}\right)_{m+1,n} + C_n^9\left(\frac{1}{\rho_p}\right)_{m+1,n-1} = D_n^9 \qquad \text{(E-2)}$$

$$A_n^9 = a_n\, v_{p_{m+\theta,n}} \qquad \text{(E-3)}$$

$$B_n^9 = u_{p_{m+\theta,n}} + a_n(K^2-1)v_{p_{m+\theta,n}} - \theta(u_{p_{m+1,n}} - u_{p_{m,n}}) - a_n\Delta v_{p_{m+\theta,n}} \quad \text{(E-4)}$$

$$C_n^9 = -a_n K^2 v_{p_{m+\theta,n}} \quad \text{(E-5)}$$

$$D_n^9 = [u_{p_{m+\theta,n}} + (1-\theta)(u_{p_{m+1,n}} - u_{p_{m,n}}) + b_n\Delta v_{p_{m+\theta,n}}](\frac{1}{\rho_p})_{m,n}$$

$$- b_n v_{p_{m+\theta,n}}\Delta(\frac{1}{\rho_p})_{m,n} \quad \text{(E-6)}$$

where

$$\Delta v_{p_{m+\theta,n}} = \theta\Delta v_{p_{m+1,n}} + (1-\theta)\Delta v_{p_{m,n}}$$

The boundary conditions at the wall and the outer edge of the boundary-layer are:

$$(\frac{1}{\rho_p})_{m+1,1} = 0 \quad \text{(E-7)}$$

$$(\frac{1}{\rho_p})_{m+1,N} = \frac{1}{\beta} \quad \text{(E-8)}$$

By solving the difference equation (E-2) with the boundary conditions (E-7) and (E-8), a numerical solution is obtained for the same freestream and wall conditions. In Figs. E-1 to E-4, these results are compared with those results obtained based on the assumption of $\rho_p = \beta\rho$ for $x > x_{cri}$. It is interesting to note that the resulting boundary-layer characteristics (i.e., shear stress, wall heat-transfer and displacement thickness) are almost the same for these two different methods, despite the fact that there are large differences between the particle density profiles, especially near the wall. It provides the evidence that the particle density has a very small effect on dusty-gas boundary-layer flows in the quasi-equilibrium and near-equilibrium regions. As mentioned before, this approximate treatment of the particle density (that is, for $x > x_{cri}$, $\rho_p = \beta\rho$ is assumed across the whole boundary layer) results in satisfactory accuracy on the boundary-layer flow-profiles and characteristic quantities except the particle density itself. It is due to the fact that the particle and gas phases are already in a near- or quasi-equilibrium state after the critical point ($x > x_{cri}$).

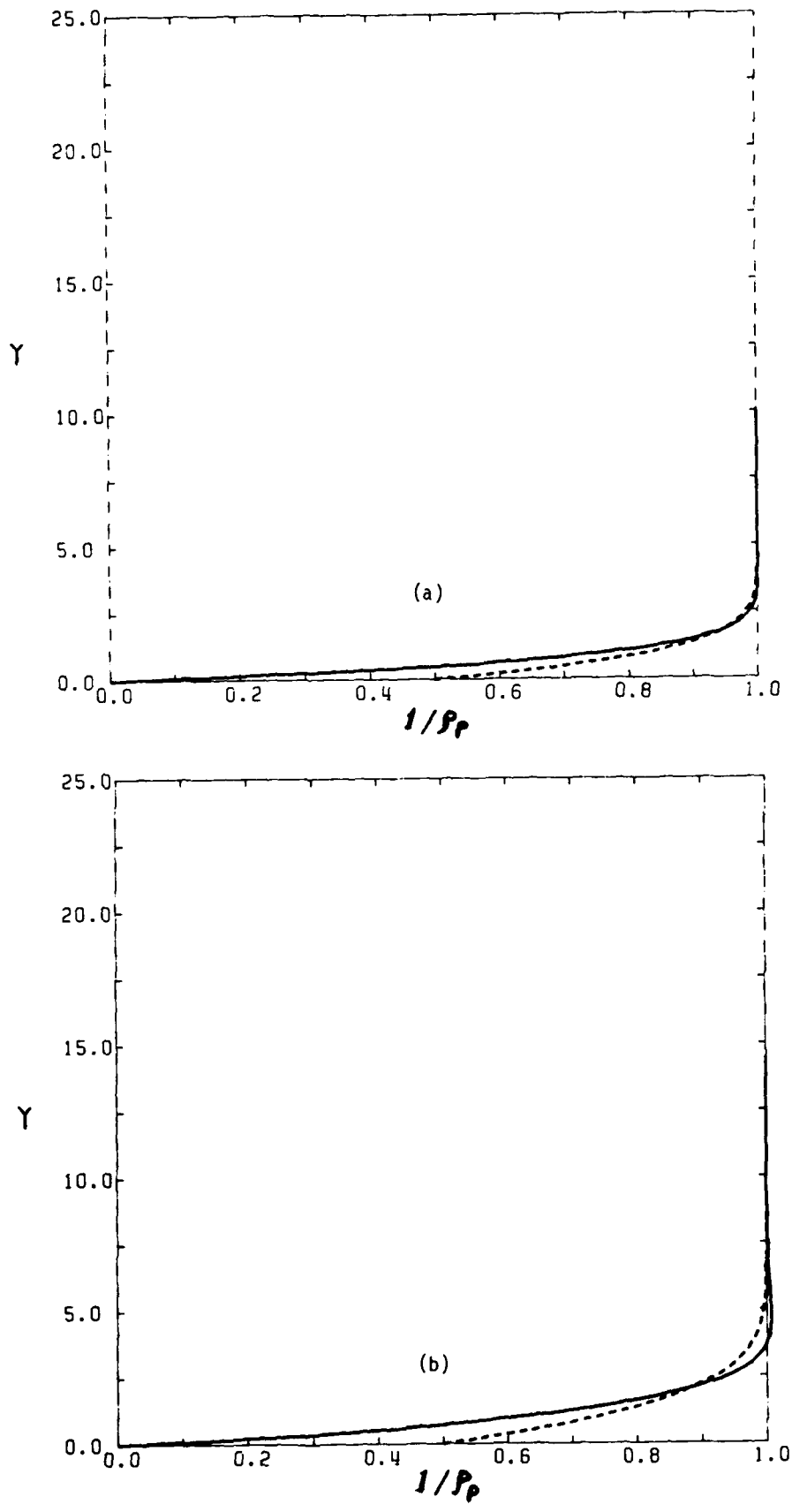

FIG. E-1 PARTICLE-DENSITY PROFILES.

(a) x = 2.05; (b) x = 5.05; (c) x = 10.05.

——— WITH ACCUMULATION; ---- WITHOUT ACCUMULATION.

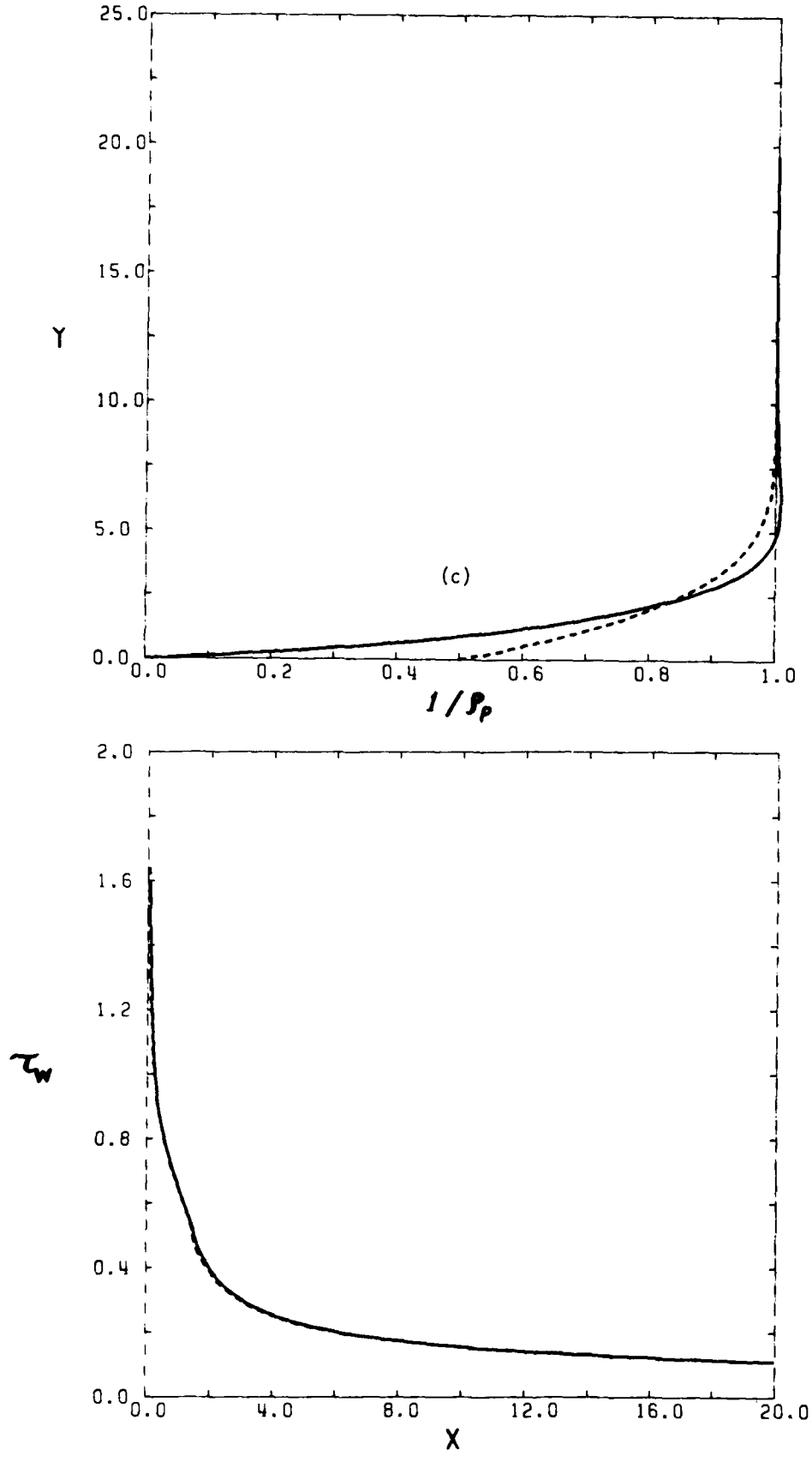

FIG. E-2 SHEAR STRESS AT THE WALL WITH DISTANCE x.

——— WITH ACCUMULATION; ---- WITHOUT ACCUMULATION.

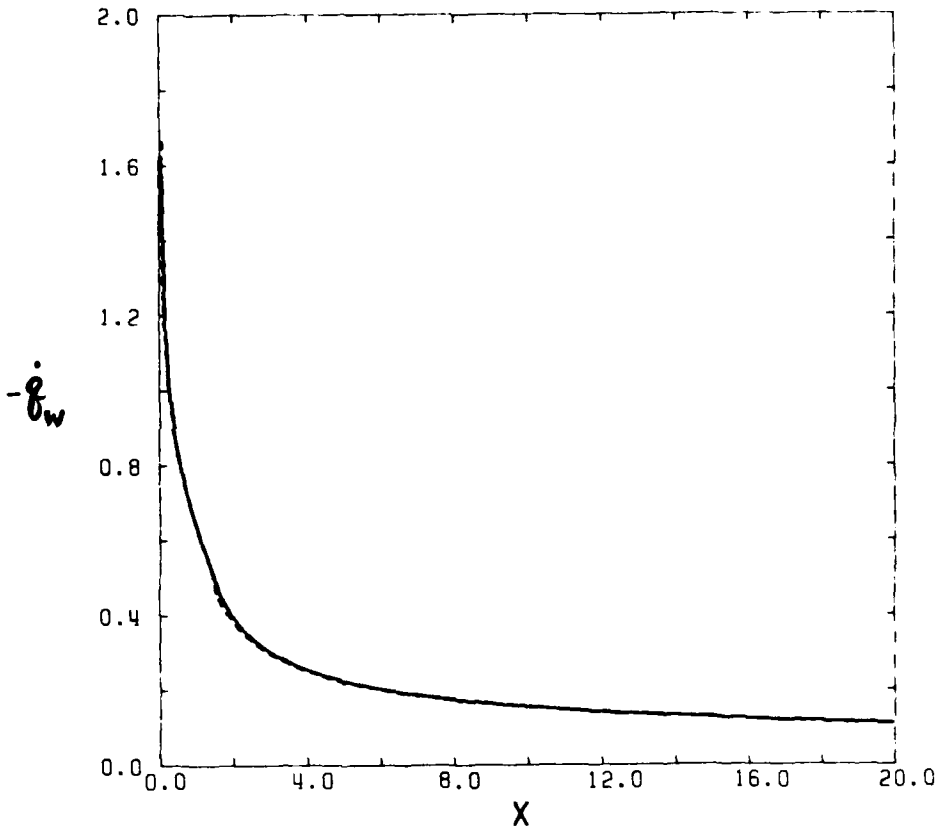

FIG. E-3 WALL HEAT-TRANSFER RATE WITH DISTANCE x.

——— WITH ACCUMULATION; ---- WITHOUT ACCUMULATION.

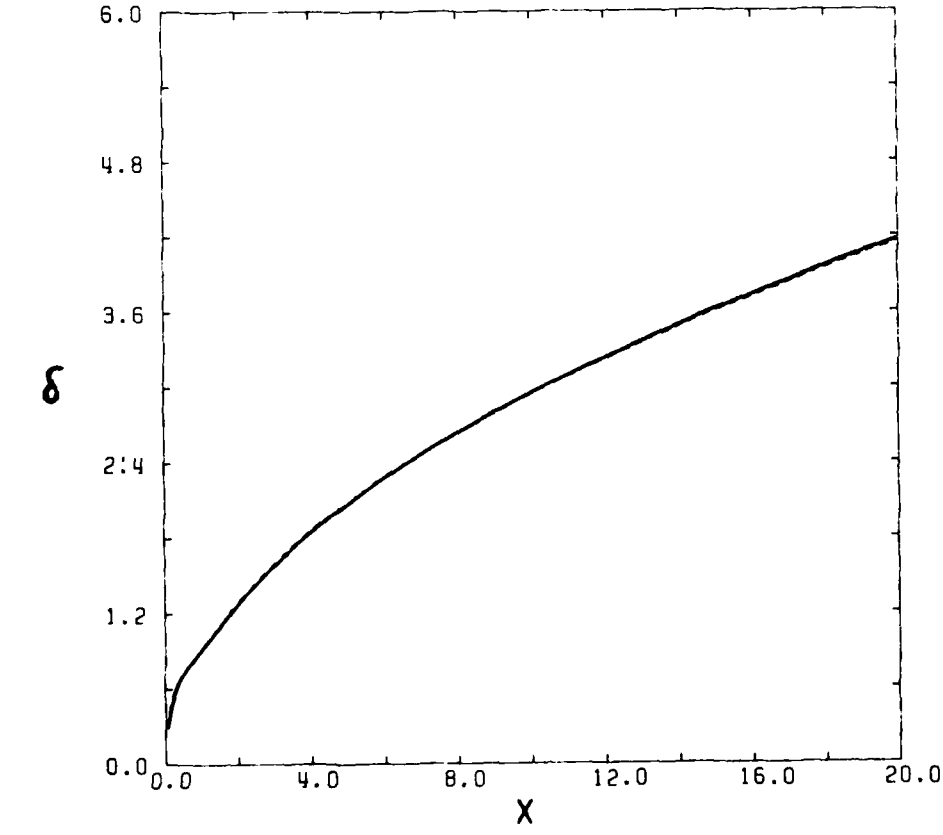

FIG. E-4 NONDIMENSIONAL DISPLACEMENT THICKNESS WITH DISTANCE x.

——— WITH ACCUMULATION; ---- WITHOUT ACCUMULATION.

UTIAS Report No. 311

University of Toronto, Institute for Aerospace Studies (UTIAS)
4925 Dufferin Street, Downsview, Ontario, Canada, M3H 5T6

FINITE-DIFFERENCE SOLUTIONS FOR COMPRESSIBLE LAMINAR BOUNDARY-LAYER FLOWS OF A DUSTY GAS OVER A SEMI-INFINITE FLAT PLATE

Wang, B. Y., Glass, I. I.

1. Dusty-gas flows 2. Two-phase flows 3. Boundary-layer flows
4. Partial-differential equations 5. Numerical analysis

A finite-difference method is used to investigate compressible, laminar boundary-layer flows of a dilute dusty gas over a semi-infinite flat plate. Details are given of the implicit finite-difference schemes as well as the boundary conditions, initial conditions and compatibility conditions for solving the gas-particle boundary-layer equations. The flow profiles for both the gas and particle phases were obtained numerically along the whole length of the plate from the leading edge to far downstream of it. The finite-difference solutions in the large-slip region and the small-slip region are compared with the asymptotic solutions and good agreement is achieved. The boundary-layer characteristics of interest, including the wall shear stress, the wall heat-transfer rate and the displacement thickness, are calculated. The alteration of the flow properties owing to the presence of particles is discussed in detail. It was found that the boundary-layer flow of a dusty gas can be divided into three distinct flow regimes which are characterized by quasi-frozen, nonequilibrium and quasi-equilibrium flows and that at a critical distance from the leading edge the particle velocity at the wall decelerates to zero and near-equilibrium is achieved between the gas and particle flows. For the laminar boundary layer of a dusty gas, the shear stress and the heat-transfer at the wall are increased and the displacement thickness is decreased compared with the pure-gas case alone.

Available copies of this report are limited. Return this card to UTIAS, if you require a copy.

UTIAS Report No. 311

University of Toronto, Institute for Aerospace Studies (UTIAS)
4925 Dufferin Street, Downsview, Ontario, Canada, M3H 5T6

FINITE-DIFFERENCE SOLUTIONS FOR COMPRESSIBLE LAMINAR BOUNDARY-LAYER FLOWS OF A DUSTY GAS OVER A SEMI-INFINITE FLAT PLATE

Wang, B. Y., Glass, I. I.

1. Dusty-gas flows 2. Two-phase flows 3. Boundary-layer flows
4. Partial-differential equations 5. Numerical analysis

A finite-difference method is used to investigate compressible, laminar boundary-layer flows of a dilute dusty gas over a semi-infinite flat plate. Details are given of the implicit finite-difference schemes as well as the boundary conditions, initial conditions and compatibility conditions for solving the gas-particle boundary-layer equations. The flow profiles for both the gas and particle phases were obtained numerically along the whole length of the plate from the leading edge to far downstream of it. The finite-difference solutions in the large-slip region and the small-slip region are compared with the asymptotic solutions and good agreement is achieved. The boundary-layer characteristics of interest, including the wall shear stress, the wall heat-transfer rate and the displacement thickness, are calculated. The alteration of the flow properties owing to the presence of particles is discussed in detail. It was found that the boundary-layer flow of a dusty gas can be divided into three distinct flow regimes which are characterized by quasi-frozen, nonequilibrium and quasi-equilibrium flows and that at a critical distance from the leading edge the particle velocity at the wall decelerates to zero and near-equilibrium is achieved between the gas and particle flows. For the laminar boundary layer of a dusty gas, the shear stress and the heat-transfer at the wall are increased and the displacement thickness is decreased compared with the pure-gas case alone.

Available copies of this report are limited. Return this card to UTIAS, if you require a copy.

UTIAS Report No. 311

University of Toronto, Institute for Aerospace Studies (UTIAS)
4925 Dufferin Street, Downsview, Ontario, Canada, M3H 5T6

FINITE-DIFFERENCE SOLUTIONS FOR COMPRESSIBLE LAMINAR BOUNDARY-LAYER FLOWS OF A DUSTY GAS OVER A SEMI-INFINITE FLAT PLATE

Wang, B. Y., Glass, I. I.

1. Dusty-gas flows 2. Two-phase flows 3. Boundary-layer flows
4. Partial-differential equations 5. Numerical analysis

A finite-difference method is used to investigate compressible, laminar boundary-layer flows of a dilute dusty gas over a semi-infinite flat plate. Details are given of the implicit finite-difference schemes as well as the boundary conditions, initial conditions and compatibility conditions for solving the gas-particle boundary-layer equations. The flow profiles for both the gas and particle phases were obtained numerically along the whole length of the plate from the leading edge to far downstream of it. The finite-difference solutions in the large-slip region and the small-slip region are compared with the asymptotic solutions and good agreement is achieved. The boundary-layer characteristics of interest, including the wall shear stress, the wall heat-transfer rate and the displacement thickness, are calculated. The alteration of the flow properties owing to the presence of particles is discussed in detail. It was found that the boundary-layer flow of a dusty gas can be divided into three distinct flow regimes which are characterized by quasi-frozen, nonequilibrium and quasi-equilibrium flows and that at a critical distance from the leading edge the particle velocity at the wall decelerates to zero and near-equilibrium is achieved between the gas and particle flows. For the laminar boundary layer of a dusty gas, the shear stress and the heat-transfer at the wall are increased and the displacement thickness is decreased compared with the pure-gas case alone.

Available copies of this report are limited. Return this card to UTIAS, if you require a copy.

UTIAS Report No. 311

University of Toronto, Institute for Aerospace Studies (UTIAS)
4925 Dufferin Street, Downsview, Ontario, Canada, M3H 5T6

FINITE-DIFFERENCE SOLUTIONS FOR COMPRESSIBLE LAMINAR BOUNDARY-LAYER FLOWS OF A DUSTY GAS OVER A SEMI-INFINITE FLAT PLATE

Wang, B. Y., Glass, I. I.

1. Dusty-gas flows 2. Two-phase flows 3. Boundary-layer flows
4. Partial-differential equations 5. Numerical analysis

A finite-difference method is used to investigate compressible, laminar boundary-layer flows of a dilute dusty gas over a semi-infinite flat plate. Details are given of the implicit finite-difference schemes as well as the boundary conditions, initial conditions and compatibility conditions for solving the gas-particle boundary-layer equations. The flow profiles for both the gas and particle phases were obtained numerically along the whole length of the plate from the leading edge to far downstream of it. The finite-difference solutions in the large-slip region and the small-slip region are compared with the asymptotic solutions and good agreement is achieved. The boundary-layer characteristics of interest, including the wall shear stress, the wall heat-transfer rate and the displacement thickness, are calculated. The alteration of the flow properties owing to the presence of particles is discussed in detail. It was found that the boundary-layer flow of a dusty gas can be divided into three distinct flow regimes which are characterized by quasi-frozen, nonequilibrium and quasi-equilibrium flows and that at a critical distance from the leading edge the particle velocity at the wall decelerates to zero and near-equilibrium is achieved between the gas and particle flows. For the laminar boundary layer of a dusty gas, the shear stress and the heat-transfer at the wall are increased and the displacement thickness is decreased compared with the pure-gas case alone.

Available copies of this report are limited. Return this card to UTIAS, if you require a copy.

END

1-87

DTIC